2008-07-17

Theory and Estimation of Acoustic Intensity and Energy Density

Derek C. Thomas
Brigham Young University - Provo

THEORY AND ESTIMATION OF ACOUSTIC INTENSITY AND ENERGY DENSITY

by

Derek C. Thomas

A thesis submitted to the faculty of

Brigham Young University

in partial fulfillment of the requirements for the degree of

Master of Science

Department of Physics and Astronomy

Brigham Young University

August 2008

BRIGHAM YOUNG UNIVERSITY

GRADUATE COMMITTEE APPROVAL

of a thesis submitted by

Derek C. Thomas

This thesis has been read by each member of the following graduate committee and by majority vote has been found to be satisfactory.

Date	Kent L. Gee, Chair
Date	Scott D. Sommerfeldt
Date	Jonathan D. Blotter

BRIGHAM YOUNG UNIVERSITY

As chair of the candidate's graduate committee, I have read the thesis of Derek C. Thomas in its final form and have found that (1) its format, citations, and bibliographical style are consistent and acceptable and fulfill university and department style requirements; (2) its illustrative materials including figures, tables, and charts are in place; and (3) the final manuscript is satisfactory to the graduate committee and is ready for submission to the university library.

Date

Kent L. Gee
Chair, Graduate Committee

Accepted for the Department

Ross L. Spencer, Department Chair
Department of Physics and Astronomy

Accepted for the College

Thomas W. Sederberg, Associate Dean
College of Physical and Mathematical Sciences

ABSTRACT

THEORY AND ESTIMATION OF ACOUSTIC INTENSITY AND ENERGY DENSITY

Derek C. Thomas

Department of Physics and Astronomy

Master of Science

In order to facilitate the acquisition and accurate interpretation of intensity and energy density data in high-amplitude pressure fields, the expressions for intensity and energy density are examined to ascertain the impact of nonlinear processes on the standard expressions. Measurement techniques for estimating acoustic particle velocity are presented. The finite-difference method is developed in an alternate manner and presented along with bias and confidence estimates. Additionally, two new methods for estimating the local particle velocity are presented. These methods appears to eliminate the errors and bias associated with the finite-difference technique for certain cases.

ACKNOWLEDGMENTS

I would like to thank all of the people who made this research possible and whose cooperation allowed me to finish in accordance with my timeline. I'm grateful to my advisor, Kent Gee, for his willingness to listen, ask questions, and review my drafts on the weekends. I would like to thank my committee for their patience and valuable insight. I owe many thanks to my fellow students including Jarom Giraud, Panu Puikkonen, Cole Duke, Buye Xu, and many others for their assistance and time spent as sounding boards. Most of all, I would like to my wife Wendy for her patience and understanding during the long hours required to finish on time, and for putting up with my endless curiosity.

Contents

List of Figures

Chapter 1

Introduction

1.1 Introduction

This thesis contains a theoretical development of the acoustic intensity and energy density as well as a review of an established method for estimating the information necessary to calculate these quantities from experimental data. The limitations of this method are discussed, and two new alternate methods are presented. These methods are analyzed and compared to the established method. This chapter presents an overview of the previous work and motivates the work presented in this thesis.

1.2 Background

An expression for the energy carried by an acoustic pressure wave was first derived by Kirchhoff in 1877 [1]. It was also considered by Lord Rayleigh in his seminal work, *The Theory of Sound* [2]. Acoustic intensity measurements have proved useful for various applications. The acoustic intensity has been used extensively for characterization of radiating sources, while acoustic energy density has been shown to be useful in both

architectural acoustics [3] and active noise control [4]. Because the energy density exhibits greater spatial uniformity than other observable field quantities, such as pressure, the number of measurement points required to characterize the field may be reduced in some cases [3]. In noise control, minimization of the energy density at one point corresponds to a greater reduction of the total energy of the pressure field due to the spatial uniformity of the energy density, often resulting in more efficient control.

Although the common expression for acoustic energy density

$$w = \frac{1}{2}\rho u^2 + \frac{p^2}{2\rho_0 c} \tag{1.1}$$

is used indiscriminately in acoustics, multiple sources [5–10] present

$$w = \frac{1}{2}\rho u^2 + \frac{p}{\gamma - 1} \tag{1.2}$$

as an energy density expression derived from first principles *without* linearizing approximations for the nondissipative case; this expression seems necessary to describe the energy density of a high-amplitude field [11]. The connection between the Eqs. (1.1) and (1.2) has been discussed in the literature [6–8], but still remains somewhat ambiguous.

The standard method for estimating particle velocity [12] from closely spaced pressure measurements relies on a finite-difference estimate of the pressure gradient as well as an average measure of the pressure. These estimates introduce significant bias into the measurement process. Elko performed extensive work on the development and evaluation of the finite-difference (p-p) method for estimating the intensity in one dimension [13]. Elko suggested [14] that mounting the sensors in a sphere for the finite-difference estimate reduces the bias.

1.3 Motivation

High-amplitude noise is a byproduct of the current demand for high-thrust jet and rocket engines in transportation, military, and scientific applications. There is a growing need to understand the nature and effects of such noise, due to increasingly stringent noise pollution regulations and possible structural and mechanical effects of high-amplitude pressure exposure. NASA has funded research with the goal of providing additional insight and understanding of acoustical phenomena relevant to rocket noise sources. Due to the utility of energy density and intensity measurements in other areas of acoustics, NASA seeks to employ similar methods in the evaluation and testing of rocket noise. A probe has been constructed which consists of four high-amplitude pressure microphones mounted on the surface of a sphere. Because of this, special attention will be paid to the effect of the sphere on the estimated quantities.

1.4 Research Objectives

There are two predominant objectives of the research contained herein. The first is to verify the standard expressions for acoustic intensity and energy density and provide a connection between these expressions and the alternate expression derived from first principles [8]. The second is to estimate the intensity and energy density of a pressure field for certain cases without the inherent bias of the finite-difference method.

1.5 Outline

The remainder of this thesis will be as follows:

- Chapter 2 begins with a development of the expressions for linear acoustic

intensity and energy density both generally and for several model cases. It contains a derivation of the fully nonlinear energetic acoustic quantities for the nondissipative case from first principles, and provides a connection between the nonlinear expressions and the standard linear forms.

- Chapter 3 presents the standard method for estimating the acoustic intensity and energy density of a pressure field using pressure sensors along with two new methods for estimating the same quantities.

- Chapter 4 contains a development of confidence intervals for intensity estimates made from acquired data. The errors induced by estimate bias and equipment are considered and numerical simulations of the various techniques are presented and compared.

- Chapter 5 summarizes the results of the research and includes suggestions for future work.

- The MATLAB code used to produce the results contained herein is presented for reference in the appendix.

Chapter 2

Acoustic Intensity and Energy Density

2.1 Fundamental Equations

A description of the behavior of a fluid requires an equation of momentum,

$$\rho \frac{D\mathbf{u}}{Dt} = -\nabla P + \nabla \cdot \mathbb{T} + \mathbf{f}, \tag{2.1}$$

where ρ is the mass density, $\mathbf{u}$ is the velocity vector field, P is the absolute pressure, $\mathbb{T}$ is the stress tensor, and $\mathbf{f}$ represents any body forces such as gravity, or electromagnetic forces. Bold faced font will be used to represent vectors, and blackboard font will be used to represent second rank tensors and matrices. Using $\nabla(\cdot)$ to represent the gradient operator, the total derivative is defined as $D(\cdot)/Dt = \partial(\cdot)/\partial t + \mathbf{u} \cdot \nabla(\cdot)$. Assuming that the stress tensor and body forces are known, additional relations are necessary to determine the pressure, density, and velocity fields. The imposition of a mass conservation law on the system induces the continuity equation

$$\frac{\partial \rho}{\partial t} + \nabla \cdot (\rho \mathbf{u}) = 0. \tag{2.2}$$

In order to close the system, additional information, such as an energy equation or an appropriate equation of state, is needed. These equations may be used to develop expressions for the energy density and energy transfer due to a fluid disturbance. The governing acoustic equations are a special cases of these general equations. First, the linear case will be considered, followed by the more general nonlinear case.

2.2 Linear Expressions for Acoustic Intensity and Energy Density

The conservation expressions in Eq. (2.1) and (2.2) are nonlinear and currently do not admit analytical solution except in certain simplified cases. For the case of small-amplitude acoustic fluctuations about an equilibrium state, considerable simplification is achieved by substituting

$$\mathbf{u} = \mathbf{u}_0 + \mathbf{u}', \tag{2.3a}$$

$$P = P_0 + p', \tag{2.3b}$$

$$\rho = \rho_0 + \rho', \tag{2.3c}$$

and neglecting second order terms. If losses and body forces also neglected and there is no mean flow ($\mathbf{u}_0 = 0$), then, to first order, the momentum and continuity equations are

$$\rho_0 \frac{\partial \mathbf{u}'}{\partial t} = -\nabla p', \tag{2.4a}$$

$$\frac{\partial \rho'}{\partial t} = -\rho_0 \nabla \cdot \mathbf{u}'. \tag{2.4b}$$

These are referred to as the linearized Euler's (momentum) and continuity equations [1].

Because the system is defined by two equations in the three quantities, ρ', p', and $\mathbf{u}'$, it is underdetermined and an additional relation is required. The adiabatic equation of state,

$$1 + \frac{p'}{P_0} = \left(1 + \frac{\rho'}{\rho_0}\right)^{\gamma}, \tag{2.5}$$

where γ is the ratio of specific heats, is appropriate for most acoustic processes in which heat transfer between elements of the system is negligible.

The intensity due to a small-amplitude acoustic disturbance may be developed by considering the linearized forms of the governing equations [1]. Taking the dot product of the velocity with the linearized Euler's equation (2.4a), applying a vector identity, and using the mass conservation equation (2.4b) yields

$$\mathbf{u}' \cdot \left[\rho_0 \frac{\partial \mathbf{u}'}{\partial t}\right] = -\nabla \cdot (p'\mathbf{u}') - \frac{p'}{\rho_0}\frac{\partial \rho'}{\partial t}. \tag{2.6}$$

Using the linear relation for the speed of sound in an adiabatic gas $\rho' = p'/c^2$ and applying the chain rule to the time derivatives produces

$$\frac{\partial}{\partial t}\left[\frac{\rho_0 \left|\mathbf{u}'\right|^2}{2} + \frac{p'^2}{2\rho_0 c^2}\right] + \nabla \cdot (p'\mathbf{u}') = 0. \tag{2.7}$$

The term in brackets on the left is referred to as the acoustic energy density

$$w = \frac{\rho_0 u'^2}{2} + \frac{p'^2}{2\rho_0 c^2}, \tag{2.8}$$

and the instantaneous acoustic intensity is defined as

$$\mathbf{I}_i = p'\mathbf{u}'. \tag{2.9}$$

If complex notation is used for the pressure and velocity, then $\mathbf{I}_i = \mathrm{Re}\{p'_{complex}\}\mathrm{Re}\{\mathbf{u}'_{complex}\}$. The complex notation will be used throughout the remainder of this work without special indication. It is also possible to define the complex intensity [15] as

$$\mathbf{I}_c = \frac{1}{2}p'\mathbf{u}^* = \mathbf{I} + \jmath\mathbf{J}, \tag{2.10}$$

where,

$$\mathbf{I} = \frac{1}{2}\mathrm{Re}\{p\mathbf{u}^*\}, \tag{2.11a}$$

$$\mathbf{J} = \frac{1}{2}\mathrm{Im}\{p\mathbf{u}^*\}. \tag{2.11b}$$

The symbol $\jmath$ is used to represent the imaginary number, $\jmath = \sqrt{-1}$. To distinguish between the real and imaginary parts of the complex intensity, the real part $\mathbf{I}$ is referred to as the active intensity and the imaginary part $\mathbf{J}$ is referred to as the reactive intensity [1,15]. The active intensity is the time average of the instantaneous intensity,

$$\frac{1}{T}\int_T \mathbf{I}_i dt = \mathbf{I}. \tag{2.12}$$

The active intensity is the average energy per cycle carried through a surface by the "traveling" portion of the pressure field. The reactive intensity represents the energy that is carried back and forth through the same surface by the "standing" portion of the pressure field, hence the average intensity of the reactive portion is zero.

2.2.1 Intensity Due to Point Sources

The pressure field produced by a single time-harmonic point source at an arbitrary location $\mathbf{r}_{s1}$ is

$$p_1 = \frac{A_1}{|\mathbf{r}_1|}e^{\jmath(\omega t - \mathbf{k}_1\cdot\mathbf{r}_1)}, \tag{2.13}$$

where A_1 is the complex source amplitude, $\mathbf{r}_1 = \mathbf{r} - \mathbf{r}_{s1}$, and $\mathbf{k}_1 = k\frac{\mathbf{r}_1}{|\mathbf{r}_1|}$ is the wave vector indicating the direction of propagation. The velocity field associated with the pressure field is found using Euler's equation, and may be written as

$$\mathbf{u}_1 = \frac{\jmath}{\rho\omega}\nabla p_1 = \frac{A_1}{\rho\omega|\mathbf{r}_1|^2}\mathbf{r}_1\left[k - \frac{\jmath}{|\mathbf{r}_1|}\right]e^{\jmath(\omega t - \mathbf{k}_1\cdot\mathbf{r}_1)}. \tag{2.14}$$

Using these expressions for pressure and particle velocity in Eq. (2.11) yields

$$\mathbf{I} = \frac{k|A_1|^2}{\rho\omega|\mathbf{r}_1|^3}\mathbf{r}_1, \tag{2.15}$$

$$\mathbf{J} = \frac{|A_1|^2}{\rho\omega|\mathbf{r}_1|^4}\mathbf{r}_1 \tag{2.16}$$

for the active and reactive intensities.

It is also straightforward to find the intensity due to the radiation of multiple point sources. The pressure at a point $\mathbf{r}$ is given by the sum of the contributions from the individual sources,

$$p = \sum_{m=1}^{N} p_m = \sum_{m=1}^{N} \frac{A_m}{|\mathbf{r}_m|} e^{\jmath(\omega t - \mathbf{k}_m \cdot \mathbf{r}_m)}, \tag{2.17}$$

where $\mathbf{r}_m = \mathbf{r} - \mathbf{r}_{sm}$, and $\mathbf{k}_m = k\frac{\mathbf{r}_m}{|\mathbf{r}_m|}$. The velocity is found in the same manner as in Eq. (2.14) to be

$$\mathbf{u} = \sum_{n=1}^{N} \mathbf{u}_n = \sum_{n=1}^{N} \frac{A_n}{\rho\omega|\mathbf{r}_n|^2}\mathbf{r}_n \left[k - \frac{\jmath}{|\mathbf{r}_n|}\right] e^{\jmath(\omega t - \mathbf{k}_n \cdot \mathbf{r}_n)}. \tag{2.18}$$

Thus, the instantaneous intensity is

$$\mathbf{I}_i = \sum_{m=1}^{N} p_m \sum_{n=1}^{N} \mathbf{u}_n = \sum_{m=1}^{N}\sum_{n=1}^{N} \frac{A_m A_n}{\rho\omega|\mathbf{r}_m||\mathbf{r}_n|^2} \left[k - \frac{\jmath}{|\mathbf{r}_n|}\right] e^{\jmath(2\omega t - \mathbf{k}_n \cdot \mathbf{r}_n - \mathbf{k}_m \cdot \mathbf{r}_m)}\mathbf{r}_n, \tag{2.19}$$

and the complex intensity is

$$\mathbf{I}_c = \frac{1}{2}\sum_{m=1}^{N} p_m \sum_{n=1}^{N} \mathbf{u}_n^* = \frac{1}{2}\sum_{m=1}^{N}\sum_{n=1}^{N} \frac{A_m A_n^*}{\rho\omega|\mathbf{r}_m||\mathbf{r}_n|^2} \left[k + \frac{\jmath}{|\mathbf{r}_n|}\right] e^{\jmath(\mathbf{k}_n \cdot \mathbf{r}_n - \mathbf{k}_m \cdot \mathbf{r}_m)}\mathbf{r}_n. \tag{2.20}$$

Taking the real part of Eq. (2.20) describes the average energy transfer due to the acoustic disturbance over one period, or over a sufficiently long time interval.

2.3 Nonlinear Expressions for Acoustic Intensity and Energy Density

Although the method presented previously for obtaining the linear acoustic intensity is mathematically elegant, it provides little insight into the physical processes that

govern energy transfer in a fluid. A more general approach may be followed to obtain expressions for the acoustic intensity and energy density from the nonlinear governing equations.

The general form for the kinetic energy density, $\mathfrak{t}$, is $\frac{1}{2}\rho u^2$, where ρ is the mass density, by appropriate definition of variables, this definition is valid for both Lagrangian and Eulerian coordinates. This expression is identical in form to the classical expression for kinetic energy having the mass replaced by the mass density. In order to determine the correct form for the potential energy density $\mathfrak{u}$ in a fluid, assume that $\mathfrak{u} = \rho e$, where e is the internal energy per unit mass. The value of e may be found using either a series expansion or by considering the thermodynamic properties of the system. The series expansion is presented by both Pierce [1] and Chu and Apfel [16]. A derivation based on thermodynamic principles is found in Seliger and Whitham's paper [17].

First, consider the first law of thermodynamics,

$$\delta\mathcal{U} = \delta\mathcal{Q} + \delta\mathcal{W}, \tag{2.21}$$

where $\mathcal{Q}$ is the heat of the system and $\mathcal{W}$ is the work done on the system. This law states that the change in the energy in the system is equal to the sum of the change in heat and the work done on the system. This may be expressed in terms of exact differentials as

$$d\mathcal{U} = \Theta dS - PdV, \tag{2.22}$$

where S is the entropy, Θ is the temperature, and P is the pressure. For the problem at hand, this equation is most usefully expressed as

$$de = \Theta ds - Pd\left(\rho^{-1}\right), \tag{2.23}$$

where e is again the energy per unit mass, s is the specific entropy, and $1/\rho$ is the specific volume (volume per unit mass). This relation may be solved for the energy

per unit mass e, if the process is assumed to be isentropic ($ds = 0$), and if the pressure is related to the density by an appropriate equation of state. The thermodynamic process of acoustic propagation is usually assumed to be adiabatic, in which case, the equation of state is

$$\frac{P}{P_0} = \left(\frac{\rho}{\rho_0}\right)^{\gamma}, \tag{2.24}$$

where $\gamma = c_p/c_v$, and c_p, and c_v are the specific heats at constant pressure, and constant volume, respectively. Using these assumptions, Eq. (2.23) becomes

$$de = -P_0 \left(\frac{\rho}{\rho_0}\right)^{\gamma} d\left(\rho^{-1}\right), \tag{2.25}$$

which may be integrated as

$$\int_{e_{ref}}^{e} de' = -\int_{\rho_{ref}^{-1}}^{\rho^{-1}} P_0 \left(\frac{\rho'}{\rho_0}\right)^{\gamma} d\left(\rho'^{-1}\right). \tag{2.26}$$

The bounds of integration are chosen to represent the change in energy in the system as it moves from a reference state to another state. The reference state may be the equilibrium state or the classical zero-energy state (vacuum). For these two cases, evaluating the integral given above yields

$$e - e_0 = \frac{P}{\rho(\gamma - 1)} - \frac{P_0}{\rho_0(\gamma - 1)}, \tag{2.27}$$

for the energy per unit mass relative to a reference state, and

$$e = \frac{P}{\rho(\gamma - 1)}, \tag{2.28}$$

for the energy per unit mass relative to the zero-energy state. Because the internal energy per unit mass appears multiplied by the mass density, it is also possible to define a potential energy density relative to a reference state as

$$\mathfrak{u} - \mathfrak{u}_0 = \rho e - [\rho e]_{ref} = \frac{P}{\gamma - 1} - \left[\frac{P}{\gamma - 1}\right]_{ref}. \tag{2.29}$$

If the zero-energy state is chosen as the reference state, then Eq. (2.29) is equal to Eq. (2.28). If the equilibrium state is chosen, then Eq. (2.29) is

$$\mathfrak{u} - \mathfrak{u}_0 = \frac{P - P_0}{\gamma - 1} \neq \rho(e - e_0) = \frac{P}{(\gamma - 1)} - \frac{\rho P_0}{\rho_0(\gamma - 1)}. \tag{2.30}$$

Thus, for an adiabatic process in a gas, the total energy density is

$$w = \mathfrak{t} + \mathfrak{u} = \frac{\rho u^2}{2} + \frac{P}{\gamma - 1}. \tag{2.31}$$

There is a rather subtle point here that should be emphasized. If the potential energy density of the system is referenced to an equilibrium energy per unit *mass*, the energy density expression becomes

$$w = \frac{\rho u^2}{2} + \frac{P}{\gamma - 1} - \frac{\rho P_0}{\rho_0(\gamma - 1)}. \tag{2.32}$$

This is the expression presented by Andreev [8] as the correct expression for acoustic energy density. However, if the energy is referenced to an energy per unit *volume*, then the expression is

$$w = \frac{\rho u^2}{2} + \frac{P - P_0}{\gamma - 1}. \tag{2.33}$$

Because the acoustic equations are most commonly used in an Eulerian form (control volume), it seems that referencing the energy density to the equilibrium energy density per unit volume is more appropriate, and in this case Eq. (2.33) is more natural. However, it will be shown later that Eq. (2.27) is the correct energy expression for a Lagrangian coordinate system.

In order to draw a connection between Eq. (2.33) and the traditional acoustic energy density, Eq. (2.8), assume that the fluctuations about equilibrium are small, and expand the pressure P about the equilibrium in a series in the density ρ. The result is

$$P - P_0 = \left[\frac{\partial p}{\partial \rho}\right]_0 (\rho - \rho_0) + \frac{1}{2!}\left[\frac{\partial^2 p}{\partial \rho^2}\right]_0 (\rho - \rho_0)^2 + \cdots, \tag{2.34}$$

where the derivatives are evaluated at equilibrium. This expansion may be used to show that for the infinitesimal case, the energy density expressions obtained from Eqs. (2.27) and (2.29) are equal. Using the ideal gas law and the adiabatic equation of state,

$$\left[\frac{\partial p}{\partial \rho}\right]_0 = \left[\frac{\gamma P}{\rho}\right]_0 = c^2, \tag{2.35}$$

and

$$\left[\frac{\partial^2 p}{\partial \rho^2}\right]_0 = \left[\frac{\gamma(\gamma-1)P}{\rho^2}\right]_0 = \frac{c^2}{\rho_0}(\gamma-1). \tag{2.36}$$

Thus,

$$\mathfrak{u} = \frac{P-P_0}{\gamma-1} = \frac{c^2}{\gamma-1}(\rho-\rho_0) + \frac{c^2}{2\rho_0}(\rho-\rho_0)^2 + \cdots. \tag{2.37}$$

Assuming that $\rho = \rho_0 + \rho'$, and discarding third-order terms in the kinetic energy density expression, we have

$$w = \frac{\rho_0 u^2}{2} + \frac{1}{\gamma-1}\left[c^2(\rho-\rho_0)\right] + \frac{c^2}{2\rho_0}(\rho-\rho_0)^2 \tag{2.38}$$

to second order. The first order relation between the density and pressure, $\rho - \rho_0 = (P-P_0)/c^2$ may be used to write the squared term in w in the more commonly used form if desired [1]. Upon substituting w into the energy conservation equation [1],

$$\frac{\partial w}{\partial t} + \nabla\cdot(w\mathbf{u} + P\mathbf{u}) = 0, \tag{2.39}$$

we see that the linear terms cancel due to the continuity equation, $\partial\rho/\partial t + \nabla\cdot(\rho\mathbf{u}) = 0$, and

$$\frac{\partial}{\partial t}\left[\frac{\rho_0 u^2}{2} + \frac{c^2}{2\rho_0}(\rho-\rho_0)^2\right] + \nabla\cdot[\mathbf{u}(P-P_0)]. \tag{2.40}$$

From this equation we define the acoustic potential energy density,

$$\mathfrak{u} = \frac{c^2}{2\rho_0}(\rho-\rho_0)^2, \tag{2.41}$$

the acoustic kinetic energy density,

$$\mathfrak{t} = \frac{\rho_0 u^2}{2}, \tag{2.42}$$

the acoustic energy density,

$$w = \mathfrak{t} + \mathfrak{u} = \frac{\rho_0 u^2}{2} + \frac{c^2}{2\rho_0}(\rho - \rho_0)^2, \tag{2.43}$$

and the acoustic intensity,

$$I = \mathbf{u}(P - P_0). \tag{2.44}$$

Although the method outlined previously provides a simple analytic form for the total energy density, the adiabatic assumption limits the application of the expression to other fluids. An alternate method for determining the potential energy density is to assume that the fluctuation from equilibrium is small, and expand ρe in a series in ρ about an equilibrium value ρ_0 as

$$\rho e = \rho_0 e_0 + \left[\frac{\partial \rho e}{\partial \rho}\right]_0 (\rho - \rho_0) + \frac{1}{2!}\left[\frac{\partial^2 \rho e}{\partial \rho^2}\right]_0 (\rho - \rho_0)^2 + \cdots, \tag{2.45}$$

where the terms inside the brackets, $[\cdot]_0$, are evaluated at equilibrium. Again using Eq. (2.23), the necessary derivatives are

$$\frac{\partial \rho e}{\partial \rho} = e + \rho \frac{\partial e}{\partial \rho} = e + \frac{p}{\rho} = h, \tag{2.46}$$

$$\frac{\partial^2 \rho e}{\partial \rho^2} = \frac{\partial h}{\partial \rho} = \frac{\partial e}{\partial \rho} + \frac{1}{\rho}\frac{\partial p}{\partial \rho} - \frac{p}{\rho} = \frac{1}{\rho}\frac{\partial p}{\partial \rho} = \frac{c^2}{\rho}, \tag{2.47}$$

where c is the isentropic sound speed and h is the enthalpy per unit mass. Thus,

$$\rho e = \rho_0 e_0 + h_0(\rho - \rho_0) + \frac{c^2}{2\rho_0}(\rho - \rho_0)^2 \tag{2.48}$$

to second order. Following the assumption that the fluctuations about equilibrium are small, and writing $\rho = \rho_0 + \rho'$, then $\rho' u^2/2$ is a third order quantity, and the total energy density is

$$w = \frac{\rho_0 u^2}{2} + \rho_0 e_0 + h_0(\rho - \rho_0) + \frac{c^2}{2\rho_0}(\rho - \rho_0)^2 \tag{2.49}$$

to second order. The energy density relative to equilibrium is

$$w = \frac{\rho_0 u^2}{2} + h_0(\rho - \rho_0) + \frac{c^2}{2\rho_0}(\rho - \rho_0)^2. \tag{2.50}$$

The standard expression for acoustic energy density is obtained by considering the energy conservation equation,

$$\frac{\partial w}{\partial t} + \nabla \cdot [(w + p)\mathbf{u}] = 0. \tag{2.51}$$

When w is substituted into the conservation equation, the linear terms again cancel and as a result,

$$\frac{\partial}{\partial t}\left[\frac{\rho_0 u^2}{2} + \frac{c^2}{2\rho_0}(\rho - \rho_0)^2\right] + \nabla \cdot [\mathbf{u}(P - P_0)] = 0. \tag{2.52}$$

Naze Tjøtta and Tjøtta [18] give the nonlinear expression of energy conservation to third order as

$$\frac{\partial}{\partial t}\mathcal{E} + \nabla \cdot \mathcal{I} = -\mathcal{D}, \tag{2.53}$$

where

$$\begin{aligned}\mathcal{E} = {} & \rho_0 \frac{u^2}{2} + \frac{(P - P_0 + \mathcal{L})^2}{2\rho_0 c_0^2} + \frac{1}{3}\left(1 - \frac{B}{A}\right)\frac{(P - P_0)^3}{\rho_0^2 c_0^4} \\ & - \frac{\partial}{\partial t}\left[(\kappa + \frac{4}{3}\mu)\frac{u^2}{2c_0^2} + \frac{\gamma - 1}{\gamma} K \frac{(P - P_0)^2}{2\rho_0 c_0^4}\right], \end{aligned} \tag{2.54a}$$

$$\mathcal{I} = (P - P_0 + E)\mathbf{u} - \mu \mathbf{u} \times \nabla \times \mathbf{u}, \tag{2.54b}$$

$$\mathcal{D} = \frac{1}{c_0^2}(\kappa + \frac{4}{3}\mu)\left|\frac{\partial \mathbf{v}}{\partial t}\right|^2 + \frac{\gamma - 1}{\gamma}\frac{K}{\rho_0 c_0^4}\left(\frac{\partial p}{\partial t}\right)^2 + \mu |\nabla \times \mathbf{v}|^2, \tag{2.54c}$$

$$E = \frac{\rho_0 u^2}{2} + \frac{(P - P_0)^2}{2\rho_0 c_0^2}, \tag{2.54d}$$

where K, κ, and μ are the coeffiecients of thermal conductivity, bulk and shear viscosity, respectively, and $\mathcal{L} = \rho u^2/2 + p^2/2\rho c^2$ is the acoustic Lagrangian density. If dissipative terms are removed, zero mean flow is assumed and the third order quantities are neglected, then Eqs. (2.53) and (2.54) reduce to

$$\frac{\partial}{\partial t}\mathcal{E} + \nabla \cdot \mathcal{I} = 0, \tag{2.55}$$

where,

$$\mathcal{E} = \rho_0 \frac{u^2}{2} + \frac{(P - P_0)^2}{2\rho_0 c_0^2} = w, \tag{2.56a}$$

$$\mathcal{I} = (P - P_0)\mathbf{u} = \mathbf{I}_i \tag{2.56b}$$

which are equivalent to the energy equations derived here.

2.4 Lagrangian Formulation

The equations of motion in a Lagrangian frame may be obtained by means of a variational principle. This formulation permits commentary on which expression for the potential energy density is most appropriate. The linear acoustic equations of motion are obtained from a variational principle in [19]. Bennett includes a brief treatment of the method in his book *Lagrangian Fluid Dynamics* [20]. Eckart considers the motion of an adiabatic ideal gas [21], but the clearest development of the nonlinear equations of motion is presented by Seliger and Whitham [17].

Let the position of some fluid particle at time $t = 0$ be represented by $\boldsymbol{\alpha} = [\ \alpha_1\ \alpha_2\ \alpha_3\ ]^{\mathrm{T}}$. The position of the particle at time t is given by

$$\mathbf{x}(\boldsymbol{\alpha}, t) = \boldsymbol{\alpha} + \boldsymbol{\xi}(\boldsymbol{\alpha}, t), \tag{2.57}$$

where $\boldsymbol{\xi} = [\ \xi_1\ \xi_2\ \xi_3\ ]^{\mathrm{T}}$ is the vector of displacements. Throughout this section it will be convenient to use subscripts to denote vector components. The summation convention, where repeated indices indicate summation *e.g.*,

$$\sum_i x_i y_i = x_i y_i \tag{2.58}$$

will also be employed. The transformation from the initial time to the current time

is characterized by the Jacobian matrix

$$\mathbb{J} = \frac{\partial x_i}{\partial \alpha_j} = \begin{bmatrix} 1 + \frac{\partial \xi_1}{\partial \alpha_1} & \frac{\partial \xi_1}{\partial \alpha_2} & \frac{\partial \xi_1}{\partial \alpha_3} \\ \frac{\partial \xi_2}{\partial \alpha_1} & 1 + \frac{\partial \xi_2}{\partial \alpha_2} & \frac{\partial \xi_2}{\partial \alpha_3} \\ \frac{\partial \xi_3}{\partial a_1} & \frac{\partial \xi_3}{\partial a_2} & 1 + \frac{\partial \xi_3}{\partial a_3} \end{bmatrix}, \tag{2.59}$$

thus, the current density ρ is related to the initial density ρ_0 by the Jacobian determinant [17],

$$J = \frac{\partial(x_1, x_2, x_3)}{\partial(\alpha_1, \alpha_2, \alpha_3)} = \frac{\partial \mathbf{x}}{\partial \alpha_1} \cdot \frac{\partial \mathbf{x}}{\partial \alpha_2} \times \frac{\partial \mathbf{x}}{\partial \alpha_3} = \begin{vmatrix} 1 + \frac{\partial \xi_1}{\partial \alpha_1} & \frac{\partial \xi_1}{\partial \alpha_2} & \frac{\partial \xi_1}{\partial \alpha_3} \\ \frac{\partial \xi_2}{\partial \alpha_1} & 1 + \frac{\partial \xi_2}{\partial \alpha_2} & \frac{\partial \xi_2}{\partial \alpha_3} \\ \frac{\partial \xi_3}{\partial \alpha_1} & \frac{\partial \xi_3}{\partial \alpha_2} & 1 + \frac{\partial \xi_3}{\partial \alpha_3} \end{vmatrix}, \tag{2.60}$$

as

$$\rho = \frac{\rho_0}{J}. \tag{2.61}$$

Once the density has been determined, it may be used to determine the pressure via the adiabatic relation,

$$P = P_0 \left(\frac{\rho}{\rho_0} \right)^{\gamma} = \frac{P_0}{J^{\gamma}}. \tag{2.62}$$

Implicit in the use of this equation is that the entropy remains constant for a given particle. The velocity of a fluid particle is given by

$$u_i = \frac{\partial x_i}{\partial t} = \frac{\partial \xi_i}{\partial t}. \tag{2.63}$$

These quantities may be used to determine the equations of motion by means of a variational principle. For a conservative system in Lagrangian coordinates, the equations of motion may be found by satisfying the condition that the action, $\mathcal{S}$, defined as

$$\mathcal{S} = \int_t \int_V [\mathfrak{t} - \mathfrak{u}] dV dt, \tag{2.64}$$

be stationary. The Lagrangian coordinate differential volume $dV = dx_1 dx_2 dx_3$ may be related to the reference coordinate volume $dW = d\alpha_1 d\alpha_2 d\alpha_3$ by $dV = J dW$.

Substituting the results of Section 2.3 into Eq. (2.64) results in

$$\mathcal{S} = \int_t \int_V \rho \left[\frac{1}{2} \left(\frac{\partial x_i}{\partial t} \right)^2 - \frac{p}{\rho(\gamma - 1)} \right] dV dt. \tag{2.65}$$

Using the relations between the Lagrangian coordinates and the pressure, mass density, and particle velocity and making the transformation to the reference coordinate system yields

$$\mathcal{S} = \int_t \int_W \rho_0 \left[\frac{1}{2} \left(\frac{\partial x_i}{\partial t} \right)^2 - \frac{p_0}{\rho_0(\gamma - 1)} J^{1-\gamma} \right] dW dt. \tag{2.66}$$

The integrand is defined as the Lagrangian density $\mathcal{L}$. It may be shown [19] that the constraint on $\mathcal{S}$ is satisfied if

$$\frac{\partial}{\partial t} \left[\frac{\partial \mathcal{L}}{\partial \frac{\partial x_i}{\partial t}} \right] + \sum_{j=1}^{3} \frac{\partial}{\partial \alpha_j} \left[\frac{\partial \mathcal{L}}{\partial \frac{\partial x_i}{\partial \alpha_j}} \right] - \frac{\partial \mathcal{L}}{\partial x_i} = 0. \tag{2.67}$$

The Lagrangian density, $\mathcal{L}$, is depends on x_i only through derivatives, so

$$\frac{\partial}{\partial t} \left[\frac{\partial \mathcal{L}}{\partial \frac{\partial x_i}{\partial t}} \right] + \sum_{j=1}^{3} \frac{\partial}{\partial \alpha_j} \left[\frac{\partial \mathcal{L}}{\partial \frac{\partial x_i}{\partial \alpha_j}} \right] = 0. \tag{2.68}$$

Carrying out the appropriate derivatives [17] results in the equation of motion

$$\frac{\partial^2 x_i}{\partial t^2} = -\frac{1}{\rho_0} \frac{\partial J}{\partial \left(\frac{\partial x_i}{\partial \alpha_j} \right)} \frac{\partial P}{\partial \alpha_j}. \tag{2.69}$$

Substituting for P and defining $c_0 = \gamma P_0 / \rho_0$ produces

$$\frac{\partial^2 x_i}{\partial t^2} = c_0 J^{-\gamma - 1} \frac{\partial J}{\partial \left(\frac{\partial x_i}{\partial \alpha_j} \right)} \frac{\partial J}{\partial \alpha_j}. \tag{2.70}$$

For one dimension, $J = 1 + \partial \xi_1 / \partial \alpha_1$, and Eq. (2.70) becomes

$$\frac{\partial^2 \xi_1}{\partial t^2} = \frac{c_0}{\left(1 + \frac{\partial \xi_1}{\partial \alpha_1} \right)^{\gamma + 1}} \frac{\partial^2 \xi_1}{\partial \alpha_1^2}, \tag{2.71}$$

which is identical to the full non-dissipative nonlinear equation derived by Beyer [22].

This formulation enables a discussion of the three expressions derived for the potential energy density in Section 2.3. The three expressions are numbered as follows to facilitate discussion. The potential energy density referenced to the zero energy (vacuum) state is given by

$$\mathfrak{u}_1 = \frac{P}{\gamma - 1}, \tag{2.72}$$

the potential energy density referenced to the equilibrium energy per unit mass is

$$\mathfrak{u}_2 = \frac{P}{\gamma - 1} - \frac{\rho P_0}{\rho_0(\gamma - 1)}, \tag{2.73}$$

and the potential energy density referenced to the equilibrium energy per unit volume is

$$\mathfrak{u}_3 = \frac{P - P_0}{\gamma - 1}. \tag{2.74}$$

The first expression, $\mathfrak{u}_1$ is valid for all cases, but there is some ambiguity as to which of the remaining two is appropriate for acoustic energy density, that is, which expression is best for fluctuations about equilibrium. The Lagrangian formulation allows immediate comparison of the two. Upon substitution, it becomes apparent that $\mathfrak{u}_3$ does not produce the correct Lagrangian equations of motion. Thus, $\mathfrak{u}_2$ is the correct form for a Lagrangian description of acoustic processes. This does not mean that $\mathfrak{u}_3$ is inaccurate, rather, $\mathfrak{u}_3$ seems more suited to the control volume formulation of Eulerian fluid dynamics because it is referenced to the energy per volume which is a much more natural quantity in an Eulerian coordinate system. The lack of knowledge of an appropriate variational principle for an Eulerian field precludes investigation of this hypothesis; however, the paper by Scholle [23] may serve as a starting point for continued investigation. Thus, $\mathfrak{u}_2$ appears to be appropriate for a Lagrangian description of the fluid motion, while $\mathfrak{u}_3$ appears to be appropriate for an Eulerian description. For infinitesimal fluctuations, this question becomes inconsequential as the two conventions are equivalent.

Chapter 3

Techniques for Estimating Acoustic Intensity and Energy Density

3.1 Introduction

Calculation of the acoustic intensity and energy density at a point in space requires knowledge of both the pressure and the particle velocity at that point. The pressure is easily measured with a microphone or other appropriate sensor. However, direct measurement of the particle velocity is difficult and the equipment is often expensive, and in some cases very fragile. Consequently, alternate methods that exploit knowledge of the acoustical field have been devised to provide relatively low cost, durable probes. One technique that uses the differences between the pressures at multiple sensor locations to estimate particle velocity has been included in the ANSI standard on sound intensity measurements [24]. The finite-difference technique is presented here along with an alternate method that provides certain advantages over the finite-difference method.

Before discussing the various methods for estimating particle velocity from pres-

sure measurements, the relationship between pressure and particle velocity is discussed. The particle velocity may be related to the pressure using the linear Euler's equation,

$$\rho_0 \frac{\partial \mathbf{u}}{\partial t} = -\nabla p. \tag{3.1}$$

If the signal is time-harmonic and complex notation is used, or if the analysis is conducted in the frequency domain via the Fourier transform, then

$$\frac{\partial \mathbf{u}(\mathbf{r}, t)}{\partial t} = j\omega \mathbf{u}(\mathbf{r}, t), \tag{3.2}$$

or,

$$\frac{\partial \tilde{\mathbf{u}}(\mathbf{r}, \omega)}{\partial t} = j\omega \tilde{\mathbf{u}}(\mathbf{r}, \omega), \tag{3.3}$$

where $\tilde{\mathbf{u}} = \mathcal{F}\{\mathbf{u}\} = \int_{-\infty}^{\infty} \mathbf{u} e^{\jmath\omega t} dt$. In these cases, Eq. (3.1) becomes

$$\jmath\omega\rho_0 \mathbf{u} = -\nabla p, \tag{3.4}$$

or

$$\jmath\omega\rho_0 \tilde{\mathbf{u}} = -\nabla \tilde{p}. \tag{3.5}$$

An alternate method [25] uses the antiderivative to find that

$$\mathbf{u} = -\rho_0^{-1} \int_0^t \nabla p \, dt, \tag{3.6}$$

assuming that the system is initially at rest. All three of these methods for estimating the particle velocity require knowledge of the pressure gradient. The standard method for approximating the pressure gradient is known as the finite-difference method. Hereafter, all analysis will be conducted in the frequency domain and the tilde indicating the Fourier transform will be omitted.

3.2 Finite-Difference Method

In one dimension, the gradient of a pressure field may be easily estimated by taking the difference between two closely spaced sensors and dividing by the separation distance d to obtain

$$\frac{\partial p}{\partial x} \approx \frac{p_1 - p_2}{d}. \tag{3.7}$$

This necessitates the use of closely phase matched sensors, although the effect of slight phase mismatch for constant frequency decreases as the separation distance increases. The maximum separation distance is limited by the finite-difference approximation of the spatial derivative which requires that the separation distance be much less than a wavelength, λ. Fahy [12] suggests that the spacing should be less than 0.13λ to avoid errors greater than 5%. These requirements limit the frequency bandwidth for which this method can be used.

The finite-difference method can be extended up to three dimensions be using one pair of sensors along each coordinate axis for a total of six sensors. However, it is not necessary to use six sensors. Since three points in space uniquely define a plane, with three sensors it is always possible to find a plane that contains all three sensors. Although variation normal to this plane cannot be resolved by the triad of sensors, this problem is corrected by adding a fourth sensor that does not lie in the plane of the other three sensors. Using this fourth sensor, variations in any direction may be estimated.

Although numerous configurations of sensors may be used [26,27], only a tetrahedral configuration will be considered here. The methods presented are applicable to an array of microphones in arbitrary locations. The tetrahedral configuration consists of four sensors located at the vertices of a tetrahedron as shown in Fig. 3.1. In a spherical coordinate system with vertices a distance a from the origin, the azimuthal

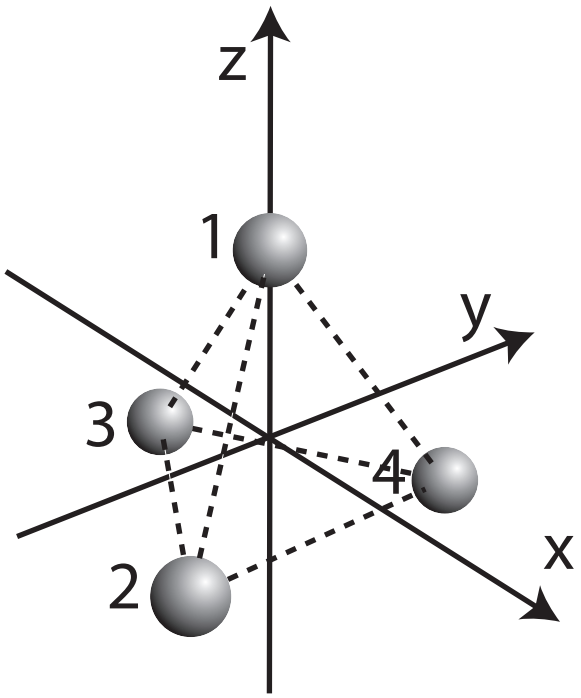

Figure 3.1 A tetrahedral sensor array. The sensors are placed at the vertices of a tetrahedron with a circumcircle of radius a. Sensor 1 lies on the z axis and sensors 2 and 4 are aligned with the y axis.

(ϕ_i) and polar (θ_i) angles for the i-th sensor are

$$\begin{aligned} \phi_1 &= 0, & \theta_1 &= 0, \\ \phi_2 &= \tfrac{5\pi}{3}, & \theta_2 &= \pi - \arccos\tfrac{1}{3}, \\ \phi_3 &= \pi, & \theta_3 &= \pi - \arccos\tfrac{1}{3}, \\ \phi_4 &= \tfrac{\pi}{3}, & \theta_4 &= \pi - \arccos\tfrac{1}{3}. \end{aligned}$$

Using these angles, the locations of the sensors may be specified in cartesian coordinates as

$$\mathbf{r}_1 = \begin{bmatrix} 0 \\ 0 \\ a \end{bmatrix}, \mathbf{r}_2 = \begin{bmatrix} \frac{a\sqrt{2}}{3} \\ -\frac{a\sqrt{6}}{3} \\ -\frac{a}{3} \end{bmatrix}, \mathbf{r}_3 = \begin{bmatrix} -\frac{2a\sqrt{2}}{3} \\ 0 \\ -\frac{a}{3} \end{bmatrix}, \text{ and } \mathbf{r}_4 = \begin{bmatrix} \frac{a\sqrt{2}}{3} \\ \frac{a\sqrt{6}}{3} \\ -\frac{a}{3} \end{bmatrix}. \tag{3.8}$$

There are certain difficulties associated with using four sensors if they are not aligned along the coordinate axes with one placed at the origin. In any alternate

configuration, the lines between sensors have projections on multiple axes and the gradient can no longer be estimated simply by taking the difference between pairs of sensors and dividing by the separation distance. Instead, the relative contribution by each pair to each component of the gradient must be calculated.

From a naive perspective, perhaps the most apparent method for calculating the contribution of each sensor pair to the estimated gradient is to take the the difference of the pressures measured at the sensors divided by the projection of the separation distance onto the appropriate coordinate axis and averaging the results. For four sensors located at $\mathbf{r}_1$, $\mathbf{r}_2$, $\mathbf{r}_3$, and $\mathbf{r}_4$, where $\mathbf{r}_i = [x_i \; y_i \; z_i]^{\mathrm{T}}$, this can be calculated systematically by defining the matrix $\mathbf{d_x}$ as

$$\mathbf{d_x} = \begin{bmatrix} d_{x11} & d_{x12} & d_{x13} & d_{x14} \\ d_{x21} & d_{x22} & d_{x23} & d_{x24} \\ d_{x31} & d_{x32} & d_{x33} & d_{x34} \\ d_{x41} & d_{x42} & d_{x43} & d_{x44} \end{bmatrix}, \tag{3.9}$$

where $d_{xij} = x_i - x_j$. Thus, $d_{xii} = 0$ and $d_{xij} = -d_{xji}$ so $\mathbf{d_x}$ is antisymmetric and $\mathrm{trace}(\mathbf{d_x}) = 0$. Defining similar matrices $\mathbf{d_y}$ and $\mathbf{d_z}$ in the same manner yields,

$$\mathbf{d_y} = \begin{bmatrix} d_{y11} & d_{y12} & d_{y13} & d_{y14} \\ d_{y21} & d_{y22} & d_{y23} & d_{y24} \\ d_{y31} & d_{y32} & d_{y33} & d_{y34} \\ d_{y41} & d_{y42} & d_{y43} & d_{y44} \end{bmatrix}, \tag{3.10}$$

$d_{yij} = y_i - y_j$, $d_{yii} = 0$, $d_{yij} = -d_{yji}$,

$$\mathbf{d_z} = \begin{bmatrix} d_{z11} & d_{z12} & d_{z13} & d_{z14} \\ d_{z21} & d_{z22} & d_{z23} & d_{z24} \\ d_{z31} & d_{z32} & d_{z33} & d_{z34} \\ d_{z41} & d_{z42} & d_{z43} & d_{z44} \end{bmatrix}, \tag{3.11}$$

$d_{zij} = z_i - z_j$, $d_{zii} = 0$, and $d_{zij} = -d_{zji}$. Next, the matrices $\mathbf{d}'_{\mathbf{x}}$, $\mathbf{d}'_{\mathbf{y}}$, and $\mathbf{d}'_{\mathbf{z}}$ are formed by inverting the nonzero elements of the corresponding $\mathbf{d}_\mu$ matrix. As an example, for nonzero elements of $\mathbf{d}_{\mathbf{x}}$, $d'_{xij} = 1/d_{xij}$. Using these matrices with the matrix $\mathbb{P}$, defined as

$$\mathbb{P} = \begin{bmatrix} p_1 & 0 & 0 & 0 \\ 0 & p_2 & 0 & 0 \\ 0 & 0 & p_3 & 0 \\ 0 & 0 & 0 & p_4 \end{bmatrix}, \tag{3.12}$$

a finite-difference operator, $\Delta_\mu(\cdot)$, may be defined as

$$\mathbf{\Delta}_\mu(\mathbb{P}) = \mathbf{d}'_\mu \mathbb{P} + (\mathbf{d}'_\mu \mathbb{P})^{\mathrm{T}}. \tag{3.13}$$

Because $\mathbb{P}$ is diagonal, and $\mathbf{d}'$ is antisymmetric, this operator may be written as

$$\mathbf{\Delta}_\mu(\mathbb{P}) = \mathbf{d}'_\mu \mathbb{P} - \mathbb{P}(\mathbf{d}'_\mu)^{\mathrm{T}}. \tag{3.14}$$

For the coordinate system defined in Eq. (3.8),

$$\mathbf{\Delta}_{\mathbf{x}}(\mathbb{P}) = \begin{bmatrix} 0 & \frac{p_2-p_1}{d_{x12}} & \frac{p_1-p_3}{d_{x13}} & \frac{p_4-p_1}{d_{x14}} \\ \frac{p_2-p_1}{d_{x12}} & 0 & \frac{p_2-p_3}{d_{x23}} & 0 \\ \frac{p_1-p_3}{d_{x13}} & \frac{p_2-p_3}{d_{x23}} & 0 & \frac{p_4-p_3}{d_{x34}} \\ \frac{p_4-p_1}{d_{x14}} & 0 & \frac{p_4-p_3}{d_{x34}} & 0 \end{bmatrix}, \tag{3.15}$$

$$\mathbf{\Delta}_{\mathbf{y}}(\mathbb{P}) = \begin{bmatrix} 0 & \frac{p_2-p_1}{d_{y12}} & 0 & \frac{p_4-p_1}{d_{y14}} \\ \frac{p_2-p_1}{d_{y12}} & 0 & \frac{p_3-p_2}{d_{y23}} & \frac{p_4-p_2}{d_{y24}} \\ 0 & \frac{p_3-p_2}{d_{y23}} & 0 & \frac{p_4-p_3}{d_{y34}} \\ \frac{p_4-p_1}{d_{y14}} & \frac{p_4-p_2}{d_{y24}} & \frac{p_4-p_3}{d_{y34}} & 0 \end{bmatrix}, \tag{3.16}$$

and

$$\mathbf{\Delta_z}(\mathbb{P}) = \begin{bmatrix} 0 & \frac{p_2-p_1}{d_{z12}} & \frac{p_3-p_1}{d_{z13}} & \frac{p_4-p_1}{d_{z14}} \\ \frac{p_2-p_1}{d_{z12}} & 0 & 0 & 0 \\ \frac{p_3-p_1}{d_{z13}} & 0 & 0 & 0 \\ \frac{p_4-p_1}{d_{z14}} & 0 & 0 & 0 \end{bmatrix}. \tag{3.17}$$

The components of these matrices are finite-difference approximations of the spatial derivatives of the field p along the chosen coordinate axes. The standard approximations for these derivatives may be found by averaging the components of the operator acting on the diagonal matrix of the measurement points. This average may be computed using

$$\frac{dp}{dx} \approx \frac{1}{N}\sum_{i,j}[\mathbf{\Delta_x}(\mathbb{P})]_{ij} = \frac{1}{N}\mathbf{i}^{\mathrm{T}}\mathbf{\Delta_x}(\mathbb{P})\mathbf{i}, \tag{3.18}$$

where N is the number of nonzero components in $\mathbf{\Delta_x}(\mathbb{P})$, and $\mathbf{i}$ is a column vector of ones. For a tetrahedral probe with microphones placed at a radial distance, a, from a common origin as defined in Eq. (3.8), the gradient is approximately

$$\nabla p \approx \begin{bmatrix} \frac{1}{N}\mathbf{i}^{\mathrm{T}}\mathbf{\Delta_x}(\mathbb{P})\mathbf{i} \\ \frac{1}{N}\mathbf{i}^{\mathrm{T}}\mathbf{\Delta_y}(\mathbb{P})\mathbf{i} \\ \frac{1}{N}\mathbf{i}^{\mathrm{T}}\mathbf{\Delta_z}(\mathbb{P})\mathbf{i} \end{bmatrix} = \frac{1}{4a}\begin{bmatrix} \frac{\sqrt{2}}{5}(-9p_1+8p_2-7p_3+8p_4) \\ \sqrt{6}(p_4-p_2) \\ 3p_1-p_2-p_3-p_4 \end{bmatrix} \tag{3.19}$$

A careful examination of the x term reveals that this expression cannot be correct as it predicts variation in the x direction in the presence of a field that varies only in the z direction. The reason for this is not clear unless the sums are analyzed term by term. It then becomes apparent that due to the symmetries of the configuration in the y-direction, the contributions of all of the sensor pairs cancel except for sensors 2 and 4 which lie along the y-axis. In the x-direction, this symmetry does not exist, and consequently, the other pairs do not cancel. If all of the sensors lie in the same plane then this won't cause any problems, however, since the sensors lie outside of the x-y plane, there are potential phase differences between the sensors that are not

accounted for. These phase differences cause errors in the gradient estimate for certain directions.

A more correct finite-difference estimate may be obtained from the assumption that the sensors are located such that the spatial variation in the field is small over the volume occupied by the probe. This is technically identical to the method used by Pascal and Li [27] although their method varies slightly in certain details. In this case, the gradient of the field may be approximately related to the pressure difference between any sensor pair by

$$\mathbf{r}'_{ij} \cdot \nabla p = {\mathbf{r}'_{ij}}^{\mathrm{T}} \nabla p \approx p_j - p_i, \tag{3.20}$$

where $\mathbf{r}'_{ij} = [r_{jx} - r_{ix}\ r_{jy} - r_{iy}\ r_{jz} - r_{iz}]^{\mathrm{T}} = \mathbf{r}_j - \mathbf{r}_i$. If $\mathbf{\Delta p} = [\ p_2 - p_1\ \cdots\ p_n - p_{n-1}\ ]^{\mathrm{T}}$, and $\mathbb{X} = [\ \mathbf{r}'_{12}\ \mid\ \mathbf{r}'_{13}\ \cdots\ \mid\ \mathbf{r}'_{n-1,n}\ ]^{\mathrm{T}}$ is an $N \times 3$ matrix, n is the number of sensors and $N = n(n-1)/2$ is the number of sensor pairs, then

$$\mathbb{X} \nabla p = \mathbf{\Delta p} + \boldsymbol{\epsilon}_{\nabla p}, \tag{3.21}$$

where $\boldsymbol{\epsilon}_{\Delta p}$ represents the error in the estimate. By minimizing the squared error, the least-squares estimate of the gradient is

$$\nabla p \approx (\mathbb{X}^{\mathrm{T}} \mathbb{X})^{-1} \mathbb{X}^{\mathrm{T}} \mathbf{\Delta p}. \tag{3.22}$$

This is a finite-difference, least-squares estimate of the gradient of the field p. The matrix $(\mathbb{X}^{\mathrm{T}}\mathbb{X})^{-1}\mathbb{X}^{\mathrm{T}}$ is a left inverse [28, 29] of $\mathbb{X}$, and may be calculated as long as the columns of $\mathbb{X}$ are linearly independent. This requirement is guaranteed to be satisfied as long as the number of sensors used is greater than the number of measurement dimensions (three dimensions, four sensors minimum). The errors associated with this approximation will be discussed in section 4.1.1. For the tetrahedral probe considered

previously, the gradient approximation is

$$\nabla p \approx \frac{1}{4a} \begin{bmatrix} \sqrt{2}(p_2 - 2p_3 + p_4) \\ \sqrt{6}(-p_2 + p_4) \\ 3p_1 - p_2 - p_3 - p_4 \end{bmatrix}. \tag{3.23}$$

The y and z components are identical to the those obtained by averaging the individual contributions of sensor pairs, but the x component is very different. It can be shown that for a variation along the y or z axis, this method predicts no variation in the x direction, as opposed to the erroneous prediction of the averaging method. Consequently, this method appears to be the best available solution.

This approximation of the gradient may be used to estimate the acoustic intensity. Substituting Eq. (3.23) into Eq. (3.5), the velocity $\mathbf{u}$ is

$$\mathbf{u} = \frac{\jmath}{\rho_0 \omega} \nabla p \approx \frac{\jmath}{4a\rho_0\omega} \begin{bmatrix} \sqrt{2}(p_2 - 2p_3 + p_4) \\ \sqrt{6}(-p_2 + p_4) \\ 3p_1 - p_2 - p_3 - p_4 \end{bmatrix} \tag{3.24}$$

From Eq. (2.11), the time-averaged intensity vector, $\mathbf{I}$ is

$$\mathbf{I} = \frac{1}{2}\mathrm{Re}\{p\mathbf{u}^*\}. \tag{3.25}$$

For the finite-difference case, the pressure p is the Fourier transform of the pressure at the acoustical center of the probe, which is approximated as the average of the pressure measured at the four sensor locations

$$p \approx \frac{p_1 + p_2 + p_3 + p_4}{4}. \tag{3.26}$$

Defining the single-sided cross-spectrum as

$$G_{ij} = 2\left[p_i^* p_j\right]_{\omega=0\ldots\infty}, \tag{3.27}$$

and substituting the estimated values for $\mathbf{u}$ and p, the time-averaged intensity is

$$\mathbf{I} \approx \frac{1}{32\rho\omega a} \begin{bmatrix} \sqrt{2}\ \mathrm{Im}\{-G_{12} + 2G_{13} - G_{14} + 3G_{23} - 3G_{34}\} \\ \sqrt{6}\ \mathrm{Im}\{G_{12} - G_{14} - G_{23} - 2G_{24} - G_{34}\} \\ 4\ \mathrm{Im}\{G_{12} + G_{13} + G_{14}\} \end{bmatrix}. \tag{3.28}$$

These expressions agree with those presented without derivation by Hori [30].

3.3 Wave Vector Method

The finite-difference method suffers from frequency-dependent estimate bias which results from both averaging and the finite-difference approximation. In spite of this limitation, it can be used with virtually no knowledge of the field to estimate both the active and reactive intensity. If certain conditions are met, then our knowledge of wave propagation may be used to more elegantly and accurately estimate the particle velocity. If the measurement location is in the acoustic far field, then the velocity and intensity may be estimated by assuming that the wavefront is approximately planar over the volume of the sphere, and that the wave is described locally by $p = p_0 e^{-\jmath \mathbf{k}\cdot\mathbf{r}}$. In this case, the direction of propagation may be estimated by comparing the relative phase of the sensors in the probe.

Consider a probe consisting of four sensors, with sensors 1, 2, 3, and 4 located at $\mathbf{r}_1$, $\mathbf{r}_2$, $\mathbf{r}_3$, and $\mathbf{r}_4$, respectively. This probe may be used to estimate the wave vector of a pressure field. It is useful to shift the coordinate system temporarily so that one of the sensors lies at the origin. Choosing to place sensor 1 at the origin results in

the shifted coordinate system, $\mathbf{r}'$. The shifted sensor positions are given by

$$\mathbf{r}'_{11} = \mathbf{r}_1 - \mathbf{r}_1, \tag{3.29a}$$

$$\mathbf{r}'_{12} = \mathbf{r}_2 - \mathbf{r}_1, \tag{3.29b}$$

$$\mathbf{r}'_{13} = \mathbf{r}_3 - \mathbf{r}_1, \tag{3.29c}$$

$$\mathbf{r}'_{14} = \mathbf{r}_4 - \mathbf{r}_1. \tag{3.29d}$$

Observe that the pressure measured at each of the sensors is given by

$$p_1 = |p(\mathbf{r}_1)|\, e^{\jmath\varphi_1}, \quad p_2 = |p(\mathbf{r}_2)|\, e^{\jmath\varphi_2}, \quad p_3 = |p(\mathbf{r}_3)|\, e^{\jmath\varphi_3}, \quad \text{and} \quad p_4 = |p(\mathbf{r}_4)|\, e^{\jmath\varphi_4}. \tag{3.30}$$

The phases of the pressures measured at sensors 2-4 relative to the pressure at sensor 1 may be found from the transfer functions,

$$H_{ij} = \frac{p_j}{p_i} = \frac{|p_j|}{|p_i|} e^{\jmath\varphi_{ij}}. \tag{3.31}$$

The phases of the sensors relative to sensor 1 are given by

$$\varphi_{11} = \arg(H_{11}) = 0, \tag{3.32a}$$

$$\varphi_{12} = \arg(H_{12}), \tag{3.32b}$$

$$\varphi_{13} = \arg(H_{13}), \tag{3.32c}$$

$$\varphi_{14} = \arg(H_{14}). \tag{3.32d}$$

For a plane wave, the spatial phase shift of any point relative to the origin is

$$\varphi = -\mathbf{k} \cdot \mathbf{r}. \tag{3.33}$$

Combining Eq. (3.32) and (3.33) provides a system of three equations relating the transfer functions to the wave vector $\mathbf{k}$

$$-\mathbf{k} \cdot \mathbf{r}'_{12} = \arg(H_{12}) = \varphi_{12}, \tag{3.34a}$$

$$-\mathbf{k} \cdot \mathbf{r}'_{13} = \arg(H_{13}) = \varphi_{13}, \tag{3.34b}$$

$$-\mathbf{k} \cdot \mathbf{r}'_{14} = \arg(H_{14}) = \varphi_{14}. \tag{3.34c}$$

If the pressure field is not planar, these equations are approximate. The error remains small except in fields dominated by the reactive pressure. These equations may be written in matrix form as

$$-\mathbb{X}_1\mathbf{k} = \boldsymbol{\varphi}_1, \tag{3.35}$$

where $\mathbf{k}$ is the wave vector, $\mathbb{X}_1 = \left[\ \mathbf{r}'_{12} \,\middle|\, \mathbf{r}'_{13} \,\middle|\, \mathbf{r}'_{14}\ \right]^{\mathrm{T}}$, and $\boldsymbol{\varphi}_1 = \left[\arg(H_{12}) \quad \arg(H_{13}) \quad \arg(H_{14})\right]^{\mathrm{T}}$. The wave vector $\mathbf{k}$ normal to the surface of constant phase may be estimated if the $\mathbf{r}_i$ are chosen so that $\mathbb{X}_1$ is invertible, in which case,

$$\mathbf{k}' = -\mathbb{X}_1^{-1}\boldsymbol{\varphi}_1. \tag{3.36}$$

This is the wave vector calculated relative to sensor 1, hereafter referred to as $\mathbf{k}'_1$. The same calculation may be carried out with any other sensor lying at the origin. The requirement that $\mathbb{X}_1$ be invertible is equivalent to requiring that the vectors $\mathbf{r}'_i$ contain orthogonal components, or in other words, that the vectors $\mathbf{r}'_{1i}$ form a three-dimensional basis.

Once the wave vector has been estimated, it can be related to the particle velocity by

$$\mathbf{u} = \frac{\mathbf{k}}{\rho_0\omega}e^{-\jmath\mathbf{k}\cdot\mathbf{r}}. \tag{3.37}$$

Following the assumption that the wavefronts are locally planar and taking the gradient of the plane wave pressure field analytically, Eq. (3.5) becomes Eq. (3.37). It is also possible to use the relation $|\mathbf{k}'| = k' = \omega/c_{ph}$, where c_{ph} is the phase speed, to express Eq. (3.37) as

$$\mathbf{u} = \frac{\mathbf{k}'}{|\mathbf{k}'|}\frac{e^{-\jmath\mathbf{k}'\cdot\mathbf{r}}}{\rho_0 c_{ph}}. \tag{3.38}$$

Special care must be taken when using this form of the equation because it uses the phase speed of the wave front, not the thermodynamic sound speed. Thus, it is only valid in regions where the two are approximately equal. The phase speed may be

calculated from the estimated vector $\mathbf{k}'$ as

$$c_{ph} = \frac{|\mathbf{k}'|}{\omega}. \tag{3.39}$$

Comparing the calculated phase speed with the thermodynamic sound speed may serve as a check of whether or not the necessary assumptions are valid.

It is also possible to use all of the inter-sensor transfer functions simultaneously to find a least-squares estimate of the wave vector. This is mathematically equivalent to estimating the wave vectors relative to each sensor and averaging the result to obtain

$$\mathbf{k}'_{ave} = \sum_{m=1}^{n} \frac{\mathbf{k}'_m}{n}. \tag{3.40}$$

This is accomplished by defining the matrix

$$\mathbb{X} = \left[\mathbb{X}_1^{\mathrm{T}} \mid \mathbb{X}_2^{\mathrm{T}} \mid \cdots \mid \mathbb{X}_n^{\mathrm{T}}\right]^{\mathrm{T}} = \left[\mathbf{r}'_{12} \mid \mathbf{r}'_{13} \mid \cdots \mid \mathbf{r}'_{n-1,n}\right], \tag{3.41}$$

and the vector

$$\boldsymbol{\varphi} = \left[\varphi_{12} \mid \varphi_{13} \mid \cdots \mid \varphi_{n-1,n}\right]^{\mathrm{T}} = \left[\arg(H_{12}) \mid \arg(H_{13}) \mid \cdots \mid \arg(H_{n-1,n})\right]^{\mathrm{T}}. \tag{3.42}$$

These quantities may be used to estimate $\mathbf{k}_{ls}$ using the full form of (3.35),

$$-\mathbb{X}\mathbf{k}'_{ls} = \boldsymbol{\varphi}. \tag{3.43}$$

The least-squares solution is

$$\mathbf{k}'_{ls} = -(\mathbb{X}^{\mathrm{T}}\mathbb{X})^{-1}\mathbb{X}^{\mathrm{T}}\boldsymbol{\varphi} = -\mathbb{C}_r^{-1}\mathbb{X}^{\mathrm{T}}\boldsymbol{\varphi}, \tag{3.44}$$

where $\mathbb{C}_r$ is the covariance matrix of inter-sensor separation distances.

The separation distance of the sensors provides an upper limit on the estimable wave number. The phase between two sensors in a given direction may only be accurately determined if the sensors are separated by less than half of a wavelength, consequently,

$$|\mathbf{k}| < \min_i \frac{2\pi}{|\mathbf{r}_{i\nu} - \mathbf{r}_{j\nu}|}, \tag{3.45}$$

where ν represents the appropriate cartesian coordinate. This limit is directly analogous to the Nyquist frequency. There is a different minimum frequency for each direction, however, a conservative estimate may be obtained by using the maximum sensor to sensor distance. Because the wave vector method directly uses the phase to estimate the wave vector in the frequency domain, in certain cases it is possible to extend the method to frequencies *above* the Nyquist limit. If there is sufficient frequency content in the signal to accurately unwrap the phase, *e.g.* a broadband signal such as the sound field of a jet or rocket field, then the method may potentially be used beyond the Nyquist limit.

The wave vector calculated using this method is the normal vector of a surface of constant phase. The geometry of the surfaces of constant phase (planar, cylindrical, spherical, or other) may be determined by appropriate placement of multiple probes and using the wave vectors to determine the principal curvatures of the surfaces of constant phase. It may be possible in certain cases to use multiple probes to estimate the source location by triangulation.

For the tetrahedral probe depict in Fig. 3.1, the sensors are located at

$$\mathbf{r}_1 = \begin{bmatrix} 0 \\ 0 \\ a \end{bmatrix}, \mathbf{r}_2 = \begin{bmatrix} \frac{a\sqrt{2}}{3} \\ -\frac{a\sqrt{6}}{3} \\ -\frac{a}{3} \end{bmatrix}, \mathbf{r}_3 = \begin{bmatrix} -\frac{2a\sqrt{2}}{3} \\ 0 \\ -\frac{a}{3} \end{bmatrix}, \text{ and } \mathbf{r}_4 = \begin{bmatrix} \frac{a\sqrt{2}}{3} \\ \frac{a\sqrt{6}}{3} \\ -\frac{a}{3} \end{bmatrix}, \tag{3.46}$$

where a is the radial distance of the sensors from the origin. By shifting the coordinate system so that sensor 1 lies at the origin,

$$\mathbf{r}'_1 = \begin{bmatrix} 0 \\ 0 \\ 0 \end{bmatrix}, \mathbf{r}'_2 = \begin{bmatrix} \frac{a\sqrt{2}}{3} \\ -\frac{a\sqrt{6}}{3} \\ -\frac{4a}{3} \end{bmatrix}, \mathbf{r}'_3 = \begin{bmatrix} -\frac{2a\sqrt{2}}{3} \\ 0 \\ -\frac{4a}{3} \end{bmatrix}, \text{ and } \mathbf{r}'_4 = \begin{bmatrix} \frac{a\sqrt{2}}{3} \\ \frac{a\sqrt{6}}{3} \\ -\frac{4a}{3} \end{bmatrix}. \tag{3.47}$$

Form the matrix

$$\mathbb{X}_1 = \begin{bmatrix} \frac{a\sqrt{2}}{3} & -\frac{a\sqrt{6}}{3} & -\frac{4a}{3} \\ -\frac{2a\sqrt{2}}{3} & 0 & -\frac{4a}{3} \\ \frac{a\sqrt{2}}{3} & \frac{a\sqrt{6}}{3} & -\frac{4a}{3} \end{bmatrix}, \tag{3.48}$$

and calculate the inverse

$$\mathbb{X}_1^{-1} = \begin{bmatrix} \frac{\sqrt{2}}{4a} & -\frac{\sqrt{2}}{2a} & \frac{\sqrt{2}}{4a} \\ -\frac{\sqrt{6}}{4a} & 0 & \frac{\sqrt{6}}{4a} \\ -\frac{1}{4a} & -\frac{1}{4a} & -\frac{1}{4a} \end{bmatrix}. \tag{3.49}$$

Thus,

$$\mathbf{k}_1' = \begin{bmatrix} k_{x1}' \\ k_{y1}' \\ k_{z1}' \end{bmatrix} = \frac{\sqrt{2}}{4a} \begin{bmatrix} -\arg(H_{12}) + 2\arg(H_{13}) - \arg(H_{14}) \\ \sqrt{3}\arg(H_{12}) - \sqrt{3}\arg(H_{14}) \\ \frac{1}{\sqrt{2}}\arg(H_{12}) + \frac{1}{\sqrt{2}}\arg(H_{13}) + \frac{1}{\sqrt{2}}\arg(H_{14}) \end{bmatrix}. \tag{3.50}$$

The least-squares estimate of the wave vector may be calculated as

$$\mathbf{k}_{ls}' = \frac{1}{16a} \begin{bmatrix} \sqrt{2}\left(-\arg(H_{12}) + 2\arg(H_{13}) - \arg H_{14}\right) + 3\arg(H_{23}) - 3\arg(H_{34})) \\ \sqrt{6}\left(\arg(H_{12}) - \arg(H_{14}) - \arg(H_{23}) - 2\arg(H_{24}) - \arg(H_{34})\right) \\ 4\left(\arg(H_{12}) + \arg(H_{13}) + \arg(H_{14})\right) \end{bmatrix} \tag{3.51}$$

For a tetrahedral probe, the sensors are equidistant and the separation distance is

$$|\mathbf{r}_i - \mathbf{r}_j| = \frac{2a\sqrt{6}}{3}. \tag{3.52}$$

Hence the lowest Nyquist frequency for the probe is

$$f_{max} = \frac{c}{2\frac{2a\sqrt{6}}{3}} = \frac{3c}{4a\sqrt{6}}. \tag{3.53}$$

For a probe with a $1/2''$ radius, $f_{max} = 8402$ Hz. The smallest separation distance for a coordinate axis is along the x-axis, where sensors 2 and 4 are separated from sensor 3 by a distance $a\sqrt{2}$. The highest Nyquist frequency for a tetrahedron is 9701 Hz.

3.4 Spherical Harmonic Method

If the sensors are located on the surface of a sphere, then the symmetry of the probe provides an alternate means for estimating the wave vector. The pressure produced by an incident plane wave of amplitude p_0 on the surface of a rigid sphere is given by

$$p\mid_{r=a} = p_0 \sum_{n'=0}^{\infty} (-\jmath)^{n'}(2n'+1)\left[j_{n'}(ka) - \frac{j'_n(ka)}{h^{(2)\prime}_{n'}(ka)} h^{(2)}_{n'}(ka)\right] \sum_{m=-n'}^{n'} Y^m_{n'}(\hat{\mathbf{r}})[Y^m_{n'}(\hat{\mathbf{k}})]^*, \tag{3.54}$$

where $\hat{\mathbf{r}}$ and $\hat{\mathbf{k}}$ represent the angular position and direction of wave propagation respectively [31]. The pressure at the position of the i-th sensor, p_i is

$$p_i = p_0 \sum_{n'=0}^{\infty} (-\jmath)^{n'}(2n'+1)\left[j_{n'}(ka) - \frac{j_{n'}(ka)}{h^{(2)\prime}_{n'}(ka)} h^{(2)}_{n'}(ka)\right] \sum_{m=-n'}^{n'} Y^m_{n'}(\hat{\mathbf{r}}_i)[Y^m_{n'}(\hat{\mathbf{k}})]^*. \tag{3.55}$$

Let the vector $\mathbf{p}$ be defined as $\mathbf{p} = [p_1\ p_2\ \ldots\ p_n]$, where n is the number of sensors. The summation in Eq. (3.55) may be related to $\mathbf{p}$. First, define the matrix of spherical harmonics and spherical Bessel functions at the sensor locations as

$$\mathbb{H} = \begin{bmatrix} a_0 Y^0_0(\hat{\mathbf{r}}_1) & a_1 Y^{-1}_1(\hat{\mathbf{r}}_1) & a_1 Y^0_1(\hat{\mathbf{r}}_1) & a_1 Y^1_1(\hat{\mathbf{r}}_1) & \cdots \\ a_0 Y^0_0(\hat{\mathbf{r}}_2) & a_1 Y^{-1}_1(\hat{\mathbf{r}}_2) & a_1 Y^0_1(\hat{\mathbf{r}}_2) & a_1 Y^1_1(\hat{\mathbf{r}}_2) & \cdots \\ & & \vdots & & \\ a_0(ka) Y^0_0(\hat{\mathbf{r}}_n) & a_1 Y^{-1}_1(\hat{\mathbf{r}}_n) & a_1 Y^0_1(\hat{\mathbf{r}}_n) & a_1 Y^1_1(\hat{\mathbf{r}}_n) & \cdots \end{bmatrix}, \tag{3.56}$$

where,

$$a_{n'} = (-\jmath)^{n'}(2n'+1) j_{n'}(ka) - \frac{j'_{n'}(ka)}{h^{(2)\prime}_{n'}(ka)} h^{(2)}_{n'}(ka). \tag{3.57}$$

Then, define the vector $\mathbf{Y}_k$ as

$$\mathbf{Y}_k = \begin{bmatrix} Y^0_0(\hat{\mathbf{k}}) & Y^{-1}_1(\hat{\mathbf{k}}) & Y^0_1(\hat{\mathbf{k}}) & Y^1_1(\hat{\mathbf{k}}) & \cdots \end{bmatrix}. \tag{3.58}$$

The vector $\mathbf{p}$ is thus,

$$\mathbf{p} = p_0 \mathbb{H} \mathbf{Y}^{\mathrm{H}}_k. \tag{3.59}$$

$\mathbb{H}$ is an $n \times \infty$ matrix and $\mathbf{Y}_k$ is an infinitely long vector. For most well-behaved cases, both may be truncated. The number of terms that must be kept depends on the maximum ka value desired. If the summation in Eq. (3.55) were truncated after M terms, then $\mathbb{H}$ would be an $n \times (M+1)^2$ matrix and $\mathbf{Y}_k$ would have $(M+1)^2$ elements. The elements of $\mathbb{H}$ are calculated from known quantities, but the vector $\mathbf{Y}_k$ and the constant p_0 contain the amplitude and direction of the incident wave which are the quantities to be estimated. The product of p_0 and $\mathbf{Y}_k$ may be estimated from the vector of pressure amplitudes and the truncated matrix $\mathbb{H}$ as

$$p_0 \mathbf{Y}_k^{\mathrm{H}} = (\mathbb{H}^{\mathrm{H}}\mathbb{H})^{-1}\mathbb{H}^{\mathrm{H}}\mathbf{p}. \tag{3.60}$$

Because this calculation is carried out numerically, care must be taken when inverting the matrix $\mathbb{H}^{\mathrm{H}}\mathbb{H}$ to avoid numerical error.

Once the product $p_0\mathbf{Y}_k$ has been calculated, the wave amplitude p_0 and the direction of propagation may be found using the definition of the spherical harmonics and an identity. The spherical harmonics are defined as

$$Y_n^m(\hat{\mathbf{k}}) = \sqrt{\frac{2n+1}{4\pi}\frac{(n-m)!}{(n+m)!}} P_n^m(\cos\theta_k) e^{\jmath m\phi_k}, \tag{3.61}$$

hence, $Y_0^0(\hat{\mathbf{k}}) = 1/\sqrt{4\pi}$. Thus, the approximate amplitude, $\hat{p}_0$, of the incoming wave may be calculated by multiplying the first element of the vector $(\mathbb{H}^{\mathrm{H}}\mathbb{H})^{-1}\mathbb{H}^{\mathrm{H}}\mathbf{p}$ by $\sqrt{4\pi}$,

$$\hat{p}_0 = \sqrt{4\pi}[(\mathbb{H}^{\mathrm{H}}\mathbb{H})^{-1}\mathbb{H}^{\mathrm{H}}\mathbf{p}]_1. \tag{3.62}$$

The expression inside of the brackets is a vector, so the subscript serves to index the elements of the vector. This is an estimate of amplitude of the incident wave *without* the presence of the sphere. Once the amplitude of the incident wave has been approximated, the direction of the wave vector may be determined using the identity

$$\frac{2n+1}{4\pi} P_n(\hat{\mathbf{x}}\cdot\hat{\mathbf{y}}) = \sum_{m=-n}^{n} Y_n^m(\hat{\mathbf{x}})\,[Y_n^m(\hat{\mathbf{y}})]^*. \tag{3.63}$$

This may be expressed using the vector notation by first defining

$$\mathbf{Y}_{ri} = \begin{bmatrix} Y_0^0(\hat{\mathbf{r}}_i) & Y_1^{-1}(\hat{\mathbf{r}}_i) & Y_1^0(\hat{\mathbf{r}}_i) & Y_1^1(\hat{\mathbf{r}}_i) & \cdots \end{bmatrix}, \tag{3.64}$$

so that,

$$P_n(\hat{\mathbf{k}} \cdot \hat{\mathbf{r}}) = \frac{4\pi}{2n+1} \left[\mathbf{Y}_{ri}\right]_{(n+1)^2-2n\ldots(n+1)^2} \left[\mathbf{Y}_k^{\mathrm{H}}\right]_{(n+1)^2-2n\ldots(n+1)^2}. \tag{3.65}$$

It is possible to determine the direction of propagation using just the second through fourth entries of the vectors $\mathbf{Y}_k$ and $\mathbf{Y}_{ri}$ by recalling the definition of the first order Legendre polynomial, $P_1(x) = x$, thus,

$$\hat{\mathbf{k}} \cdot \hat{\mathbf{r}}_i = \arccos\left(\frac{4\pi}{3} \left[\mathbf{Y}_{ri}\right]_{2\ldots4} \left[\mathbf{Y}_k^{\mathrm{H}}\right]_{2\ldots4}\right). \tag{3.66}$$

Thus, a system of equations for $\hat{\mathbf{k}}$ may be written in matrix form as

$$\hat{\mathbb{X}}\hat{\mathbf{k}} = \mathbf{c}, \tag{3.67}$$

where

$$\hat{\mathbb{X}} = \begin{bmatrix} \hat{\mathbf{r}}_1 & \hat{\mathbf{r}}_2 & \cdots & \hat{\mathbf{r}}_n \end{bmatrix}^{\mathrm{T}} \tag{3.68}$$

is the matrix of unit sensor position vectors, and

$$\mathbf{c} = \begin{bmatrix} \arccos\left(\frac{4\pi}{3} \left[\mathbf{Y}_{r1}\right]_{2\ldots4} \left[\mathbf{Y}_k^{\mathrm{H}}\right]_{2\ldots4}\right) \\ \arccos\left(\frac{4\pi}{3} \left[\mathbf{Y}_{r2}\right]_{2\ldots4} \left[\mathbf{Y}_k^{\mathrm{H}}\right]_{2\ldots4}\right) \\ \vdots \\ \arccos\left(\frac{4\pi}{3} \left[\mathbf{Y}_{rn}\right]_{2\ldots4} \left[\mathbf{Y}_k^{\mathrm{H}}\right]_{2\ldots4}\right) \end{bmatrix}. \tag{3.69}$$

The unit vector $\hat{\mathbf{k}}$ is given approximately as

$$\hat{\mathbf{k}} = (\hat{\mathbb{X}}^{\mathrm{T}}\hat{\mathbb{X}})^{-1}\hat{\mathbb{X}}^{\mathrm{T}}\mathbf{c}. \tag{3.70}$$

The magnitude of the wave vector is given by the relation $k = \omega/c$, so

$$\mathbf{k} = \frac{\omega}{c}\hat{\mathbf{k}}. \tag{3.71}$$

Once the wave vector has been determined, the particle velocity and the intensity may be calculated using Eqs. (3.37) and (2.11).

Chapter 4

Comparison of Intensity Estimation Techniques

The methods presented in Chapter 3 for estimating the particle velocity are of little use without knowledge of their limitations and the accuracy of their results. It is necessary to know the effect of sensor phase mismatch and signal noise. If the probe consists of sensors mounted on the surface of a sphere, and the scattering is not included in the calculations as it is for the spherical harmonic method, it is necessary to determine the effect that scattering from the sphere has on the estimated quantities.

4.1 Estimate Confidence

4.1.1 Finite-Difference Method Estimate Confidence

Throughout this chapter, $E\{\cdot\}$ will be used to represent the expected value. In order to determine reasonable confidence bounds for the estimators presented in Chapter 3, assume that the errors in the signals are uncorrelated. If this is true, then the

covariance matrix, defined as

$$\mathbb{C}_{\Delta p} = E\{(\mathbf{\Delta p} - \mathbf{\Delta p}_0)(\mathbf{\Delta p} - \mathbf{\Delta p}_0)^{\mathrm{H}}\}, \tag{4.1}$$

where $\mathbf{\Delta p}_0 = E\{\begin{bmatrix} p_2 - p_1 & p_3 - p_1 & \cdots & p_N - p_{N-1} \end{bmatrix}^{\mathrm{T}}\}$is the mean of the pressure differences, reduces to $\mathbb{C}_{\Delta p} = \sigma^2_{\Delta p}\mathbb{I}$, where $\sigma^2_{\Delta p}$ is the variance. It is necessary to estimate the variance from the data as [32, 33]

$$\sigma^2_{\Delta p} = \frac{\mathbf{\Delta p}^{\mathrm{H}}(\mathbb{I} - \mathbb{R})\mathbf{\Delta p}}{N - r} \tag{4.2}$$

where $\mathbb{I}$ is the identity matrix, $\mathbb{R} = \mathbb{X}(\mathbb{X}^{\mathrm{T}}\mathbb{X})^{-1}\mathbb{X}^{\mathrm{T}}$, N is the number of sensor pairs, and r is the rank of the matrix $\mathbb{R}$. The pressures may be modeled as being normally distributed about the mean $\mathbf{\Delta p}_0$ with a probability density function f given as

$$f(\mathbf{\Delta p}) = \frac{1}{(2\pi)^{\frac{N}{2}}\left|\mathbb{C}_{\Delta p}\right|^{\frac{1}{2}}} \exp\left[-\frac{1}{2}\left[(\mathbf{\Delta p}^{\mathrm{H}} - \mathbf{\Delta p}_0^{\mathrm{H}})\mathbb{C}^{-1}_{\Delta p}(\mathbf{\Delta p} - \mathbf{\Delta p}_0)\right]\right]. \tag{4.3}$$

For uncorrelated signal noise,

$$f(\mathbf{\Delta p}) = \frac{1}{(2\pi\sigma^2_{\Delta p})^{\frac{N}{2}}} \exp\left[-\frac{1}{2\sigma^2_{\Delta p}}\left[(\mathbf{\Delta p}^{\mathrm{H}} - \mathbf{\Delta p}_0^{\mathrm{H}})\mathbb{I}(\mathbf{\Delta p} - \mathbf{\Delta p}_0)\right]\right]. \tag{4.4}$$

It is possible to define a probability density function for the estimated gradient by recalling that

$$\mathbf{\Delta p} = \mathbb{X}\nabla p. \tag{4.5}$$

Thus, after defining a vector $\overline{\nabla p} = \mathbb{C}_r^{-1}\mathbb{X}^{\mathrm{T}}(\mathbf{\Delta p} - \mathbf{\Delta p}_0)$, where $\mathbb{C}_r = \mathbb{X}^{\mathrm{T}}\mathbb{X}$ is the covariance matrix of the inter-sensor separation distances, the probability density function of the estimated gradient ∇p is

$$f(\nabla p) = \mathcal{N}_{\nabla p} \exp\left[-\frac{1}{2\sigma^2_{\Delta p}}\overline{\nabla p}^{\mathrm{H}}\mathbb{C}_r\overline{\nabla p}\right], \tag{4.6}$$

where $\mathcal{N}_{\nabla p}$ is a normalization constant. The value of this constant is unimportant for the analysis at hand. Because the covariance matrix $\mathbb{C}_r$ is self-adjoint, the eigenvectors are orthogonal, and $\mathbb{C}_r$ may be factored as

$$\mathbb{C}_r = \mathbb{E}\mathbb{D}_r\mathbb{E}^{\mathrm{H}} \tag{4.7}$$

where $\mathbb{E}$ is a unitary matrix having the eigenvectors of $\mathbb{C}_r$ as columns, and $\mathbb{D}_r$ is a diagonal matrix with the eigenvalues of $\mathbb{C}_r$ along the diagonal [28]. The matrix $\mathbb{E}^{\mathrm{H}}$ is a unitary transformation matrix that rotates a vector into the principal axes of the column space of $\mathbb{C}_r$. Thus, the vector $\widehat{\nabla p} = \mathbb{E}^{\mathrm{H}}\overline{\nabla p}$ represents the variation in ∇p from the optimal value in an orthonormal basis of the eigenvectors of $\mathbb{C}_r$, and the probability density function of ∇p is

$$f(\nabla p) = \mathcal{N}_{\nabla p} \exp\left[-\frac{1}{2\sigma_{\Delta p}^2}\widehat{\nabla p}^{\,\mathrm{H}}\mathbb{D}_r\widehat{\nabla p}\right]. \tag{4.8}$$

Concentration ellipsoids may be defined from Eq. (4.8) by setting the exponent equal to a constant [33]. Choosing a constant $\chi^2_{\nu|g}$, where ν represents the degrees of freedom, and g represents the confidence level, defines an ellipsoid in the gradient parameter space with the equation

$$\chi^2_{\nu|g} = \frac{1}{\sigma^2_{\nabla p1}}\left[\frac{\widehat{\partial p}}{\partial x}\right]^2 + \frac{1}{\sigma^2_{\nabla p2}}\left[\frac{\widehat{\partial p}}{\partial y}\right]^2 + \frac{1}{\sigma^2_{\nabla p3}}\left[\frac{\widehat{\partial p}}{\partial z}\right]^2, \tag{4.9}$$

centered at $\overline{\nabla p_0} = \mathbb{C}_r^{-1}\mathbb{X}^{\mathrm{T}}\mathbf{\Delta p}_0$, with principal axes aligned with the eigenvectors of $\mathbb{C}_r$, with lengths given by

$$\sigma_{\nabla pi} = \sqrt{\frac{\sigma^2_{\Delta p}}{\mathbb{D}_{rii}}}. \tag{4.10}$$

Fig. 4.1 illustrates the concentration ellipse for two-dimensional cartesian coordinates. For a suitably large ensemble of estimates, a fraction g will lie within the ellipsoid. The concentration ellipsoids may then be mapped to the velocity space using the relation $\mathbf{u} = \jmath\nabla p/\rho_0\omega$.

For the tetrahedron, the covariance matrix of inter-sensor separation distances, $\mathbb{C}_r$, is

$$\mathbb{C}_r = \begin{bmatrix} \frac{16}{3}a^2 & 0 & 0 \\ 0 & \frac{16}{3}a^2 & 0 \\ 0 & 0 & \frac{16}{3}a^2 \end{bmatrix}. \tag{4.11}$$

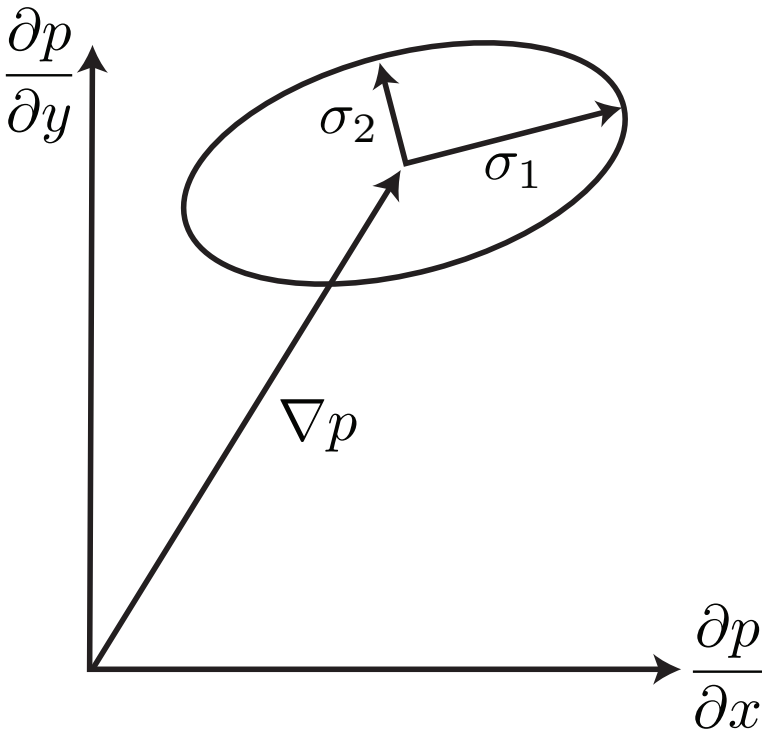

Figure 4.1 A concentration ellipsoid defined by the variance in intersensor pressure differences. The principal axes are aligned with the eigenvectors of the covariance matrix of intersensor separation distances.

Because $\mathbb{C}_r$ is diagonal, there is no need to rotate the axes of the concentration ellipsoids. Moreover, because the diagonal entries are equal, the concentration ellipsoids are spheres with radii given by

$$\sigma_{\nabla pi} = \sqrt{\frac{\sigma_{\Delta p}^2}{\mathbb{D}_{rii}}} = \frac{\sigma_{\Delta p}\sqrt{3}}{4a}. \tag{4.12}$$

The solid angle subtended by the concentration spheres in the parameter space is

$$\begin{aligned}\Omega_{\nabla p} &= 2\pi\left(1 - \left(1 - \frac{\sigma_{\nabla p}}{\left|\overline{\nabla p}_0\right|}\right)^{-1/2}\right) \\ &= 2\pi\left(1 - \left(1 - \frac{\sigma_{\Delta p}\sqrt{3}}{4a\left|\mathbb{C}_r^{-1}\mathbb{X}^{\mathrm{T}}\mathbf{\Delta p}_0\right|}\right)^{-1/2}\right).\end{aligned} \tag{4.13}$$

The solid angle provides an indicator of the accuracy of the direction of the estimate. Because the concentration ellipsoid is a sphere, the maximum and minimum radial distances of the ellipsoid lie in the same direction as $\overline{\nabla p}_0$ and are found by adding or subtracting $\sigma_{\Delta p}^2$ from $\left|\overline{\nabla p}_0\right|$.

4.1.2 Wave Vector Method Estimate Confidence

Concentration ellipses for the velocity estimate may also be developed for the wave vector method. In the wave vector method a least squares estimate of the wave vector is found using the relative phases of sensor pairs. Again assuming that errors in the phase measurements are normally distributed about the mean, the covariance matrix of the relative phase vector $\boldsymbol{\varphi}$ is

$$\mathbb{C}_{\Delta p} = \sigma_\varphi^2 \mathbb{I}. \tag{4.14}$$

The variance, σ_φ^2, of the phase measurements is given by

$$\sigma_\varphi^2 = \frac{\boldsymbol{\varphi}^{\mathrm{H}}(\mathbb{I} - \mathbb{R})\boldsymbol{\varphi}}{N - r}, \tag{4.15}$$

where $\mathbb{R} = \mathbb{X}(\mathbb{X}^{\mathrm{T}}\mathbb{X})^{-1}\mathbb{X}^{\mathrm{T}}$, N is the number of sensor pairs, and r is the rank of the matrix $\mathbb{R}$. The probability density function for the normal distribution is

$$f(\boldsymbol{\varphi}) = \frac{1}{(2\pi\sigma_{\varphi}^2)^{\frac{N}{2}}} \exp\left[-\frac{1}{2\sigma_{\varphi}^2}\left[(\boldsymbol{\varphi}^{\mathrm{H}} - \boldsymbol{\varphi}_0^{\mathrm{H}})\mathbb{I}(\boldsymbol{\varphi} - \boldsymbol{\varphi}_0)\right]\right]. \tag{4.16}$$

The wave vector $\mathbf{k}$ is related to the relative phase vector by $-\mathbb{X}\mathbf{k} = \boldsymbol{\varphi}$, so defining the mean wave vector $\mathbf{k}_0 = \mathbb{C}_r^{-1}\mathbb{X}^{\mathrm{T}}\boldsymbol{\varphi}_0$, the probability density function of $\mathbf{k}$ is

$$f(\mathbf{k}) = \mathcal{N}_k \exp\left[-\frac{1}{2\sigma_{\varphi}^2}(\mathbf{k}^{\mathrm{H}} - \mathbf{k}_0^{\mathrm{H}})\mathbb{E}\mathbb{D}_r\mathbb{E}^{\mathrm{H}}(\mathbf{k} - \mathbf{k}_0)\right]. \tag{4.17}$$

The exponent may be used to define concentration ellipsoids for the wave vector or, by appropriate transformations, for the velocity and intensity vectors. The solid angle and magnitude error bounds may be determined in the same manner as for the finite-difference method. Because the variance of the pressure measurements and the phase may be determined from experimental data, it is possible to estimate the confidence we may have in the estimated quantity. For example, if the phase error is normally distributed with variance of one degree, then the radius of the concentration ellipsoid in wave vector space for a probe with a radius of $1/2''$ is

$$\sigma_{k'} = \frac{\sqrt{3}}{4a} \approx 17.32. \tag{4.18}$$

If this is small compared to the wave vector amplitude, then the estimate may be used. For low frequencies, the standard deviation may be larger than the estimated vector and the estimate must be considered carefully. The confidence may be improved by either decreasing the phase variation, or increasing the radius of the probe.

4.2 Measurement and Equipment Induced Bias and Error

4.2.1 Finite-Difference Estimator Bias

The least-squares estimator is an unbiased estimator, but, in order to estimate the gradient of the pressure, it is assumed in Eq. (3.20),

$$\mathbf{r}'^{\mathrm{T}}_{ij} \nabla p \approx p_j - p_i, \tag{4.19}$$

that the spatial relationship between pressure sample points is approximately linear. For a small amplitude acoustic process, the spatial relationship is described by a second-order differential equation. For acoustic disturbances with a wavelength that is large compared to the sensor spacing, the pressure change is approximately linear. However, as the wavelength decreases, this approximation becomes less accurate. This results in a physical bias of the estimate. The bias due to the finite-difference is not the only source of bias. The velocity estimated is the velocity at the acoustic center of the probe. Because there is no sensor at the acoustic center of the sphere, it is necessary to estimate the pressure there from the existing sensors by averaging the pressures. This is a source of significant bias, as is illustrated for one dimension in Fig. 4.2. If the derivative of the curve at point c is approximated by the slope of the line $a - b$, the error is fairly small. In contrast, if the pressure at point c is approximated by the average of the pressures at points a and b, marked by d, then there is significant error. The average is a reasonably accurate estimate for estimating the pressure at the acoustic center of the sensors for frequencies where the sensor spacing is less than a quarter of the wavelength. If the sensor spacing is greater than a quarter wavelength, then the accuracy decreases rapidly. As is apparent in Fig. 4.3, the bias of the pressure estimate is much worse than the bias of the velocity

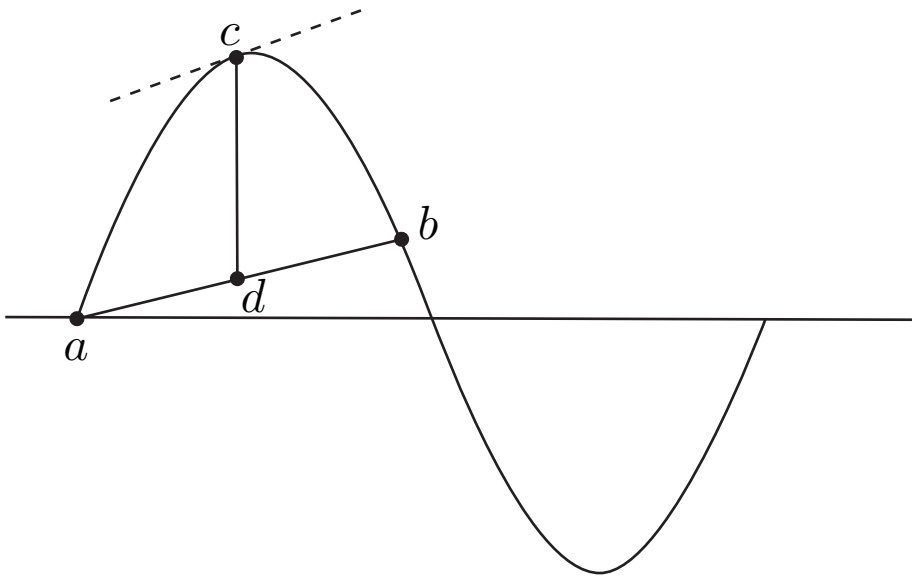

Figure 4.2 The finite-difference and average methods are illustrated.

estimate. The intensity bias is also shown in Fig. 4.3.

4.2.2 Effect of a Spherical Probe on the Finite-Difference Estimate

Because the intensity/energy density probe developed for NASA consists of four sensors mounted on the surface of a rigid sphere, the effect of a spherical housing on both methods for estimating the intensity is especially relevant.

In [14], Elko considers the effect that mounting the sensors on opposite sides of a sphere has on a finite-difference approximation of the pressure gradient. His method follows. Begin with the pressure produced by a plane wave, traveling in the $-z$ direction ($p = p_0 e^{jkz}$), incident on the surface of a rigid sphere with radius a, given by Bowman [31] as

$$p'(ka,\theta) = \frac{-jp_0}{(ka)^2} \sum_{n=0}^{\infty} (\jmath)^n (2n+1) \frac{P_n(cos\theta)}{h_n^{(2)\prime}(ka)}, \tag{4.20}$$

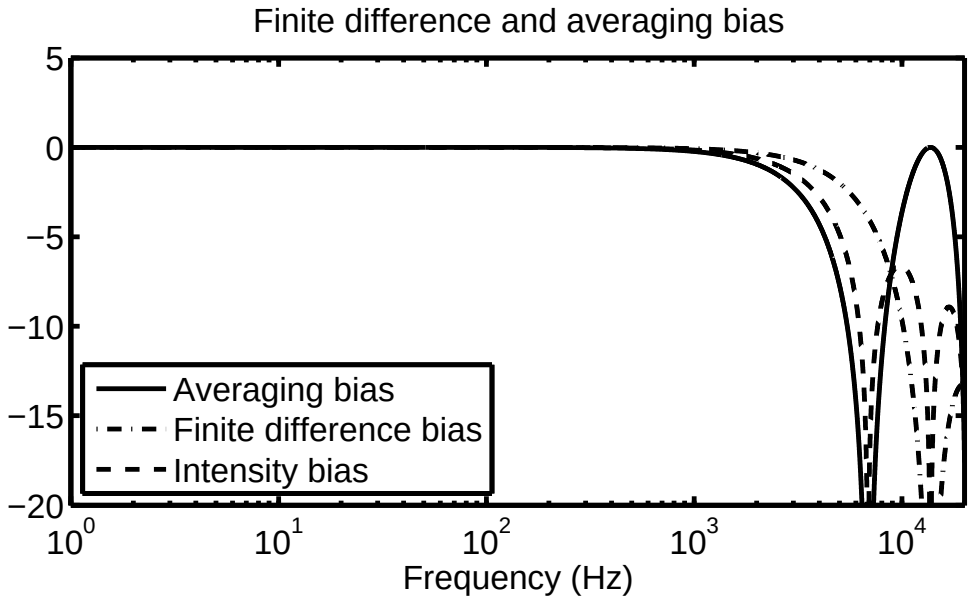

Figure 4.3 Bias of the finite-difference approximation, average pressure, and intensity for a one-dimensional probe with a sensor separation distance of 0.025m.

where P_n represents the Legendre polynomials and $h_n^{(2)} = j_n - y_n$ represents the spherical Hankel function of the second kind. Assuming that $ka \ll 1$, applying a small argument approximation to the summation, and keeping only two terms, we obtain

$$p'(ka, \theta) \approx p_0 \left[1 + \frac{3}{2} \jmath ka \cos\theta\right]. \tag{4.21}$$

For sensors located on the surface of the sphere at $\theta_1 = 0$ and $\theta_2 = \pi$, the pressures measured are approximately

$$p_1'(ka, \theta) \approx p_0 \left[1 + \frac{3}{2} \jmath ka\right], \tag{4.22a}$$

$$p_2'(ka, \theta) \approx p_0 \left[1 - \frac{3}{2} \jmath ka\right]. \tag{4.22b}$$

Using these pressures to estimate the pressure gradient yields

$$\frac{dp}{dz} \approx \frac{p_1' - p_2'}{\Delta z'} \approx \frac{3\jmath p_0 ka}{\Delta z'}. \tag{4.23}$$

Next, consider the finite-difference estimate of the pressure gradient without the sphere

$$\frac{dp}{dz} \approx \frac{p_1 - p_2}{\Delta z'} = \frac{p_0\left(e^{\jmath ka} - e^{-\jmath ka}\right)}{\Delta z} \approx \frac{\jmath 2 p_0 ka}{2a}. \tag{4.24}$$

Comparing (4.23) and (4.24), it becomes apparent that the presence of the sphere creates an effective separation distance of $\Delta z \approx 3a$ for small ka. Elko interprets this as a positive bias that counteracts the negative bias associated with the finite-difference estimation technique. However, this bias estimate is only appropriate for sensors mounted on opposite sides of the sphere. For sensors that are not mounted on orthogonal axes, the bias is different for every coordinate direction. Following the same process for the tetrahedral probe, the effective spacings are found to be

$$\Delta x' \approx \frac{3\sqrt{2}}{2}a, \tag{4.25a}$$

$$\Delta y' \approx \sqrt{6}a, \tag{4.25b}$$

$$\Delta z' \approx 2a. \tag{4.25c}$$

Elko's method may be generalized to a plane wave incident from an arbitrary direction by replacing the $\cos\theta$ term by $-\hat{\mathbf{k}}\cdot\hat{\mathbf{r}}$, where $\hat{\mathbf{k}}$ and $\hat{\mathbf{r}}$ are unit vectors indicating the direction of wave propagation and sensor location, and the dot product of the two unit vectors is given by $\hat{\mathbf{k}}\cdot\hat{\mathbf{r}} = \cos\theta_k\cos\theta + \sin\theta_k\sin\theta\cos(\phi - \phi_k)$, where ϕ_k and θ_k are the azimuthal and polar angles indicating the direction of wave propagation. For this case, Eqs. (4.23) and (4.24) become

$$\frac{dp}{dz} \approx \frac{p_1' - p_2'}{\Delta z'} \approx -\frac{3\jmath p_0 ka\hat{\mathbf{k}}\cdot(\hat{\mathbf{r}}_i - \hat{\mathbf{r}}_j)}{\Delta z'}, \tag{4.26a}$$

$$\frac{dp}{dz} \approx \frac{p_0\left(e^{-\jmath ka\hat{\mathbf{k}}\cdot\hat{\mathbf{r}}_i} - e^{-\jmath ka\hat{\mathbf{k}}\cdot\hat{\mathbf{r}}_j}\right)}{\Delta z} \approx -\frac{\jmath 2 p_0 ka\hat{\mathbf{k}}\cdot(\hat{\mathbf{r}}_i - \hat{\mathbf{r}}_j)}{\Delta z}. \tag{4.26b}$$

Taking the ratio of these two expressions, and setting it equal to one, since the

gradient estimates should be the same,

$$\frac{3\jmath p_0 ka\hat{\mathbf{k}}\cdot(\hat{\mathbf{r}}_i-\hat{\mathbf{r}}_j)}{\Delta z'}\frac{\Delta z}{\jmath 2p_0 ka\hat{\mathbf{k}}\cdot(\hat{\mathbf{r}}_i-\hat{\mathbf{r}}_j)}=1, \tag{4.27}$$

we see that

$$\Delta z'=\frac{3}{2}\Delta z \tag{4.28}$$

for a plane wave incident from an arbitrary angle. Thus for small ka, the sphere produces an effective separation of 3/2 times the physical separation distance for any sensor orientation.

Elko uses small argument approximations to reach his conclusions. However, if a small argument approximation is not made, then the pressure due to a plane wave traveling in the ϕ_k, θ_k direction measured by the i-th sensor at $a\hat{\mathbf{r}}_i$ on the surface of a sphere is

$$p_i'=p_0e^{-\jmath\mathbf{k}\cdot\hat{\mathbf{r}}_i a}-p_0\sum_{n=0}^{\infty}(-\jmath)^n(2n+1)\frac{j_n'(ka)}{h_n^{(2)\prime}(ka)}h_n^{(2)}(ka)P_n(\hat{\mathbf{k}}\cdot\hat{\mathbf{r}}_i) \tag{4.29}$$

$$=p_0\sum_{n=0}^{\infty}(-\jmath)^n(2n+1)\left[j_n(ka)-\frac{j_n'(ka)}{h_n^{(2)\prime}(ka)}h_n^{(2)}(ka)\right]P_n(\hat{\mathbf{k}}\cdot\hat{\mathbf{r}}_i). \tag{4.30}$$

Here the identity

$$\frac{2n+1}{4\pi}P_n(\hat{\mathbf{x}}\cdot\hat{\mathbf{y}})=\sum_{m=-n}^{n}Y_n^m(\hat{\mathbf{x}})\left[Y_n^m(\hat{\mathbf{y}})\right]^*, \tag{4.31}$$

has been used to simplify the usual expressions. Again setting the ratio of the two estimates equal to one,

$$\begin{aligned}\frac{(p_i'-p_j')\Delta\mu}{(p_i-p_j)\Delta\mu'}=&\frac{\Delta\mu}{\Delta\mu'}\left[p_0e^{-\jmath\mathbf{k}\cdot\hat{\mathbf{r}}_i a}-p_0e^{-\jmath\mathbf{k}\cdot\hat{\mathbf{r}}_j a}\right]^{-1}\left[p_0e^{-\jmath\mathbf{k}\cdot\hat{\mathbf{r}}_i a}-p_0e^{-\jmath\mathbf{k}\cdot\hat{\mathbf{r}}_j a}\right]\\&-\frac{\Delta\mu}{\Delta\mu'}\left[p_0e^{-\jmath\mathbf{k}\cdot\hat{\mathbf{r}}_i a}-p_0e^{-\jmath\mathbf{k}\cdot\hat{\mathbf{r}}_j a}\right]^{-1}\times\\&\left[p_0\sum_{n=0}^{\infty}(-\jmath)^n(2n+1)\frac{j_n'(ka)}{h_n^{(2)\prime}(ka)}h_n^{(2)}(ka)\left[P_n(\hat{\mathbf{k}}\cdot\hat{\mathbf{r}}_i)-P_n(\hat{\mathbf{k}}\cdot\hat{\mathbf{r}}_j)\right]\right]\\&=1,\end{aligned}$$

where μ represents the appropriate cartesian coordinate, we see that

$$\frac{\Delta\mu'}{\Delta\mu} = 1 - \sum_{n=0}^{\infty} \frac{(-\jmath)^n(2n+1)j_n'(ka)}{h_n^{(2)\prime}(ka)} h_n^{(2)}(ka) \frac{P_n(\hat{\mathbf{k}}\cdot\hat{\mathbf{r}}_i) - P_n(\hat{\mathbf{k}}\cdot\hat{\mathbf{r}}_j)}{e^{-\jmath\mathbf{k}\cdot\hat{\mathbf{r}}_i a} - e^{-\jmath\mathbf{k}\cdot\hat{\mathbf{r}}_j a}}. \tag{4.32}$$

This expression is valid for all values of ka and for an arbitrary incident plane wave. By keeping only the first two terms of the summation and using an appropriate small angle approximation, it can be shown that this reduces to Elko's expression.

4.2.3 Effect of a Spherical Probe on the Wave Vector Estimate

The effect that mounting the sensors on the surface of a sphere has on the wave vector method for estimating the particle velocity may be predicted by considering the pressure on the surface of a rigid sphere at the sensor locations $\mathbf{r}_i = a\,\hat{\mathbf{r}}$, given by

$$p_i = p_0 \sum_{n=0}^{\infty} (-\jmath)^n(2n+1) \left[j_n(ka) - \frac{j_n'(ka)}{h_n^{(2)\prime}(ka)} h_n^{(2)}(ka) \right] P_n(\hat{\mathbf{k}}\cdot\hat{\mathbf{r}}_i). \tag{4.33}$$

Because the wave vector method is a phase based calculation, it is necessary to calculate the phase at each sensor location. This is accomplished by defining

$$\begin{aligned}
\eta_i = \mathrm{Re}\{p_i\} = p_0 \sum_{n=0}^{\infty} & (-1)^n(4n+1) \\
& \times \left[j_{2n}(ka) - \frac{j_{2n}(ka)(j_{2n}'(ka))^2 + j_{2n}'(ka)y_{2n}(ka)y_{2n}'(ka)}{\left|h_{2n}^{(2)\prime}(ka)\right|} \right] P_{2n}(\hat{k}\cdot\hat{r}_i) \\
& + (-1)^{n+1}(4n+3) \\
& \times \left[\frac{y_{2n+1}(ka)(j_{2n+1}'(ka))^2 - j_{2n+1}(ka)j_{2n+1}'(ka)y_{2n+1}'(ka)}{\left|h_{2n+1}^{(2)\prime}(ka)\right|} \right] P_{2n+1}(\hat{k}\cdot\hat{r}_i),
\end{aligned} \tag{4.34}$$

and,

$$\begin{aligned}\zeta_i =&\mathrm{Im}\{p_i\} = p_0 \sum_{n=0}^{\infty}(-1)^n(4n+3) \\ &\times \left[j_{2n+1}(ka) - \frac{j_{2n+1}(ka)(j'_{2n+1}(ka))^2 + j'_{2n+1}(ka)y_{2n+1}(ka)y'_{2n+1}(ka)}{\left|h^{(2)\prime}_{2n+1}(ka)\right|} \right] P_{2n+1}(\hat{k}\cdot\hat{r}_i) \\ &+ (-1)^n(4n+1) \left[\frac{y_{2n}(ka)(j'_{2n}(ka))^2 - j_{2n}(ka)j'_{2n}(ka)y'_{2n}(ka)}{\left|h^{(2)\prime}_{2n}(ka)\right|} \right] P_{2n}(\hat{k}\cdot\hat{r}_i).\end{aligned} \tag{4.35}$$

Using these definitions, the phase is given by

$$\phi_i = \mathrm{atan2}(\zeta_i, \eta_i) \tag{4.36}$$

where $\mathrm{atan2}(y,x)$ is defined as

$$\mathrm{atan2}(y,x) = \begin{cases} \tan^{-1}\left|\frac{y}{x}\right| \ \mathrm{sgn}(y) & x > 0 \\ \frac{\pi}{2}\ \mathrm{sgn}(y) & x = 0 \\ \left(\pi - \tan^{-1}\left|\frac{y}{x}\right|\right)\mathrm{sgn}(y) & x < 0. \end{cases} \tag{4.37}$$

The pressure at any of the sensors may be expressed as

$$p_i = \sqrt{|\eta_i|^2 + |\zeta_i|^2}e^{\jmath\phi_i}, \tag{4.38}$$

and the transfer function between the sensors at $\mathbf{r}_i$ and $\mathbf{r}_j$ is

$$H_{ij} = \frac{p_j}{p_i} = \sqrt{\frac{|\eta_j|^2 + |\zeta_j|^2}{|\eta_i|^2 + |\zeta_i|^2}}e^{\jmath(\phi_i - \phi_j)}. \tag{4.39}$$

Mounting the sensors on the surface of a sphere causes amplitude and phase shifts that appear to invalidate assumptions that form the basis for calculations of the wave vector and consequently the velocity vector. The phase of the microphones relative to one another becomes strongly related to the position of the sensors on the sphere relative to the direction of the incoming signal. Define the excess phase γ_i as the

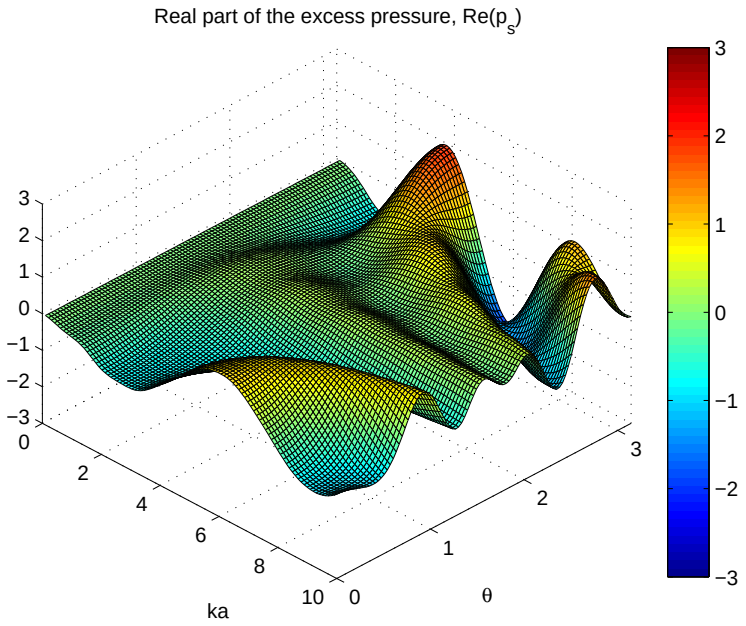

Figure 4.4 Real part of the excess pressure on the surface of a hard sphere as a function of angle.

difference between the phase in the presence of the sphere and the phase without the sphere,

$$\gamma_i = \phi_i - \varphi_i. \tag{4.40}$$

Then the least-squares estimate of the wave vector using a tetrahedral probe becomes

$$\mathbf{k} = \frac{1}{4a}\begin{bmatrix} \sqrt{2}(-\varphi_2 - \gamma_2 + 2(\varphi_3 + \gamma_3) - \varphi_4 - \gamma_4) \\ \sqrt{6}(\varphi_2 + \gamma_2 - \varphi_4 - \gamma_4) \\ -3(\varphi_1 + \gamma_1) + \varphi_2 + \gamma_2 + \varphi_3 + \gamma_3 + \varphi_4 + \gamma_4 \end{bmatrix}. \tag{4.41}$$

The excess phase has the potential to strongly affect the estimated vector, especially at higher frequencies. The real and imaginary parts of the excess, or scattered pressure defined as $p_s = p' - p$, are illustrated in Figs. 4.4 and 4.5 as functions of the angular position on the sphere and ka. It is clear from the figures that the sphere drastically affects the pressures measured at the sensor locations. Although this effect is somewhat beneficial for the finite-difference method at small values of ka, the effect

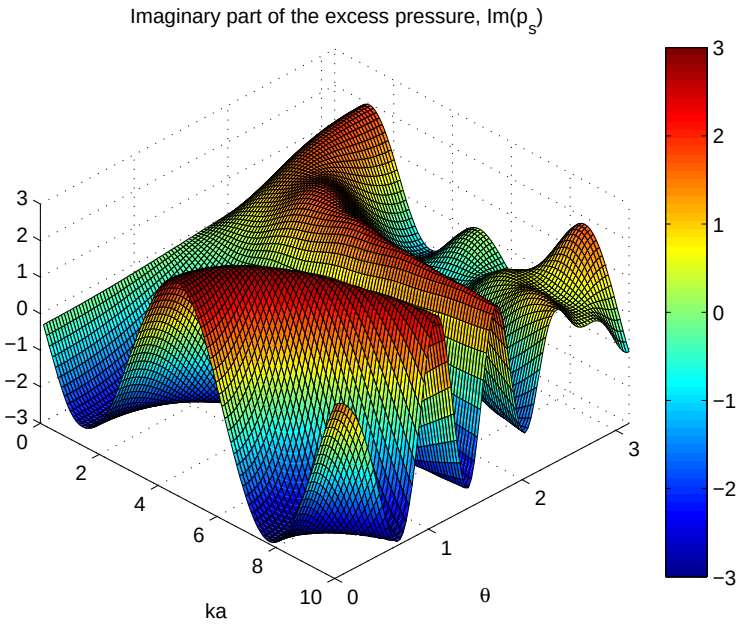

Figure 4.5 Imaginary part of the excess pressure on the surface of a hard sphere as a function of angle.

on the wave vector method is detrimental to the performance of the method. It may be possible to implement an iterative method to improve the estimate of the wave vector method in the presence of a sphere, but no work has been done to investigate this possibility.

4.2.4 Effect of Sensor Phase Mismatch

The phase mismatch of physical sensors also has the potential to significantly impact the accuracy of the estimated quantities. Let the phase mismatch of each microphone be represented by α_i, which can be a function of frequency. Using this convention, the pressure at each sensor is related to the actual pressure by

$$p_i = pe^{\jmath\alpha_i}. \tag{4.42}$$

Phase matching of the sensors is especially important at low frequencies, because the phase is proportional to the wavelength. Even a small phase error (less than one degree) corresponds to a large spatial distance for a long wavelength. Although the wave vector method appears especially sensitive to phase error because it uses the phase to directly calculate the velocity and the intensity, the finite-difference method also uses the phase indirectly, because it relies on the physical delay in the signal between two sensors to estimate the gradient. At low frequencies, even small phase errors between the sensors can cause large errors in the estimated gradient. To illustrate this, consider a plane wave of frequency f sampled at locations $\mathbf{r}_1$ and $\mathbf{r}_2$. If both sensors have phase errors given by α_1 and α_2, the estimated pressure gradient is given by

$$\frac{\partial p}{\partial x} \approx p_0 \frac{e^{-\jmath(\mathbf{k}\cdot\mathbf{r}_{1x}-\alpha_1)} - e^{-\jmath(\mathbf{k}\cdot\mathbf{r}_{2x}-\alpha_2)}}{|\mathbf{r}_{1x} - \mathbf{r}_{2x}|}. \tag{4.43}$$

By defining $\alpha_i' = \alpha_i/k$,

$$\frac{\partial p}{\partial x} \approx p_0 \frac{e^{-\jmath k(\hat{\mathbf{k}}\cdot\mathbf{r}_{1x}-\alpha_1')} - e^{-\jmath k(\hat{\mathbf{k}}\cdot\mathbf{r}_{2x}-\alpha_2')}}{|\mathbf{r}_{1x} - \mathbf{r}_{2x}|}. \tag{4.44}$$

If the wavelength of the incident wave is greater than the sensor separation distance, then α_i' will significantly affect the estimated gradient since $\hat{\mathbf{k}} \cdot \mathbf{r}_i < \alpha_i'$. The phase error between the sensors appears in the wave vector method as

$$\mathbf{k} = \frac{1}{4a} \begin{bmatrix} \sqrt{2}(-\varphi_2 - \alpha_2 + 2(\varphi_3 + \alpha_3) - \varphi_4 - \alpha_4) \\ \sqrt{6}(\varphi_2 + \alpha_2 - \varphi_4 - \alpha_4) \\ -3(\varphi_1 + \alpha_1) + \varphi_2 + \alpha_2 + \varphi_3 + \alpha_3 + \varphi_4 + \alpha_4 \end{bmatrix}. \tag{4.45}$$

By comparing Eqs. (4.44) and (4.45) it is apparent that the finite-difference method is actually more sensitive to phase error because the phase term appears in the exponent, whereas, in the wave vector method, the error affects the estimate only linearly.

4.3 Numerical Simulations

4.3.1 Plane Wave

The estimates of the active intensity produced by the finite-difference method and the wave vector method are compared by considering the accuracy of the numerically estimated quantities relative to the analytically predicted quantities. The intensity of a plane wave of amplitude p_0 is easily calculated analytically to be

$$\mathbf{I} = \frac{p_0^2}{2\rho_0 c}\hat{\mathbf{k}}. \tag{4.46}$$

The pressures measured at the four sensors are given by

$$p_i = p_0 e^{-\jmath(\mathbf{k}\cdot\mathbf{r}_i+\alpha_i)} \tag{4.47}$$

where again, α_i represents the phase error of the sensor. The predicted pressures are used to estimate the intensity as presented in chapter 3. $\mathbf{I}_{fd}$ represents the intensity estimated using the finite-difference method, $\mathbf{I}_{ls}$ represents the least-squares estimate based on the wave vector method, and $\mathbf{I}_1$ represents the wave vector estimate relative to sensor 1. The logarithmic error in the intensity component estimates given by

$$10\log_{10}\left|\frac{\left|\mathbf{I}_{[\cdot]\nu}\right|}{|\mathbf{I}_\nu|}\right| \tag{4.48}$$

and the logarithmic error in the ℓ_1 norm of the intensity estimate given by

$$10\log_{10}\left|\frac{\left|\mathbf{I}_{[\cdot]x}\right| + \left|\mathbf{I}_{[\cdot]z}\right| + \left|\mathbf{I}_{[\cdot]z}\right|}{|\mathbf{I}_x| + |\mathbf{I}_y| + |\mathbf{I}_z|}\right| \tag{4.49}$$

are shown in Figs. 4.6 through 4.14. The subscript brackets serve as placeholders for the estimate method label. The ℓ_1 norm was chosen to compare the magnitude of the estimates in order to avoid erroneous cancelation of constants in the numerical estimates. It is also a conservative estimate of the error because the ℓ_1 norm is always

greater than or equal to the standard Euclidean norm. The MATLAB code used to generate these plots is included in appendix A.

The logarithmic error in the estimates of each of the three coordinate components is presented in each of the plots to evaluate the performance of each component of the estimates as a function of the incident angle. It is clear from the error plots that the wave vector method outperforms the finite-difference method in all cases. The wave vector method is consistent in its estimates up to the Nyquist limit, in contrast to the finite-difference method which exhibits significant bias for all but the lowest frequencies. The wave vector estimate relative to one sensor performs better than the least-squares average estimate. It seems that this is due to the bias caused by averaging the pressures in the intensity calculation. It may be possible to correct for this error in the least-squares estimate once the wave vector has been estimated by multiplying the pressure by an appropriate constant to remove the effects of propagation before averaging. The average then becomes

$$\frac{1}{N}\sum_{i=1}^{N} p_i e^{j\mathbf{k}_{ls}\cdot\mathbf{r}_i}. \tag{4.50}$$

For 100 Hz, both the least-squares (Fig. 4.6) and single sensor (Fig. 4.7) wave vector methods exhibit minimal error, although the single sensor error is approximately 5 orders of magnitude smaller. In contrast, even at such a low frequency, the finite-difference method (Fig. 4.8) functions reasonably well for the $y-$ and $z-$components, but the $x-$component consistently underestimates the intensity. This is apparent in the component error plots and also can be observed in the norm error plot. The $x-$axis is located at $\phi_k = 0, \pi$, and 2π, and $\theta = \pi/2$. The error is largest at these points and decreases to nearly zero on the $y-$ and $z-$ axes ($\phi_k = \pi/2$, $3\pi/2$, and $\theta_k = 0, \pi$).

For 1000 Hz, the error in the single sensor wave vector estimate (Fig. 4.10)

remains unchanged. The error in both the least-squares wave vector estimate (Fig. 4.9) and the finite-difference estimate (Fig. 4.11) becomes more significant. The error in the least-squares wave vector estimate is still very small, but the error in the finite-difference estimate is large.

At 8000 Hz, the error in the single sensor wave vector estimate (Fig. 4.13) is still minimal, but both the finite-difference (Fig. 4.14) and least-squares wave vector (Fig. 4.12) estimates exhibit very significant error. This is not due to the bias of the finite-difference approximation, but rather to the bias inherent in averaging the measured pressures to estimate the pressure at the center of the probe.

The effect of sensor phase mismatch is also shown in Figs. 4.15 through 4.17. As expected from the theoretical predictions, the phase mismatch has less effect on the wave vector method than the finite-difference method. For the wave vector method, the phase error has the largest effect on the smallest components. As an example, there is significant error in the x component estimate when the wave vector of the incident wave lies in the $y - z$ plane. This suggests that although the logarithmic error is large, the actual error in the vector estimate is fairly small. This is supported by the fact that the logarithmic error in the ℓ_1 norm is small.

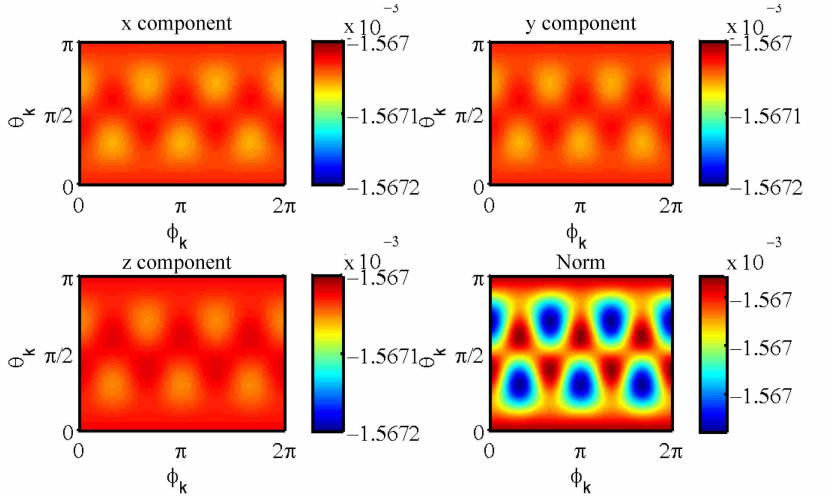

Figure 4.6 Logarithmic (dB) error in wave vector method least-squares estimate of the intensity of a 100 Hz plane wave as a function of incident angle.

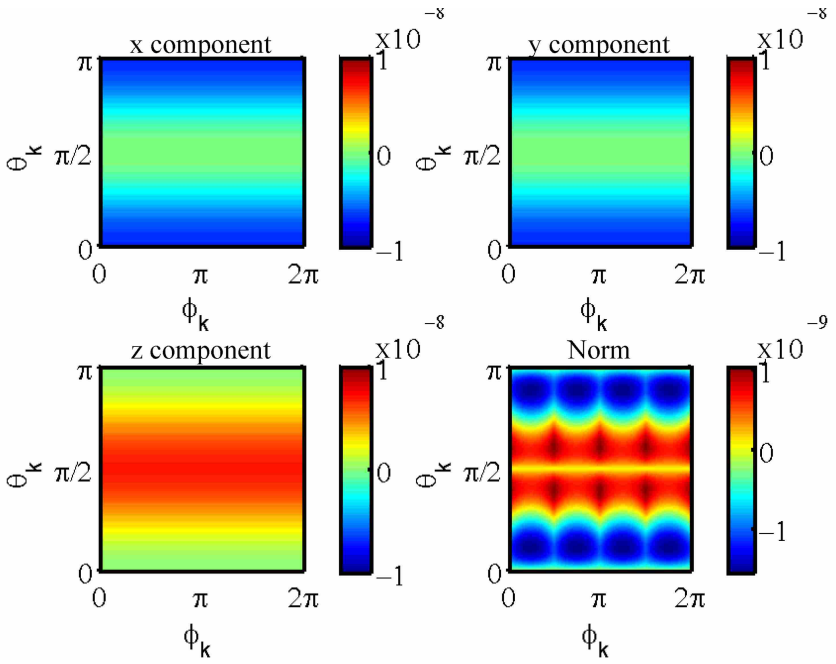

Figure 4.7 Logarithmic (dB) error in wave vector method estimate referenced to sensor 1 of the intensity of a 100 Hz plane wave as a function of incident angle.

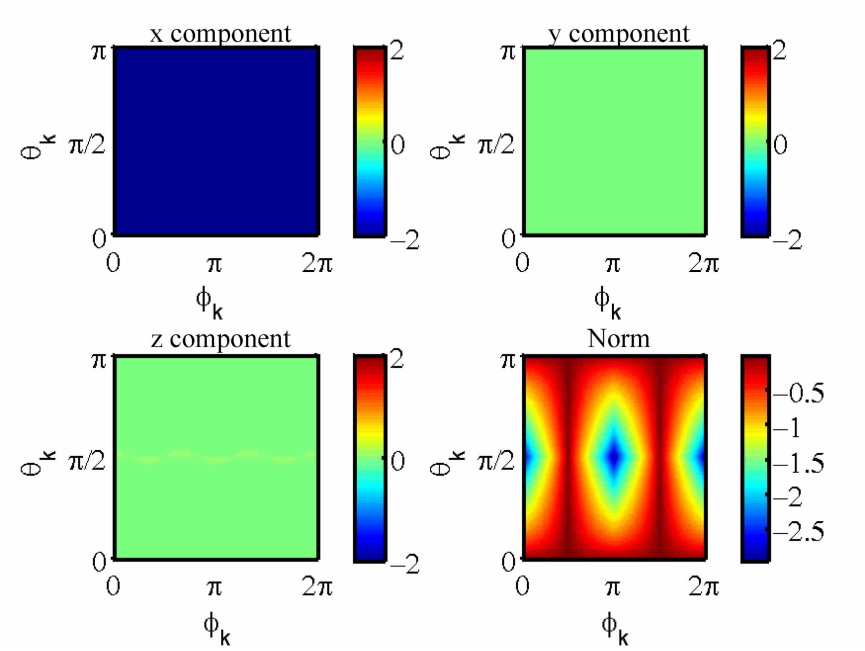

Figure 4.8 Logarithmic (dB) error in finite-difference estimate of the intensity of a 100 Hz plane wave as a function of incident angle.

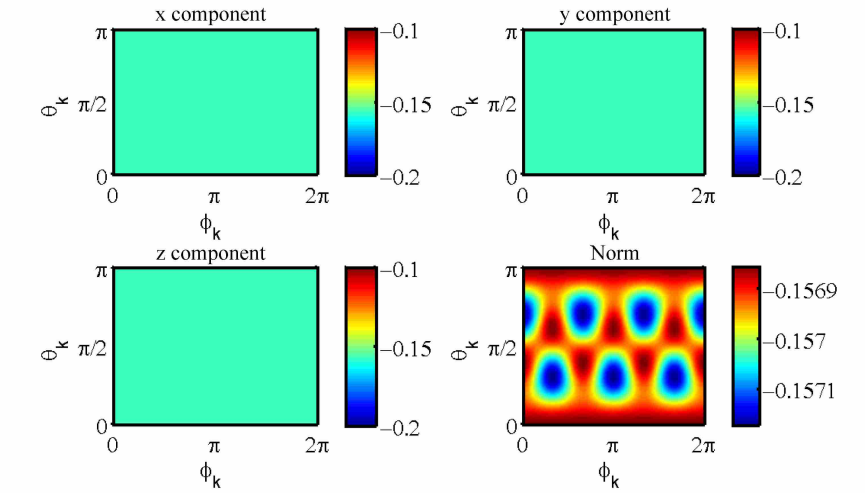

Figure 4.9 Logarithmic (dB) error in wave vector method least-squares estimate of the intensity of a 1000 Hz plane wave as a function of incident angle.

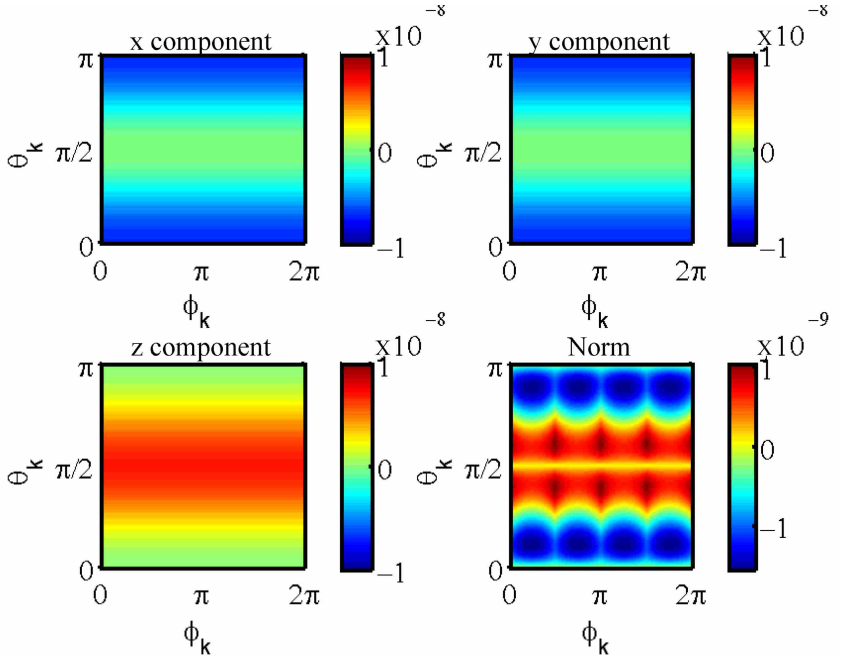

Figure 4.10 Logarithmic (dB) error in wave vector method estimate referenced to sensor 1 of the intensity of a 1000 Hz plane wave as a function of incident angle.

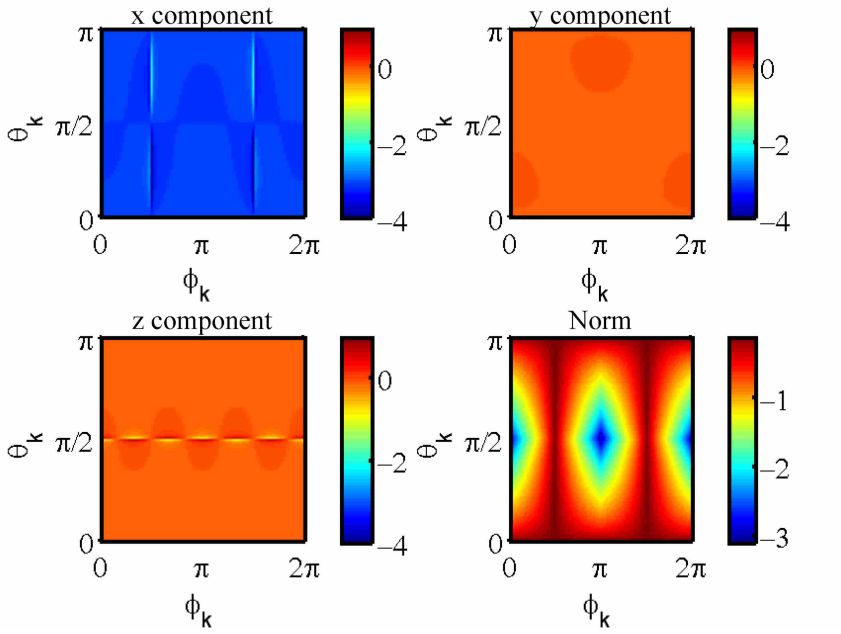

Figure 4.11 Logarithmic (dB) error in finite-difference estimate of the intensity of a 1000 Hz plane wave as a function of incident angle.

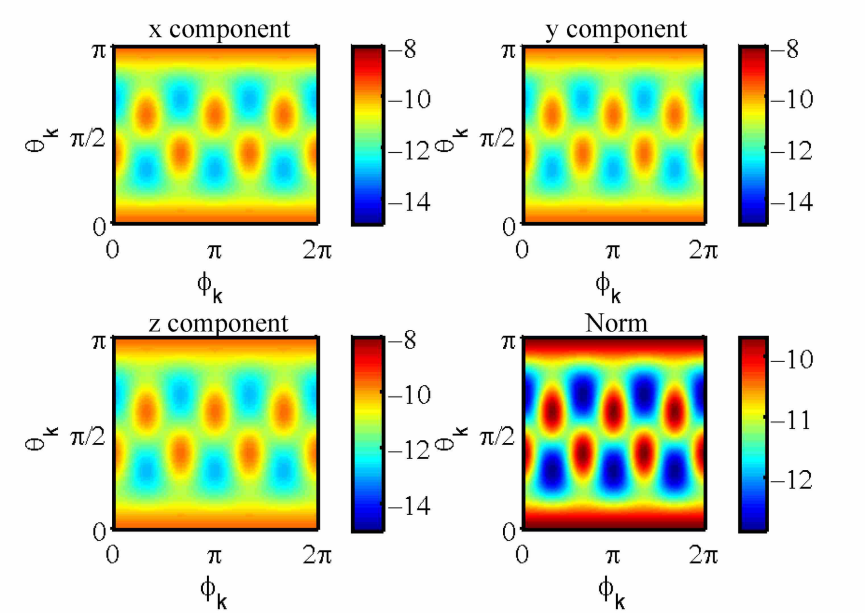

Figure 4.12 Error in wave vector method least-squares estimate of the intensity of a 8000 Hz plane wave as a function of incident angle.

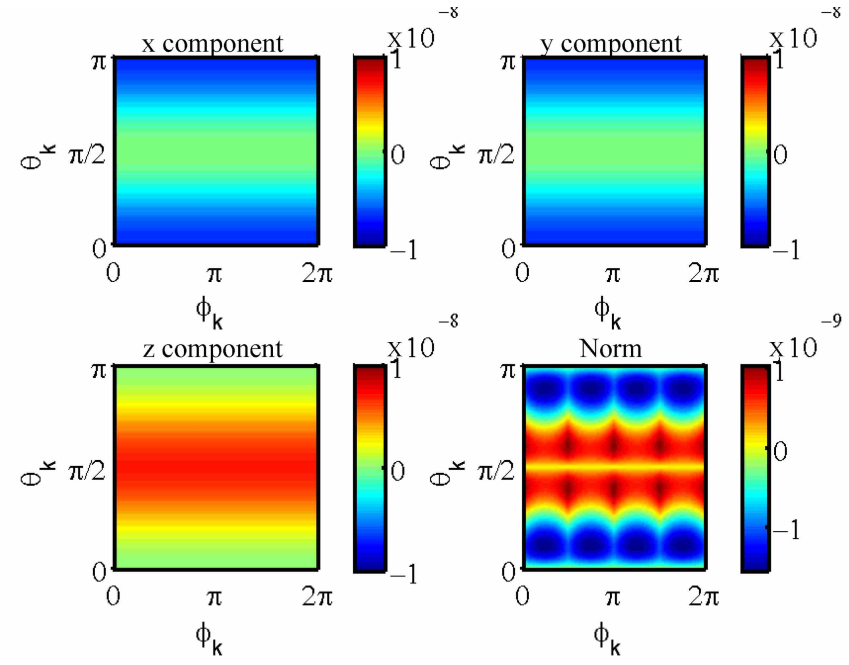

Figure 4.13 Logarithmic (dB) error in wave vector method estimate referenced to sensor 1 of the intensity of a 8000 Hz plane wave as a function of incident angle.

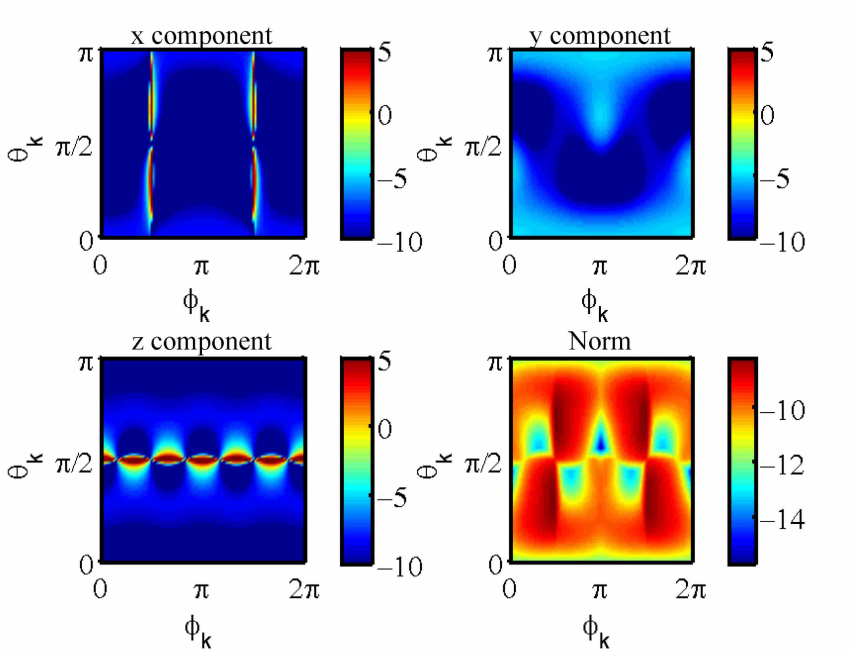

Figure 4.14 Logarithmic (dB) error in finite-difference estimate of the intensity of a 8000 Hz plane wave as a function of incident angle.

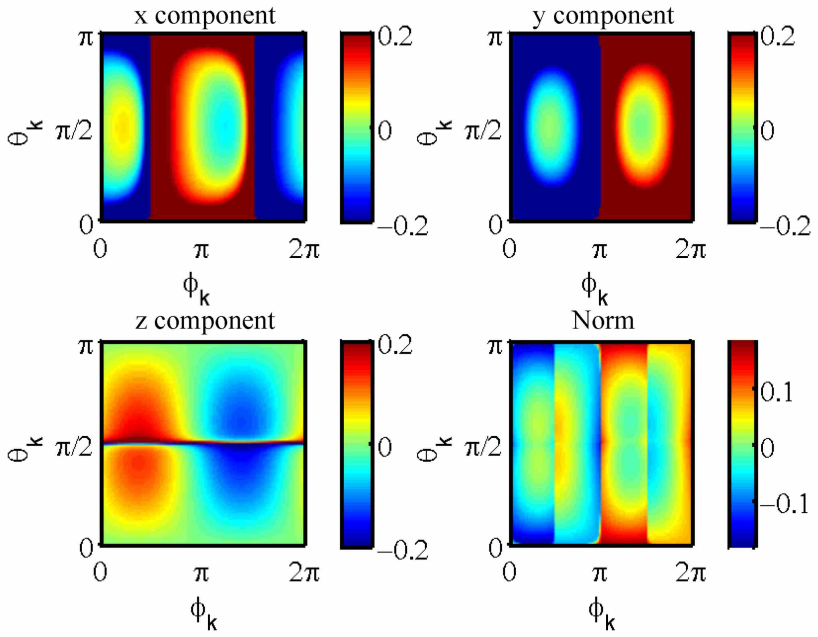

Figure 4.15 Logarithmic (dB) error due to phase mismatch in wave vector method estimate of the intensity of a 1000 Hz plane wave as a function of incident angle.

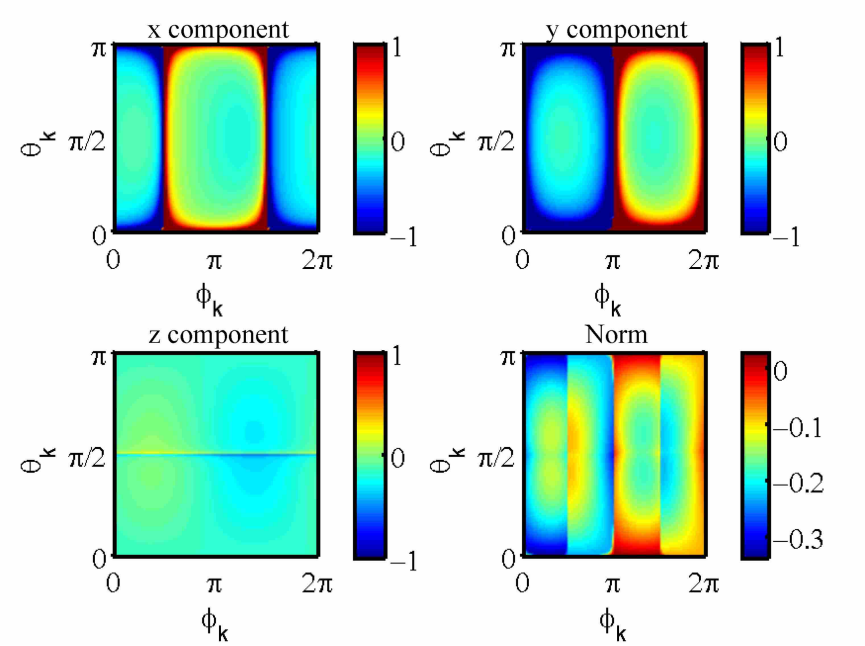

Figure 4.16 Logarithmic (dB) error due to phase mismatch in least-squares wave vector method estimate of the intensity of a 1000 Hz plane wave as a function of incident angle.

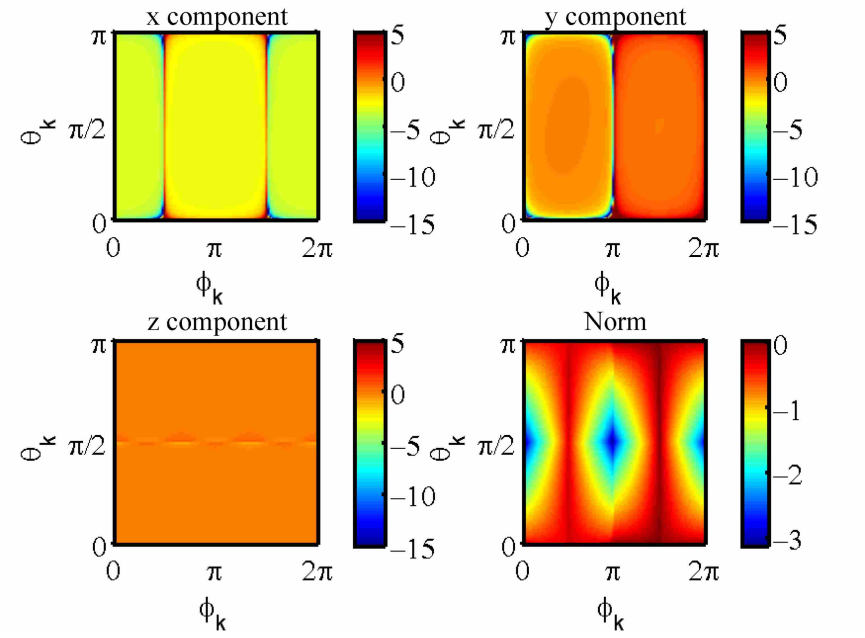

Figure 4.17 Logarithmic (dB) error due to phase mismatch in finite-difference estimate of the intensity of a 1000 Hz plane wave as a function of incident angle.

4.3.2 Monopole Source

Analytical expressions for the intensity due to a point source were presented in Chapter 2. The logarithmic errors in the estimates produced by the finite-difference (FD) method and the wave vector (WV) method are compared in Figs. 4.18 and 4.19. The magnitudes of the estimated intensity vectors are compared to the magnitude of the analytical expression by

$$10\log_{10}\frac{(|\mathbf{I}_{[\cdot]x}|+|\mathbf{I}_{[\cdot]z}|+|\mathbf{I}_{[\cdot]z}|)^{1/2}}{(|\mathbf{I}_x|+|\mathbf{I}_y|+|\mathbf{I}_z|)^{1/2}}. \tag{4.51}$$

Note that the Euclidean norm is used here instead of the ℓ_1 norm because the possibility of erroneous results using the Euclidean norm does not exist for this case. The nondimensional parameter ka, where a is the radius of the circumsphere of the tetrahedral probe, is used here. The wave vector method performs well even in the near field of the monopole. This is initially surprising until the wave vector method is analyzed more carefully. The pressure at the i-th sensor is given by

$$p_i = A_0\frac{e^{-\jmath\mathbf{k}\cdot\mathbf{r}_i}}{|\mathbf{r}_i|}. \tag{4.52}$$

Because the wave vector method only uses the phase differences, the radial amplitude variation does not effect the estimated wave vector. If the single sensor wave vector method is used, then the radial variation in pressure does not effect the estimated intensity either, and for the special case of the monopole, the wave vector actually outperforms the finite difference method. For the dipole, where the near field is significantly more complicated, this is not the case.

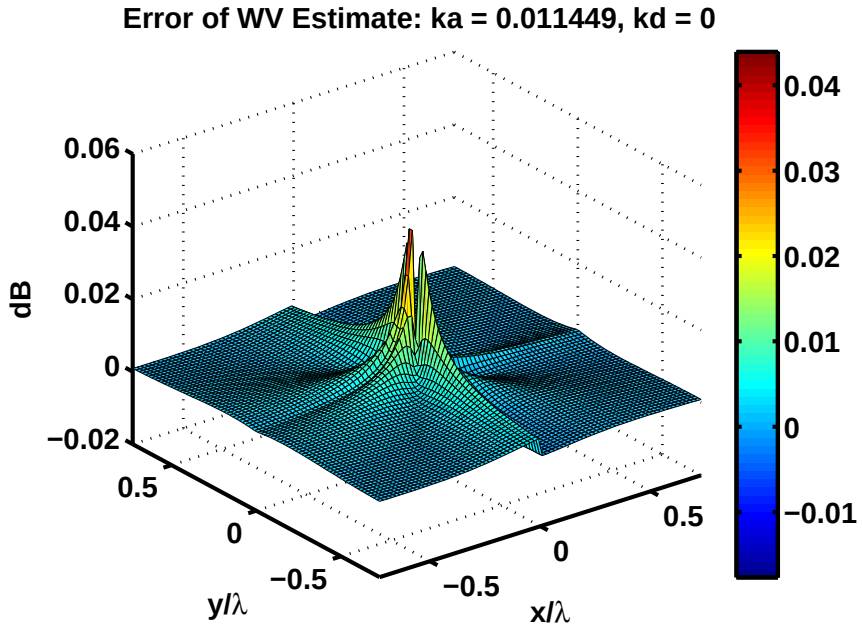

Figure 4.18 Error in wave vector method estimate in the near field of a monopole source. Axis units are in fractions of a wavelength.

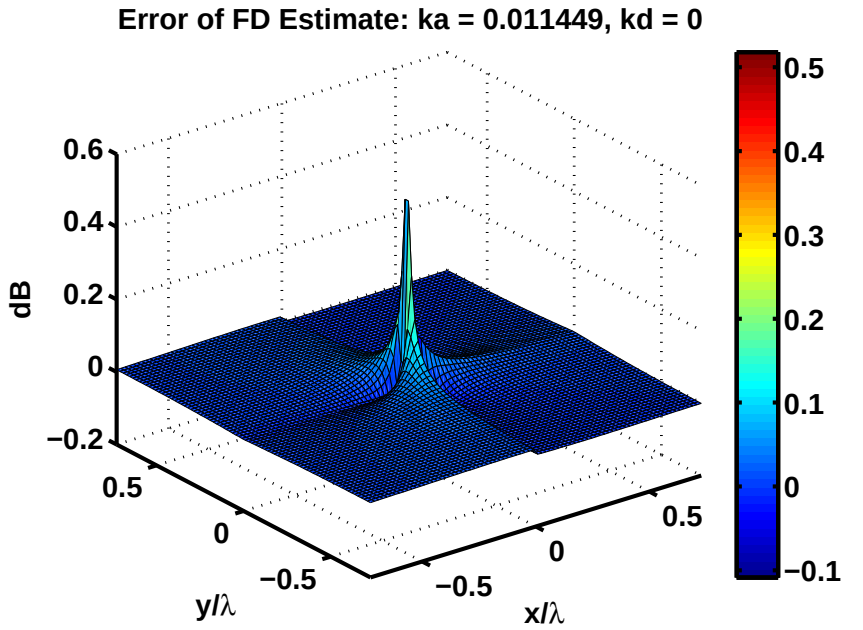

Figure 4.19 Error in finite-difference method estimate in the near field of a monopole source. Axis units are in fractions of a wavelength.

4.3.3 Dipole Source

The dipole is an excellent source configuration for comparing the finite-difference and wave vector methods. Although it is a relatively simple source configuration, the field contains strong reactive components and is significantly more complicated than the monopole field. The analytical expressions for the intensity due to multiple sources were derived in Chapter 2. When discussing dipoles it is useful to define the nondimensional parameter kd, where k is the wavenumber, and d is the source separation distance. It is also useful to nondimensionalize the characteristics of the probe to generalize the results. For the tetrahedral sensor configuration, the parameter ka, where a is again the radius of the circumsphere of the tetrahedron, is appropriate. The relevant information is included in the title or caption of the figures in order to allow comparison and generalization of the results. The analytically predicted and estimated fields for a dipole with $kd = 4.6$ are presented in Figs. 4.20-4.22. A visual inspection reveals that at this frequency, the analytical and estimated fields are very similar.

In order to compare the accuracy of the different methods, the logarithmic error defined previously is averaged over the 40m×40m×40m volume surrounding the dipole and the results are plotted against frequency in Fig. 4.23. Initially, it appears that the finite-difference method outperforms the wave vector method only marginally at low frequencies, and is much worse at high frequencies. However, if the averaging volume is reduced to 10m×10m×10m, the plots are significantly different. This case is shown in Fig. 4.24. Clearly, in the near field, the finite-difference method outperforms the wave vector method for frequencies of interest. This is expected since the wave vector method relies on the assumption that the pressure field is locally planar and this is not the case in the near field of a dipole. The spatial distribution of the error is apparent in Figs. 4.25 and 4.26. The wave vector method exhibits smaller

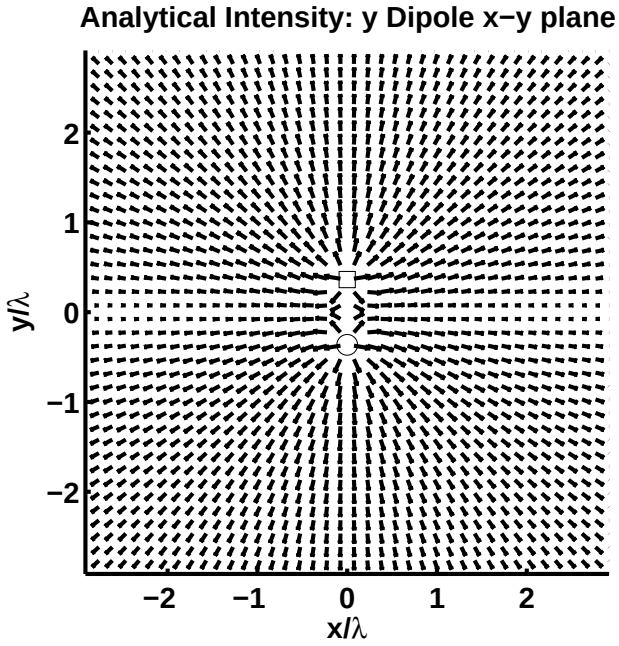

Figure 4.20 Analytically predicted dipole intensity field, $kd = 4.6$.

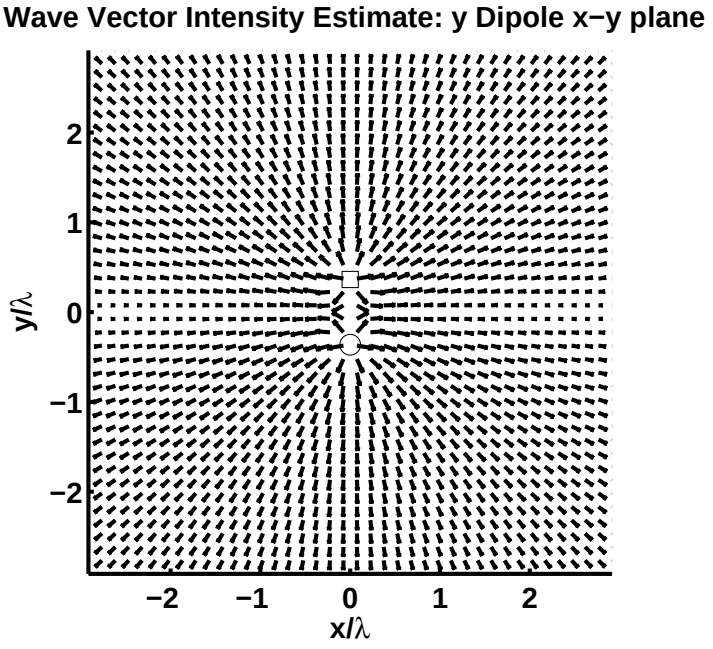

Figure 4.21 Dipole intensity field estimated using the wave vector method, $ka = 0.011$, $kd = 4.6$.

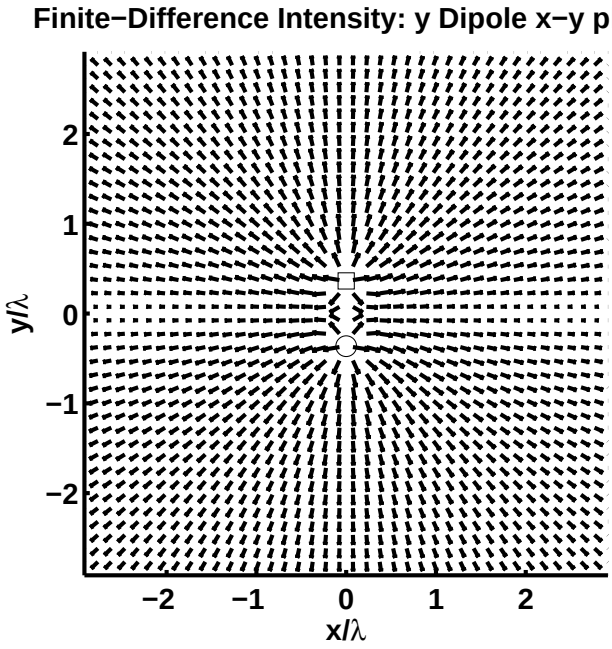

Figure 4.22 Dipole intensity field estimated using the finite-difference method, $ka = 0.011$, $kd = 4.6$.

error in the far field but the finite-difference method performs better in the near field.

It is also important to consider the effect of phase errors on the estimates. The average error with a normally distributed random phase error with a standard deviation of one degree is shown in Fig. 4.27. The phase has very little effect on the average error of both methods. The effect of the phase error on the amplitude estimate is shown in Fig. 4.28. Perhaps unexpectedly, the wave vector method outperforms the finite-difference method on average and especially at low frequencies.

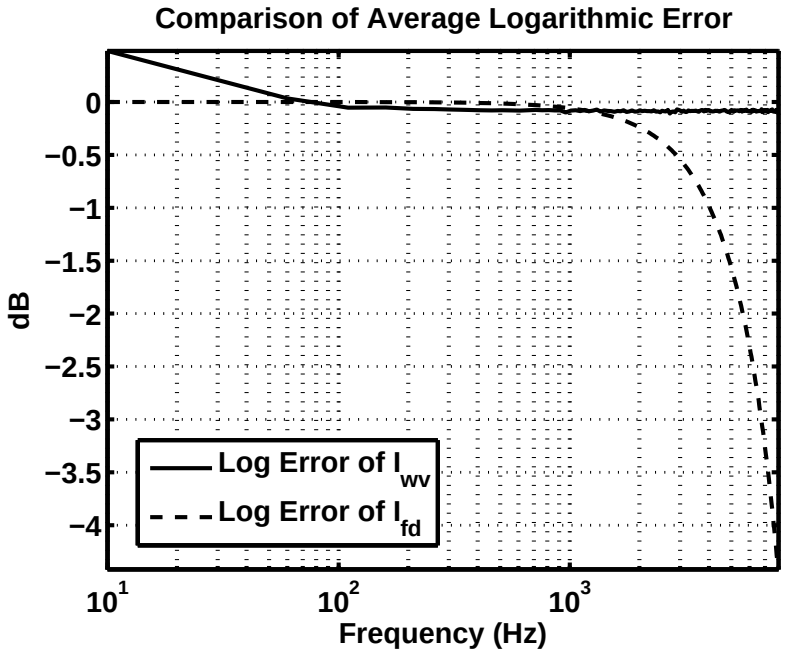

Figure 4.23 Comparison of average logarithmic error of the estimated intensity vector field in the 6400m^3 volume surrounding a dipole intensity field, $a = 0.025$m, $d = 5$m.

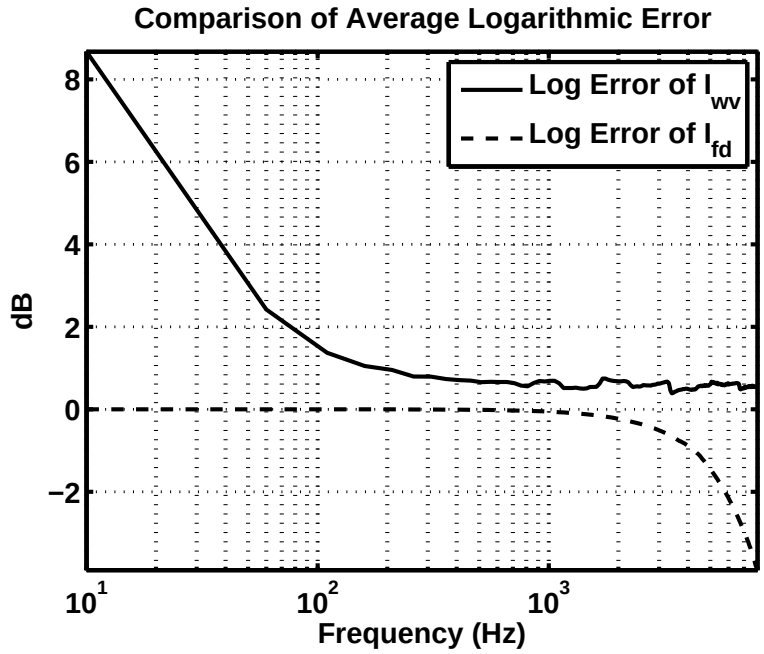

Figure 4.24 Comparison of average logarithmic error of the estimated intensity vector field in the 100m^3 volume surrounding a dipole intensity field, $a = 0.025\text{m}$, $d = 5\text{m}$.

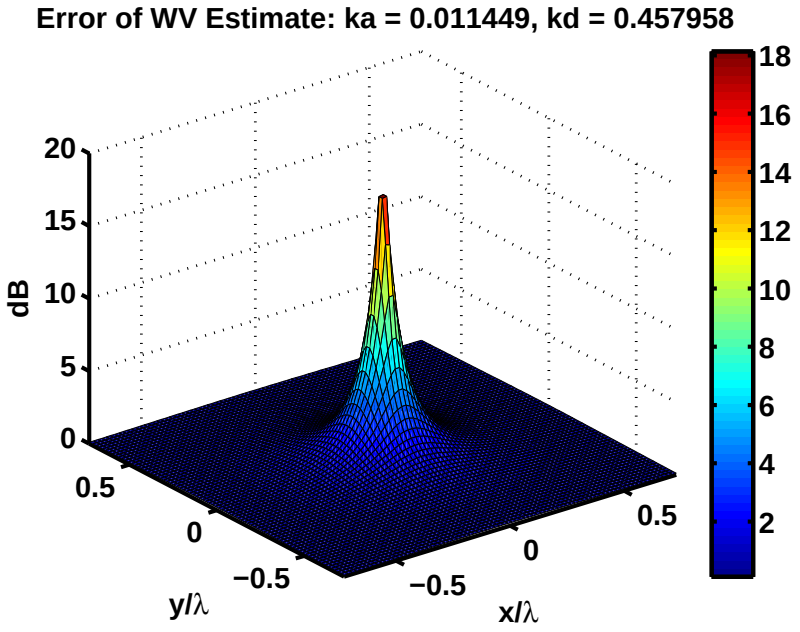

Figure 4.25 Logarithmic error of the intensity vector field estimated using the wave vector method in the $x-y$ plane surrounding a dipole, $ka = 0.011$, $kd = 4.6$.

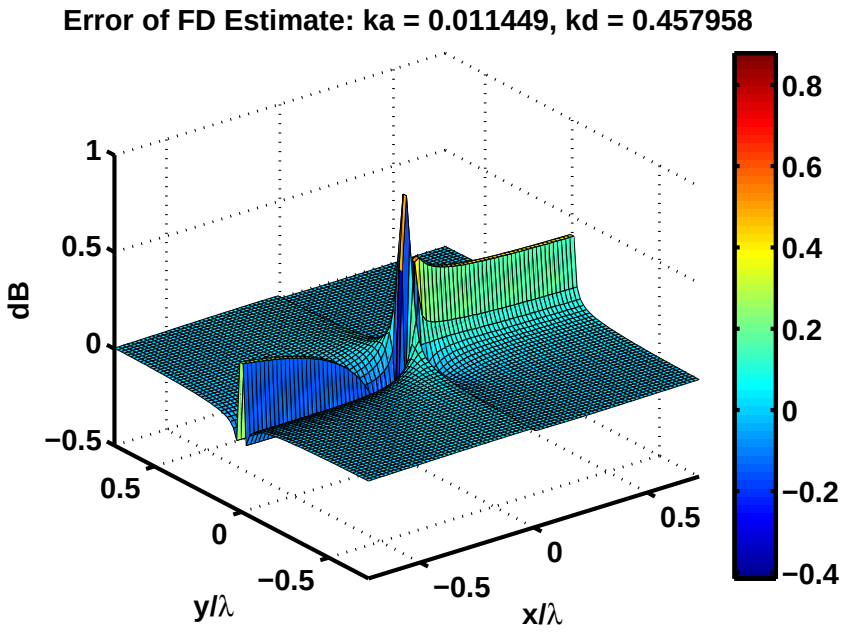

Figure 4.26 Logarithmic error of the intensity vector field estimated using the finite-difference method in the $x - y$ plane surrounding a dipole, $ka = 0.011$, $kd = 4.6$.

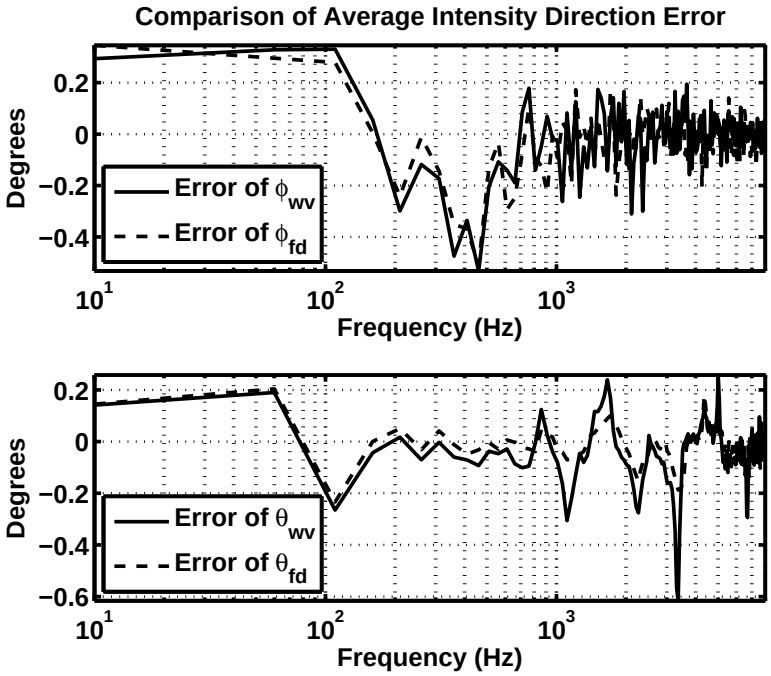

Figure 4.27 Comparison of average angular error of the estimated intensity vector field in the 100m^3 volume surrounding a dipole intensity field, $a = 0.025\text{m}$, $d = 5\text{m}$.

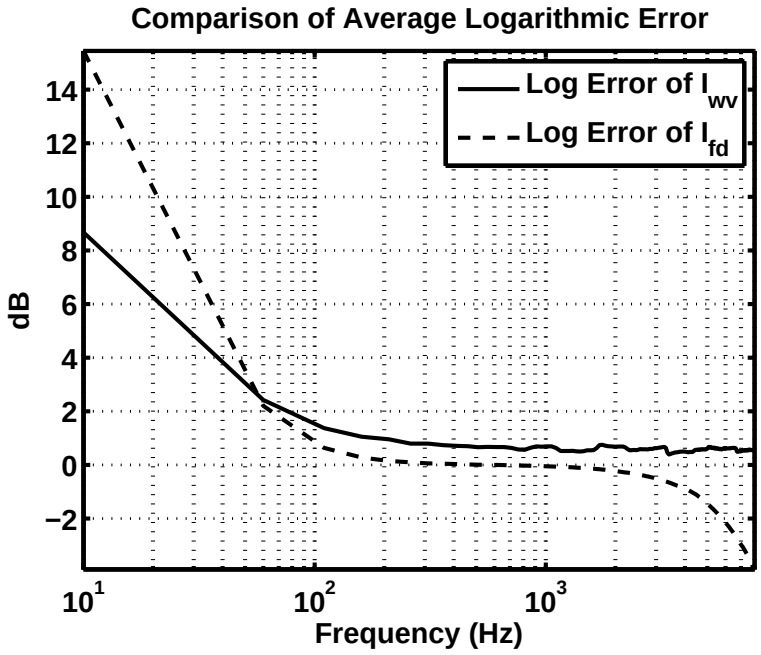

Figure 4.28 Comparison of average logarithmic error of the estimated intensity vector field in the 100m^3 volume surrounding a dipole intensity field, $a = 0.025\text{m}$, $d = 5\text{m}$.

Chapter 5

Conclusion

5.1 Summary

Both the linearized and nonlinear expressions for acoustic intensity and acoustic energy density were derived from fundamental equations or first principles. The connection between the linearized expression for the potential energy density and the nonlinear expression was shown using a power series expansion about the equilibrium. The large linear term present in the potential energy density expression cancels due to the conservation of mass when the expression is inserted into the energy conservation relation.

The finite-difference method for estimating the pressure gradient was developed generally and for the specific case of the tetrahedral probe. In addition, an alternate method for estimating the particle velocity and, consequently, the intensity from the relative phase differences was presented. A method for determining the amplitude and direction of propagation for the special case of a probe consisting of sensors mounted on the surface of a rigid sphere was developed using linear scattering theory. The wave vector and spherical harmonic methods are new methods for estimating

acoustic velocity and intensity. Currently both of these methods are limited to the acoustic far field.

Expressions for determining the confidence of the estimates produced by the methods introduced in Chapter 3 were developed using statistical arguments. The effect of finite-difference and averaging biases on the intensity estimate was investigated, as well as the effect of sensor phase mismatch. The effect of scattering induced phase variations on the estimate was also considered. The finite-difference and wave vector methods were compared in numerical simulations.

5.2 Conclusion

The expressions commonly used in acoustics applications for acoustic intensity and acoustic energy density represent conserved quantities, and are valid for processes described by second-order approximations of the governing equations. The linear term present in the expression for the potential energy derived from thermodynamic principles disappears from the energy conservation equation following the application of the mass conservation equation. It seems, although it has not been shown, that this term corresponds to the fluctuations relative to the absolute energy caused by the acoustic disturbance. These fluctuations do not contribute to the motion of the fluid since the process is primarily adiabatic and consequently, thermal transmission is negligible.

The finite-difference method for estimating the intensity exhibits significant bias in the estimates for all but the lowest frequencies. In contrast, the particle velocity estimates produced using the wave vector method remain accurate until reaching the spatial Nyquist limit. For broadband noise, it may be possible to surpass the spatial Nyquist limit by unwrapping the measured intersensor phase difference before using

the wave vector method to estimate the particle velocity.

5.3 Future Work

Both the wave vector method and the spherical harmonic method require more extensive testing. The spherical harmonic method has been developed theoretically and presented here for reference; an experimental evaluation of the performance of the method is required for validation. The wave vector method for estimating the particle velocity relies on the assumption that the field is approximately planar across the volume of the probe, and that the reactive intensity is negligible in the vicinity of the probe. It may be possible to eliminate the farfield requirement by a careful consideration of the near field of a point source, and separate the contribution of the propagating, or active intensity from the standing or reactive intensity. A similar analysis of the application of the spherical harmonic method in the neighborhood of a point source may also be fruitful. It would be useful to consider the generic case of the superposition of an arbitrary propagating wave and an arbitrary standing wave at the probe location in space. If the amplitude of the propagating wave could be separated from the amplitude of the standing wave, as well as the wave vectors of both waves, then this would serve as a method for measuring active and reactive intensity in an unknown field, *i.e.* without the farfield assumption.

Bibliography

[1] A. D. Pierce, *Acoustics: An Introduction to Its Physical Principles and Applications* (Acoustical Society of America, Melville, NY, 1989), p. 189.

[2] J. W. S. Rayleigh, *The theory of sound*, 2nd ed. (Dover, London, 1937).

[3] D. B. Nutter, T. W. Leishman, S. D. Sommerfeldt, and J. D. Blotter, "Measurement of sound power and absorption in reverberation chambers using energy density," J. Acoust. Soc. Am. **121,** 2700–2710 (2007).

[4] J. W. Parkins, S. D. Sommerfeldt, and J. Tichy, "Narrowband and broadband active control in an enclosure using the acoustic energy density," J. Acoust. Soc. Am. **108,** 192–203 (2000).

[5] E. Tadmor, "Skew selfadjoint form for systems of conservation laws," J. Math. Anal. Applic. **103,** 428–442 (1984).

[6] J. J. Markham, "Second-Order Acoustic Fields: Energy Relations," Phys. Rev. **86,** 712–714 (1952).

[7] J. J. Markham, "Second-Order Acoustic Fields: Relations between Energy and Intensity," Phys. Rev. **89,** 972–977 (1953).

[8] N. N. Andreev, "Concerning Certain Second-Order Quantities in Acoustics," Sov. Phys. Acoust. **1,** 2–11 (1955).

[9] J. Lighthill, *Waves in Fluids* (Cambridge University Press, 1978).

[10] H. Lamb, *Hydrodynamics*, sixth ed. (Dover, 1932).

[11] Y. Inoue and T. Yano, "Propagation of strongly nonlinear plane waves," J. Acoust. Soc. Am. **94,** 1632–1642 (1993).

[12] F. J. Fahy, *Sound Intensity*, 2nd ed. (E & FN Spon, London, UK, 1995).

[13] G. W. Elko, Ph.D. thesis, The Pennsyvania State University, 1984.

[14] G. W. Elko, "An acoustic vector-field probe with calculable obstacle bias," In *Proceedings of the 1991 Noise & Vibration Conference*, D. A. Quinlan and M. G. Prasad, eds., pp. 525–532 (1991).

[15] J. A. Mann, J. Tichy, and A. J. Romano, "Instantaneous and time-averaged energy transfer in acoustic fields," J. Acoust. Soc. Am. **82,** 17–30 (1987).

[16] B.-T. Chu and R. E. Apfel, "Are acoustic intensity and potential energy density first- or second-order quantities?," Am. J. Phys. **51,** 916–918 (1983).

[17] R. L. Seliger and G. B. Whitham, "Variational Principles in Continuum Mechanics," Proceedings of the Royal Society of London. Series A, Mathematical and Physical Sciences **305,** 1–25 (1968).

[18] J. Naze Tjøtta and S. Tjøtta, "Nonlinear Equations of Acoustics," In *Frontiers of Nonlinear Acoustics: Proceedings of 12th ISNA*, M. F. Hamilton and D. T. Blackstock, eds., pp. 80–97 (Elsevier Science Publishers Ltd, New York, 1990).

[19] H. Goldstein, *Classical Mechanics* (Addison-Wesley, Reading, MA, 1950).

[20] A. F. Bennett, *Lagrangian Fluid Dynamics*, *Cambridge monographs on mechanics* (Cambridge University Press, 2006).

[21] C. Eckart, "Variation Principles of Hydrodynamics," Physics of Fluids **3,** 421–427 (1960).

[22] R. T. Beyer, *Nonlinear acoustics* (Acoustical Society of America, Woodbury, NY, 1997).

[23] M. Scholle, "Construction of Lagrangians in Continuum Theories," Proceedings: Mathematical, Physical and Engineering Sciences **460,** 3241–3260 (2004).

[24] *Instruments for the Measurement of Sound Intensity*, 1996, also ASA 117-1996.

[25] S. Nagata, K. Furihata, T. Wada, D. K. Asano, and T. Yanagisawa, "A three-dimensional sound intensity measurement system for sound source identification and sound power determination by ln models," J. Acoust. Soc. Am. **118,** 3691–3705 (2005).

[26] G. Rasmussen, "Measurement of Vector Fields," In *Proceedings of the Second International Congress on Acoustic Intensity*, pp. 53–58 (1985).

[27] S. Nagata, K. Furihata, T. Wada, D. K. Asano, and T. Yanagisawa, "A systematic method to obtain 3D finite-difference formulations for acoustic intensity and other energy quantities," J. Sound. Vib. **310,** 1093–1111 (2008).

[28] T. K. Moon and W. C. Stirling, *Mathematical Methods and Algorithms for Signal Processing* (Prentice Hall, Upper Saddle River, NJ, 2000).

[29] C. W. Therrien, *Discrete Random Signals and Statistical Signal Processing* (Prentice Hall, Englewood Cliffs, NJ, 1992).

[30] K. Hori, "4 Microphones Power Advanced, 3-Dimensional Sound Intensity Measuring System," J. Electron. Eng. **31,** 47–49 (1984).

[31] *Electromagnetic and Acoustic Scattering by Simple Shapes* (North-Holland Publishing Company, New York, 1969).

[32] C. R. Rao, *Linear Statistical Inference and Its Applications* (John Wiley and Sons, New York, 1965).

[33] C. A. L. Szuberla and J. V. Olson, "Uncertainties associated with parameter estimation in atmospheric infrasound arrays," J. Acoust. Soc. Am. **115,** 253–258 (2003).

Appendix A

Matlab Code

```
clear all;
close all;
set(0,'DefaultAxesFontName','arial');
set(0,'DefaultAxesFontSize',14);
set(0,'DefaultAxesFontWeight','normal')
set(0,'DefaultAxesLineWidth',2);
set(0,'DefaultLineLineWidth',2);
f = 1000;
ph = 0; % Set to 1 to include random phase mismatch
w = 2.*pi.*f;
c = 343;
rho = 1.21;
k = w./c;
cmax = 2e-1;
cmin = -2e-1;
cmaxa = 1;
cmina = -1;
cmaxp = 5;
cminp = -15;
cminm = -1;
cmaxm = 1;
a = 0.0254./2;
N = 100;
dphik=2.*pi./(N-1);
dthetak=pi./(N-1);
[phik,thetak]=meshgrid(0:dphik:2.*pi,0:dthetak:pi);

kx = k.*cos(phik).*sin(thetak);
ky = k.*sin(phik).*sin(thetak);
kz = k.*cos(thetak);
% Microphone 1 position (on top of the sphere)
```

```
theta1 = 0;
phi1 = 0;
% Normalized dot product of the position vector of
% mic 1 with the wave vector
rk1 = 1./2.*(cos(theta1-thetak).*(1+cos(phi1-phik))...
    +cos(theta1+thetak).*(1-cos(phi1-phik)));
% Microphone 2 position
theta2 = 1.910633237;
phi2 = -pi./3;
% Normalized dot product of the position vector of
% mic 2 with the wave vector
rk2 = 1./2.*(cos(theta2-thetak).*(1+cos(phi2-phik))...
    +cos(theta2+thetak).*(1-cos(phi2-phik)));
% Microphone 3 position
theta3 = 1.910633237;
phi3 = pi;
% Normalized dot product of the position vector of
% mic 3 with the wave vector
rk3 = 1./2.*(cos(theta3-thetak).*(1+cos(phi3-phik))...
    +cos(theta3+thetak).*(1-cos(phi3-phik)));
% Microphone 4 position
theta4 = 1.910633237;
phi4 = pi./3;
% Normalized dot product of the position vector of
% mic 4 with the wave vector
rk4 = 1./2.*(cos(theta4-thetak).*(1+cos(phi4-phik))...
    +cos(theta4+thetak).*(1-cos(phi4-phik)));
p0 = 1; % Amplitude of the incident wave
kr = k.*a;
ka = k.*a;
kr1 = k.*a.*rk1;
kr2 = k.*a.*rk2;
kr3 = k.*a.*rk3;
kr4 = k.*a.*rk4;
psi2 = ph*0.0175/4*(2*rand(1)-1);
psi3 = ph*0.0175/4*(2*rand(1)-1);
psi4 = ph*0.0175/4*(2*rand(1)-1);
p1 = p0.*exp(-j.*kr1); % Pressure at mic 1
p2 = p0.*exp(-j.*kr2).*exp(j.*psi2); % Pressure at mic 2
p3 = p0.*exp(-j.*kr3).*exp(j.*psi3); % Pressure at mic 3
p4 = p0.*exp(-j.*kr4).*exp(j.*psi4); % Pressure at mic 4

p=(p1+p2+p3+p4)/4;

% kx1 = sqrt(2)./4./a.*(angle(p3.^2./p2./p4));
% ky1 = sqrt(6)./4./a.*(angle(p2./p4));
% kz1 = 1./4./a.*(angle(p2.*p3.*p4./p1.^3));
% k1 = sqrt(kx1.^2+ky1.^2+kz1.^2);

kx1 = sqrt(2)./4./a.*(-angle(p2./p1)+2...
.*angle(p3./p1)-angle(p4./p1));
```

```
ky1 = sqrt(6)./4./a.*(angle(p2./p1)-angle(p4./p1));
kz1 = 1./4./a.*(angle(p2./p1)+angle(p3./p1)+angle(p4./p1));
k1 = sqrt(kx1.^2+ky1.^2+kz1.^2);

kx2 = sqrt(2)./4./a.*(2.*angle(p3./p2)-angle(p4./p2));
ky2 = -sqrt(6)./4./a.*angle(p4./p2);
kz2 = -1./4./a.*(3.*angle(p1./p2)-angle(p3./p2)-angle(p4./p2));
k2 = sqrt(kx2.^2+ky2.^2+kz2.^2);

kx3 = -sqrt(2)./4./a.*(angle(p2./p3)+angle(p4./p3));
ky3 = sqrt(6)./4./a.*(angle(p2./p3)-angle(p4./p3));
kz3 = -1./4./a.*(3.*angle(p1./p3)-angle(p2./p3)-angle(p4./p3));
k3 = sqrt(kx3.^2+ky3.^2+kz3.^2);

kx4 = -sqrt(2)./4./a.*(angle(p2./p4)-2.*angle(p3./p4));
ky4 = sqrt(6)./4./a.*angle(p2./p4);
kz4 = -1./4./a.*(3.*angle(p1./p4)-angle(p2./p4)-angle(p3./p4));
k4 = sqrt(kx4.^2+ky4.^2+kz4.^2);

vx = kx./rho./w.*p0;
vy = ky./rho./w.*p0;
vz = kz./rho./w.*p0;
v=sqrt(abs(vx).^2+abs(vy).^2+abs(vz).^2);
Ix = p0*conj(vx)/2;
Iy = p0*conj(vy)/2;
Iz = p0*conj(vz)/2;
I = sqrt(abs(vx).^2+abs(vy).^2+abs(vz).^2);

vx1 = kx1./rho./c./k1.*p1;
vy1 = ky1./rho./c./k1.*p1;
vz1 = kz1./rho./c./k1.*p1;
v1=sqrt(abs(vx1).^2+abs(vy1).^2+abs(vz1).^2);

Ix1 = real(p1.*conj(vx1)/2);
Iy1 = real(p1.*conj(vy1)/2);
Iz1 = real(p1.*conj(vz1)/2);
I1 = sqrt(abs(Ix1).^2+abs(Iy1).^2+abs(Iz1).^2);

vx2 = kx2./rho./c./k2.*p2;
vy2 = ky2./rho./c./k2.*p2;
vz2 = kz2./rho./c./k2.*p2;
v2=sqrt(abs(vx2).^2+abs(vy2).^2+abs(vz2).^2);

Ix2 = real(p2.*conj(vx2)/2);
Iy2 = real(p2.*conj(vy2)/2);
Iz2 = real(p2.*conj(vz2)/2);
I2 = sqrt(abs(Ix2).^2+abs(Iy2).^2+abs(Iz2).^2);

vx3 = kx3./rho./c./k3.*p3;
vy3 = ky3./rho./c./k3.*p3;
vz3 = kz3./rho./c./k3.*p3;
```

```
v3=sqrt(abs(vx3).^2+abs(vy3).^2+abs(vz3).^2);

Ix3 = real(p3.*conj(vx3)/2);
Iy3 = real(p3.*conj(vy3)/2);
Iz3 = real(p3.*conj(vz3)/2);
I3 = sqrt(abs(Ix3).^2+abs(Iy3).^2+abs(Iz3).^2);

vx4 = kx4./rho./c./k4.*p4;
vy4 = ky4./rho./c./k4.*p4;
vz4 = kz4./rho./c./k4.*p4;
v4=sqrt(abs(vx4).^2+abs(vy4).^2+abs(vz4).^2);

Ix4 = real(p4.*conj(vx4)/2);
Iy4 = real(p4.*conj(vy4)/2);
Iz4 = real(p4.*conj(vz4)/2);
I4 = sqrt(abs(Ix4).^2+abs(Iy4).^2+abs(Iz4).^2);

vxa = (vx1+vx2+vx3+vx4)/4;
vya = (vy1+vy2+vy3+vy4)/4;
vza = (vz1+vz2+vz3+vz4)/4;
va = (abs(vxa).^2+abs(vya).^2+abs(vza).^2).^(1/2);

Ixa = real(p.*conj(vxa)/2);
Iya = real(p.*conj(vya)/2);
Iza = real(p.*conj(vza)/2);
Ia = sqrt(abs(Ixa).^2+abs(Iya).^2+abs(Iza).^2);

vxp = j./rho./w.*(p2-2*p3+p4)/(4*a);
vyp = j./rho./w.*sqrt(6)*(-p2+p4)/(4*a);
vzp = j./rho./w.*(3*p1-p2-p3-p4)/(4*a);
vp=sqrt(abs(vxp).^2+abs(vyp).^2+abs(vzp).^2);

Ixp = real(p.*conj(vxp)/2);
Iyp = real(p.*conj(vyp)/2);
Izp = real(p.*conj(vzp)/2);
Ip = sqrt(abs(Ixp).^2+abs(Iyp).^2+abs(Izp).^2);

lerrIx1 = 20.*log10(abs((Ix1)./(Ix)));
lerrIy1 = 20.*log10(abs((Iy1)./(Iy)));
lerrIz1 = 20.*log10(abs((Iz1)./(Iz)));
lerrI1 = 20.*(log10((abs(Ix1)+abs(Iy1)+abs(Iz1))...
    ./(abs(Ix)+abs(Iy)+abs(Iz))));

lerrIx2 = 20.*log10(abs(Ix2./Ix));
lerrIy2 = 20.*log10(abs(Iy2./Iy));
lerrIz2 = 20.*log10(abs(Iz2./Iz));
lerrI2 = 20.*(log10((abs(Ix2)+abs(Iy2)+abs(Iz2))...
    ./(abs(Ix)+abs(Iy)+abs(Iz))));

lerrIx3 = 20.*log10(abs(Ix3./Ix));
lerrIy3 = 20.*log10(abs(Iy3./Iy));
```

```
lerrIz3 = 20.*log10(abs(Iz3./Iz));
lerrI3 = 20.*(log10((abs(Ix3)+abs(Iy3)+abs(Iz3))...
    ./(abs(Ix)+abs(Iy)+abs(Iz))));

lerrIx4 = 20.*log10(abs(Ix4./Ix));
lerrIy4 = 20.*log10(abs(Iy4./Iy));
lerrIz4 = 20.*log10(abs(Iz4./Iz));
lerrI4 = 20.*(log10((abs(Ix4)+abs(Iy4)+abs(Iz4))...
    ./(abs(Ix)+abs(Iy)+abs(Iz))));

lerrIxa = 20.*log10(abs(Ixa./Ix));
lerrIya = 20.*log10(abs(Iya./Iy));
lerrIza = 20.*log10(abs(Iza./Iz));
lerrIa = 20.*log10((abs(Ixa)+abs(Iya)+abs(Iza))...
    ./(abs(Ix)+abs(Iy)+abs(Iz)));

lerrIxp = 20.*log10(abs(Ixp./Ix));
lerrIyp = 20.*log10(abs(Iyp./Iy));
lerrIzp = 20.*log10(abs(Izp./Iz));
lerrIp = 20.*log10((abs(Ixp)+abs(Iyp)+abs(Izp))...
    ./(abs(Ix)+abs(Iy)+abs(Iz)));

PHI=phik;
THETA=thetak;
subplot(2,2,1)
pcolor(phik,thetak,(lerrIx1));
shading interp
axis([0 2*pi 0 pi])
caxis([cmin cmax])
xlabel('\phi_k ')
ylabel('\theta_k ')
set(gca,'XTick',[0 pi 2*pi]);
set(gca,'XTickLabel',{'0';'p';'2p'});
set(gca,'YTick',[0 pi/2 pi])
set(gca,'YTickLabel',{'0';'p/2';'p'},'fontname','symbol');
colorbar

subplot(2,2,2)
pcolor(phik,thetak,(lerrIy1));
shading interp
axis([0 2*pi 0 pi])
caxis([cmin cmax])
xlabel('\phi_k ')
ylabel('\theta_k ')
set(gca,'XTick',[0 pi 2*pi]);
set(gca,'XTickLabel',{'0';'p';'2p'});
set(gca,'YTick',[0 pi/2 pi])
set(gca,'YTickLabel',{'0';'p/2';'p'},'fontname','symbol');
colorbar

subplot(2,2,3)
```

```
pcolor(phik,thetak,(lerrIz1));
shading interp
axis([0 2*pi 0 pi])
caxis([cmin cmax])
xlabel('\phi_k ')
ylabel('\theta_k ')
set(gca,'XTick',[0 pi 2*pi]);
set(gca,'XTickLabel',{'0';'p';'2p'});
set(gca,'YTick',[0 pi/2 pi])
set(gca,'YTickLabel',{'0';'p/2';'p'},'fontname','symbol');
colorbar

subplot(2,2,4)
pcolor(phik,thetak,(lerrI1));
shading interp
axis([0 2*pi 0 pi])
xlabel('\phi_k ')
ylabel('\theta_k ')
set(gca,'XTick',[0 pi 2*pi]);
set(gca,'XTickLabel',{'0';'p';'2p'});
set(gca,'YTick',[0 pi/2 pi])
set(gca,'YTickLabel',{'0';'p/2';'p'},'fontname','symbol');

colorbar

figure
subplot(2,2,1)
pcolor(phik,thetak,(lerrIxp));
shading interp
axis([0 2*pi 0 pi])
caxis([cminp cmaxp])
xlabel('\phi_k ')
ylabel('\theta_k ')
set(gca,'XTick',[0 pi 2*pi]);
set(gca,'XTickLabel',{'0';'p';'2p'});
set(gca,'YTick',[0 pi/2 pi])
set(gca,'YTickLabel',{'0';'p/2';'p'},'fontname','symbol');
colorbar

subplot(2,2,2)
pcolor(phik,thetak,(lerrIyp));
shading interp
axis([0 2*pi 0 pi])
caxis([cminp cmaxp])
xlabel('\phi_k ')
ylabel('\theta_k ')
set(gca,'XTick',[0 pi 2*pi]);
set(gca,'XTickLabel',{'0';'p';'2p'});
set(gca,'YTick',[0 pi/2 pi])
set(gca,'YTickLabel',{'0';'p/2';'p'},'fontname','symbol');
colorbar
```

```
subplot(2,2,3)
pcolor(phik,thetak,(lerrIzp));
shading interp
axis([0 2*pi 0 pi])
caxis([cminp cmaxp])
xlabel('\phi_k ')
ylabel('\theta_k ')
set(gca,'XTick',[0 pi 2*pi]);
set(gca,'XTickLabel',{'0';'p';'2p'});
set(gca,'YTick',[0 pi/2 pi])
set(gca,'YTickLabel',{'0';'p/2';'p'},'fontname','symbol');
colorbar

subplot(2,2,4)
pcolor(phik,thetak,(lerrIp));
shading interp
axis([0 2*pi 0 pi])
xlabel('\phi_k ')
ylabel('\theta_k ')
set(gca,'XTick',[0 pi 2*pi]);
set(gca,'XTickLabel',{'0';'p';'2p'});
set(gca,'YTick',[0 pi/2 pi])
set(gca,'YTickLabel',{'0';'p/2';'p'},'fontname','symbol');
colorbar

figure
subplot(2,2,1)
pcolor(phik,thetak,(lerrIxa));
shading interp
axis([0 2*pi 0 pi])
caxis([cmina cmaxa])
xlabel('\phi_k ')
ylabel('\theta_k ')
set(gca,'XTick',[0 pi 2*pi]);
set(gca,'XTickLabel',{'0';'p';'2p'});
set(gca,'YTick',[0 pi/2 pi])
set(gca,'YTickLabel',{'0';'p/2';'p'},'fontname','symbol');
colorbar

subplot(2,2,2)
pcolor(phik,thetak,(lerrIya));
shading interp
axis([0 2*pi 0 pi])
caxis([cmina cmaxa])
xlabel('\phi_k ')
ylabel('\theta_k ')
set(gca,'XTick',[0 pi 2*pi]);
set(gca,'XTickLabel',{'0';'p';'2p'});
set(gca,'YTick',[0 pi/2 pi])
set(gca,'YTickLabel',{'0';'p/2';'p'},'fontname','symbol');
```

```
colorbar

subplot(2,2,3)
pcolor(phik,thetak,(lerrIza));
shading interp
axis([0 2*pi 0 pi])
caxis([cmina cmaxa])
xlabel('\phi_k ')
ylabel('\theta_k ')
set(gca,'XTick',[0 pi 2*pi]);
set(gca,'XTickLabel',{'0';'p';'2p'});
set(gca,'YTick',[0 pi/2 pi])
set(gca,'YTickLabel',{'0';'p/2';'p'},'fontname','symbol');
colorbar

subplot(2,2,4)
pcolor(phik,thetak,(lerrIa));
shading interp
axis([0 2*pi 0 pi])
xlabel('\phi_k ')
ylabel('\theta_k ')
set(gca,'XTick',[0 pi 2*pi]);
set(gca,'XTickLabel',{'0';'p';'2p'});
set(gca,'YTick',[0 pi/2 pi])
set(gca,'YTickLabel',{'0';'p/2';'p'},'fontname','symbol');
colorbar
```

```
clear all;
close all;
a = 0.025;
p0 = 1;
c = 343;
rho = 1.21;
fmax = 20000;
N = 100;
M = 50;
df = fmax/(N-1);
f = 0:df:fmax;
w = 2*pi*f;
k = w/c;
kamax = 10;
dka = kamax/(N-1);
KA = 0:dka:kamax;
thetamax = pi;
dtheta = thetamax/(N-1);
THETA = 0:dtheta:thetamax;
[ka,theta] = meshgrid(KA,THETA);
ps = zeros(size(ka));
LPm2 = ones(size(ka));
LPm1 = cos(theta);
```

```
m = 0;
jmm1 = sqrt(pi./(2*ka)).*besselj(m+1/2-1,ka);
jmp1 = sqrt(pi./(2*ka)).*besselj(m+1/2+1,ka);
ymm1 = sqrt(pi./(2*ka)).*bessely(m+1/2-1,ka);
ymp1 = sqrt(pi./(2*ka)).*bessely(m+1/2+1,ka);
dhm = 1./(2*m+1).*(m*(jmm1+i*ymm1)-(m+1)*(jmp1+i*ymp1));
ps = ps+p0*(-i)^m*(2*m+1)*LPm2./dhm;
m = 1;
jmm1 = sqrt(pi./(2*ka)).*besselj(m+1/2-1,ka);
jmp1 = sqrt(pi./(2*ka)).*besselj(m+1/2+1,ka);
ymm1 = sqrt(pi./(2*ka)).*bessely(m+1/2-1,ka);
ymp1 = sqrt(pi./(2*ka)).*bessely(m+1/2+1,ka);
dhm = 1./(2*m+1).*(m*(jmm1+i*ymm1)-(m+1)*(jmp1+i*ymp1));
ps = ps+p0*(-i)^m*(2*m+1)*LPm1./dhm;
for m = 2:M
    LP = 2*cos(theta).*LPm1-LPm2-1/m*(cos(theta).*LPm1-LPm2);
    jmm1 = sqrt(pi./(2*ka)).*besselj(m+1/2-1,ka);
    jmp1 = sqrt(pi./(2*ka)).*besselj(m+1/2+1,ka);
    ymm1 = sqrt(pi./(2*ka)).*bessely(m+1/2-1,ka);
    ymp1 = sqrt(pi./(2*ka)).*bessely(m+1/2+1,ka);
    dhm = 1./(2*m+1).*(m*(jmm1+i*ymm1)-(m+1)*(jmp1+i*ymp1));
    ps = ps+p0*(-i)^m*(2*m+1)*LP./dhm;
    LPm2 = LPm1;
    LPm1 = LP;
end
ps = i./ka.^2.*ps;
% surf(ka,theta,abs(ps));
% subplot(211)
surf(ka,theta,real(ps-p0*exp(i*ka.*cos(theta))));%p0*exp(i*ka.*cos(theta))-
axis([0 kamax 0 thetamax -3 3]);
caxis([-3 3])
title('Real part of the excess pressure, Re(p_s)')
xlabel('ka')
ylabel('\theta')
view(45,45)
colorbar
figure
surf(ka,theta,imag(ps-p0*exp(i*ka.*cos(theta))));
% surf(ka,theta,(unwrap(angle(ps),0.1)));%
% axis([0 kamax 0 thetamax -3 3]);
% caxis([-3 3])
view(45,45)
title('Imaginary part of the excess pressure, Im(p_s)')
xlabel('ka')
ylabel('\theta')
colorbar
```

```
% Calculate the intensity due to multiple point sources
clear all;
close all;
```

```
set(0,'DefaultAxesFontName','Arial');

set(0,'DefaultAxesFontSize',14);

set(0,'DefaultAxesFontWeight','demi')

set(0,'DefaultAxesLineWidth',2);

set(0,'DefaultLineLineWidth',2);

set(0,'DefaultLineMarkersize',10);

colvect=[0,0,0; 0,0,0; .5,.5,.5; 0,.8,0; .7,.3,.3;];

set(0,'DefaultAxesColorOrder',colvect);

set(0,'DefaultAxesLineStyleOrder',{'-','--'});
f = 5000;
w = 2*pi*f;
c = 343;
k = w/c;
lambda = 2*pi/k;
a = 0.025/2;
rho = 1.21;
d = 0.25;
p0 = 0.1*[1,0];
rs = [0 d/2 0;0 -d/2 0];
% p0 = 0.1*[1,-1,1,-1,1,-1,1,-1,1,-1,1,-1,1,-1];
% rs = [0 d/2 0;0 -d/2 0;0 3*d/2 0;0 -3*d/2 0;0 5*d/2 0;0 -5*d/2 0;0 7*d/2 0;0 -7*d/2 0;0 9
p0 = sin(k*rs(:,2)+pi/8)./(k*rs(:,2));
N = 40;
U = 0;
TITLE = [sprintf('   Wave Vector Intensity Estimate: y Dipole y-z plane
');...
    sprintf('Finite-Difference Intensity Estimate: y Dipole y-z plane');...
    sprintf('        Analytical Intensity: y Dipole y-z plane        ');...
    sprintf('   Wave Vector Intensity Estimate: y Dipole x-z plane   ');...
    sprintf('Finite-Difference Intensity Estimate: y Dipole x-z plane');...
    sprintf('        Analytical Intensity: y Dipole x-z plane        ');...
    sprintf('   Wave Vector Intensity Estimate: y Dipole x-y plane   ');...
    sprintf('     Finite-Difference Intensity: y Dipole x-y plane    ');...
    sprintf('        Analytical Intensity: y Dipole x-y plane        ')]
for ND = 1:3;
    U = U+1;
    % rmax = 3;
    % dr = rmax/(N-1);
    % r = 0:dr:3;
    % dphi = 2*pi/(N-1);
    % phi = 0:dphi:2*pi;
    % % phi = 0;
    % dtheta = pi/(N-1);
```

```
% theta = 0:dtheta:pi;
% % theta = 0;
% [R,PHI,THETA] = meshgrid(r,phi,theta);
Xmin = -2;
Xmax = 2;
dX = (Xmax-Xmin)/(N-1);
X = Xmin:dX:Xmax;
if ND == 1
    X = 0;
end
Ymin = -2;
Ymax = 2;
dY = (Ymax-Ymin)/(N-1);
Y = Ymin:dY:Ymax;
if ND == 2
    Y = 0;
end
Zmin = -2;
Zmax = 2;
dZ = (Zmax-Zmin)/(N-1);
Z = Zmin:dZ:Zmax;
if ND == 3
    Z = 0;
end

[x,y,z] = meshgrid(X,Y,Z);
%     x = (x);
%     y = (y);
%     z = (z);
R = sqrt(x.^2+y.^2+z.^2);
PHI = atan2(y,x);
THETA = acos(z./sqrt(x.^2+y.^2+z.^2));
% x = R.*cos(PHI).*sin(THETA);
% y = R.*sin(PHI).*sin(THETA);
% z = R.*cos(THETA);

rm1 = [0 0 a];
rm2 = [a*sqrt(2)/3 -a*sqrt(6)/3 -a/3];
rm3 = [-2*a*sqrt(2)/3 0 -a/3];
rm4 = [a*sqrt(2)/3 a*sqrt(6)/3 -a/3];
%     r1(1,:,:,:) = rm1(1)+x-rs(1,1);
pa = zeros(size(x));
uax = zeros(size(pa));
uay = zeros(size(pa));
uaz = zeros(size(pa));

p1 = zeros(size(pa));
p2 = zeros(size(pa));
p3 = zeros(size(pa));
p4 = zeros(size(pa));
%     figure(3)
```

```
    for o = 1:length(p0)
        rax = x-rs(o,1);
        ray = y-rs(o,2);
        raz = z-rs(o,3);

        kax = w/c*rax./(rax.^2+ray.^2+raz.^2).^(1/2);
        kay = w/c*ray./(rax.^2+ray.^2+raz.^2).^(1/2);
        kaz = w/c*raz./(rax.^2+ray.^2+raz.^2).^(1/2);

        pa = pa + p0(o).*exp(-j*(kax.*rax+kay.*ray+kaz.*raz))./(rax.^2+ray.^2+raz.^2).^(1/2

        uax = uax+p0(o)/rho/w*rax.*(w/c-j./(rax.^2+ray.^2+raz.^2).^(1/2))...
            .*exp(-j*(kax.*rax+kay.*ray+kaz.*raz))./(rax.^2+ray.^2+raz.^2);
        uay = uay+p0(o)/rho/w.*ray.*(w/c-j./(rax.^2+ray.^2+raz.^2).^(1/2))...
            .*exp(-j*(kax.*rax+kay.*ray+kaz.*raz))./(rax.^2+ray.^2+raz.^2);
        uaz = uaz+p0(o)/rho/w.*raz.*(w/c-j./(rax.^2+ray.^2+raz.^2).^(1/2))...
            .*exp(-j*(kax.*rax+kay.*ray+kaz.*raz))./(rax.^2+ray.^2+raz.^2);

        r1x = rm1(1)+x-rs(o,1);
        r1y = rm1(2)+y-rs(o,2);
        r1z = rm1(3)+z-rs(o,3);

        k1x = w/c*r1x./(r1x.^2+r1y.^2+r1z.^2).^(1/2);
        k1y = w/c*r1y./(r1x.^2+r1y.^2+r1z.^2).^(1/2);
        k1z = w/c*r1z./(r1x.^2+r1y.^2+r1z.^2).^(1/2);

        r2x = rm2(1)+x-rs(o,1);
        r2y = rm2(2)+y-rs(o,2);
        r2z = rm2(3)+z-rs(o,3);

        k2x = w/c*r2x./sqrt(r2x.^2+r2y.^2+r2z.^2);
        k2y = w/c*r2y./sqrt(r2x.^2+r2y.^2+r2z.^2);
        k2z = w/c*r2z./sqrt(r2x.^2+r2y.^2+r2z.^2);

        r3x = rm3(1)+x-rs(o,1);
        r3y = rm3(2)+y-rs(o,2);
        r3z = rm3(3)+z-rs(o,3);

        k3x = w/c*r3x./sqrt(r3x.^2+r3y.^2+r3z.^2);
        k3y = w/c*r3y./sqrt(r3x.^2+r3y.^2+r3z.^2);
        k3z = w/c*r3z./sqrt(r3x.^2+r3y.^2+r3z.^2);

        r4x = rm4(1)+x-rs(o,1);
        r4y = rm4(2)+y-rs(o,2);
        r4z = rm4(3)+z-rs(o,3);

        k4x = w/c*r4x./sqrt(r4x.^2+r4y.^2+r4z.^2);
        k4y = w/c*r4y./sqrt(r4x.^2+r4y.^2+r4z.^2);
        k4z = w/c*r4z./sqrt(r4x.^2+r4y.^2+r4z.^2);

        p1 = p1+(p0(o)*exp(-j*(k1x.*r1x+k1y.*r1y+k1z.*r1z))./sqrt(r1x.^2+r1y.^2+r1z.^2));
```

```
        p2 = p2+(p0(o)*exp(-j*(k2x.*r2x+k2y.*r2y+k2z.*r2z))./sqrt(r2x.^2+r2y.^2+r2z.^
        p3 = p3+(p0(o)*exp(-j*(k3x.*r3x+k3y.*r3y+k3z.*r3z))./sqrt(r3x.^2+r3y.^2+r3z.^
        p4 = p4+(p0(o)*exp(-j*(k4x.*r4x+k4y.*r4y+k4z.*r4z))./sqrt(r4x.^2+r4y.^2+r4z.^
        %         subplot(221)
        %         surf(squeeze(p1))
        %         subplot(222)
        %         surf(squeeze(p2))
        %         subplot(223)
        %         surf(squeeze(p3))
        %         subplot(224)
        %         surf(squeeze(p4))
        %         pause
    end
%     p1 = p1.*exp(j*0.0175*randn(size(p1)));
%     p2 = p2.*exp(j*0.0175*randn(size(p1)));
%     p3 = p3.*exp(j*0.0175*randn(size(p1)));
%     p4 = p4.*exp(j*0.0175*randn(size(p1)));
    %         subplot(221)
    %         surf(abs(p1))
    %         subplot(222)
    %         surf(abs(p2))
    %         subplot(223)
    %         surf(abs(p3))
    %         subplot(224)
    %         surf(abs(p4))
    %         pause
    kwvx = sqrt(2)/4/a*(-angle(p2./p1)+2*angle(p3./p1)-angle(p4./p1));
    kwvy = sqrt(6)/4/a*(angle(p2./p1)-angle(p4./p1));
    kwvz = 1/4/a*(angle(p2./p1)+angle(p3./p1)+angle(p4./p1));

    kwv = (kwvx.^2+kwvy.^2+kwvz.^2).^(1/2);
    %         p(1) = (2*p3+p2+p4)/4;
    %         p(2) = (p2+p4)/4;
    %         p(3) = (3*p1+p2+p3+p4)/6;
    uwvx = kwvx.*p1./kwv/rho/c;
    uwvy = kwvy.*p1./kwv/rho/c;
    uwvz = kwvz.*p1./kwv/rho/c;

    upx = -1/j/w/rho/4/a*sqrt(2)*(p2-2*p3+p4);
    upy = -1/j/w/rho/4/a*sqrt(6)*(p4-p2);
    upz = -1/j/w/rho/4/a*(3*p1-p2-p3-p4);

    Iax = real(pa.*conj(uax))/2;
    Iay = real(pa.*conj(uay))/2;
    Iaz = real(pa.*conj(uaz))/2;

    Ialog = 10*log10(sqrt(abs(Iax).^2+abs(Iay).^2+abs(Iaz).^2)/(10e-12));
    phiIa = atan2(Iay,Iax);
    thetaIa = acos(Iaz./sqrt(Iax.^2+Iay.^2+Iaz.^2));
    Iaxlog = Ialog.*sin(thetaIa).*cos(phiIa);
    Iaylog = Ialog.*sin(thetaIa).*sin(phiIa);
```

```
    Iazlog = Ialog.*cos(thetaIa);

    Iwvx = real(p1.*conj(uwvx))/2;
    Iwvy = real(p1.*conj(uwvy))/2;
    Iwvz = real(p1.*conj(uwvz))/2;

    p = (p1+p2+p3+p4)/4;

    Ipx = real(p.*conj(upx))/2;
    Ipy = real(p.*conj(upy))/2;
    Ipz = real(p.*conj(upz))/2;

    Iwvlog = 10*log10(sqrt(abs(Iwvx).^2+abs(Iwvy).^2+abs(Iwvz).^2)/(10e-12));
    phiI = atan2(Iwvy,Iwvx);
    thetaI = acos(Iwvz./sqrt(Iwvx.^2+Iwvy.^2+Iwvz.^2));
    Iwvxlog = Iwvlog.*sin(thetaI).*cos(phiI);
    Iwvylog = Iwvlog.*sin(thetaI).*sin(phiI);
    Iwvzlog = Iwvlog.*cos(thetaI);

    Iplog = 10*log10(sqrt(abs(Ipx).^2+abs(Ipy).^2+abs(Ipz).^2)/(10e-12));
    phiIp = atan2(Ipy,Ipx);
    thetaIp = acos(Ipz./sqrt(Ipx.^2+Ipy.^2+Ipz.^2));
    Ipxlog = Iplog.*sin(thetaIp).*cos(phiIp);
    Ipylog = Iplog.*sin(thetaIp).*sin(phiIp);
    Ipzlog = Iplog.*cos(thetaIp);
    %         I1 = I1/max(max(abs(I1)));
    %         I1log = 10*sign(I1).*log10(abs(I1)/10e-12)/200;
    % r11 = r1-r1;
    % r21 = r2-r1;
    % r31 = r3-r1;
    % r41 = r4-r1;
    %             quiver3(r0(1),r0(2),r0(3),k(1),k(2),k(3),'b');
    %         quiver3(r0(1),r0(2),r0(3),k1(1),k1(2),k1(3),'b');
    figure(U)

%     subplot(2,2,ND)
    hold on
    quiver3(x,y,z,Iwvxlog,Iwvylog,Iwvzlog,'k','LineWidth',2);
    for o = 1:length(p0)
        if p0(o)>0
            shape = 'sk';
        elseif p0(o)<0
            shape = 'ok';
        end
        scatter3(rs(o,1),rs(o,2),rs(o,3),shape)
    end
    hold off
    %         quiver3(r0(1),r0(2),r0(3),0,I1log(2),I1log(3),'r');
    %             quiver3(r0(1),r0(2),r0(3),u1(1),u1(2),u1(3),'r');
    xlabel('x');
    ylabel('y');
```

```
    zlabel('z');
    axis equal
    axis([Xmin Xmax Ymin Ymax Zmin Zmax])
    az = 90*(1-sign(mod(1,ND)));
    el = 90*(1-sign(mod(3,ND)))-90*(1-sign(mod(1,ND)));
    view(az,el)
    title(TITLE(U,:))
    U = U+1;

    figure(U)
%     subplot(2,2,ND)
    hold on
    quiver3(x,y,z,Ipxlog,Ipylog,Ipzlog,'k','LineWidth',2);
    for o = 1:length(p0)
        if p0(o)>0
            shape = 'sk';
        elseif p0(o)<0
            shape = 'ok';
        end
        scatter3(rs(o,1),rs(o,2),rs(o,3),shape)
    end
    hold off
    %         quiver3(r0(1),r0(2),r0(3),0,I1log(2),I1log(3),'r');
    %             quiver3(r0(1),r0(2),r0(3),u1(1),u1(2),u1(3),'r');
    xlabel('x');
    ylabel('y');
    zlabel('z');
    axis equal
    axis([Xmin Xmax Ymin Ymax Zmin Zmax])
    az = 90*(1-sign(mod(1,ND)));
    el = 90*(1-sign(mod(3,ND)))-90*(1-sign(mod(1,ND)));
    view(az,el)
    title(TITLE(U,:))
    U = U+1;

    figure(U)
    %     subplot(2,2,ND)
    hold on
    quiver3(x,y,z,Iaxlog,Iaylog,Iazlog,'k','LineWidth',2);
    for o = 1:length(p0)
        if p0(o)>0
            shape = 'sk';
        elseif p0(o)<0
            shape = 'ok';
        end
        scatter3(rs(o,1),rs(o,2),rs(o,3),shape)
    end
    hold off
    %         quiver3(r0(1),r0(2),r0(3),0,I1log(2),I1log(3),'r');
    %             quiver3(r0(1),r0(2),r0(3),u1(1),u1(2),u1(3),'r');
    xlabel('x');
```

```
    ylabel('y');
    zlabel('z');
    axis equal
    axis([Xmin Xmax Ymin Ymax Zmin Zmax])
    az = 90*(1-sign(mod(1,ND)));
    el = 90*(1-sign(mod(3,ND)))-90*(1-sign(mod(1,ND)));
    view(az,el)
    title(TITLE(U,:))
end
% avphiIwv = 1/N^2*sum(sum((squeeze(phiI-phiIa))));
% avthetaIwv = sum(sum(squeeze(thetaI-thetaIa)));
% avphiIp = 1/N^2*sum(sum((squeeze(phiIp-phiIa))));
% avthetaIp = sum(sum(squeeze(thetaIp-thetaIa)));
%
figure
surf(squeeze(x)/lambda,squeeze(y)/lambda,10*log10(squeeze((abs(Iwvx)+abs(Iwvy)+abs(Iwvz))./
axis([Xmin/lambda Xmax/lambda Ymin/lambda Ymax/lambda])
view(3)
xlabel('x/\lambda')
ylabel('y/\lambda')
zlabel('dB')
topline = sprintf('Error of WV Estimate: ka = %g, kd = %g',k*a,k*d)
title(topline)
colorbar
figure
surf(squeeze(x)/lambda,squeeze(y)/lambda,10*log10(squeeze((abs(Ipx)+abs(Ipy)+abs(Ipz))./(a
axis([Xmin/lambda Xmax/lambda Ymin/lambda Ymax/lambda])
view(3)
xlabel('x/\lambda')
ylabel('y/\lambda')
zlabel('dB')
topline = sprintf('Error of FD Estimate: ka = %g, kd = %g',k*a,k*d)
title(topline)
colorbar
% figure(6)
% subplot(211)
% surf(squeeze(x),squeeze(y),(squeeze(phiI-phiIa)))
% subplot(212)
% surf(squeeze(x),squeeze(y),(squeeze(thetaI-thetaIa)))
% figure(7)
% subplot(211)
% surf(squeeze(x),squeeze(y),(squeeze(phiIp-phiIa)))
% subplot(212)
% surf(squeeze(x),squeeze(y),(squeeze(thetaIp-thetaIa)))
```